Open Access
ISSN: 2769-5247 (Online)

CHEMICAL SYNTHESIS

50 Years Selenium Organic Chemistry

selenium
34
Se
78.96

Guest Editor:
Prof. Bao-Lian Su

www.chesynjournal.com

Topic: 50 Years Selenium Organic Chemistry

Prof. Bao-Lian Su

Laboratory of Inorganic Materials Chemistry (CMI), University of Namur, Namur, Belgium; State Key Laboratory of Advanced Technology for Materials Synthesis and Processing, Wuhan University of Technology, Wuhan, Hubei, China.
Email: bao-lian.su@unamur.be

Bao-Lian Su, Member of the European Academy of Sciences, Member of the Royal Academy of Belgium, Honorary Fellow of the Chinese Chemical Society, Fellow of the Royal of Society of Chemistry, UK and Life Member of Clare Hall College, University of Cambridge. He is currently a professor in the University of Namur and the Wuhan University of Technology. His current research fields include the synthesis, the property study and the molecular engineering of hierarchically porous and bio-inspired materials for artificial photosynthesis, (photo) catalysis, energy conversion and storage, biotechnology, cell therapy and biomedical applications.

Special Issue introduction:

Dr. Alain Krief, the Emeritus Professor of the University of Namur, has contributed a lot to the development of selenium organic chemistry, and this field has gained evolving interest. He also played an important role as Executive Director of the International Organization for Chemistry Development (IOCD). On his 80th anniversary, we would like to celebrate his scientific achievements in this fascinating field.

EDITORIAL BOARD

GENERAL INFORMATION

About the Journal

Chemical Synthesis (*CS*) is an international peer-reviewed, open access, online journal. *Chemical Synthesis* is an open access peer-reviewed journal publishing original research involving all areas of the chemical sciences. The journal aims to be the premier resource of seminal and insightful research and showcases for researchers in both academia and industry, providing a platform of inspiration for the future of chemistry. *Chemical Synthesis* intends to serve as the preeminent international chemistry journal and has the ambition to be among the first choices of chemists for publication of their discoveries.

The scope of the journal focuses on the breadth of the chemical synthetic sciences, covering fields from synthetic methodologies, property studies by theoretical calculations or instrumental approaches at molecular and/or nano levels of the obtained products (materials) to the applications in catalysis, energy conversion and storage, biomedicals, pharmaceuticals, environment protection and remediation, *etc.*

Information for Authors

Manuscripts should be prepared in accordance with Author Instructions.
Please check www.chesynjournal.com/pages/view/author_instructions for details.
All manuscripts should be submitted online at https://oaemesas.com/login?JournalId=cs.

Copyright

Permissions

For information on how to request permissions to reproduce articles/information from this journal, please visit www.chesynjournal.com.

Disclaimer

The information and opinions presented in the journal reflect the views of the authors and not of the journal or its Editorial Board or the Publisher. Publication does not constitute endorsement by the journal. Neither the *CS* nor its publishers nor anyone else involved in creating, producing or delivering the *CS* or the materials contained therein, assumes any liability or responsibility for the accuracy, completeness, or usefulness of any information provided in the *CS*, nor shall they be liable for any direct, indirect, incidental, special, consequential or punitive damages arising out of the use of the *CS*. The *CS*, nor its publishers, nor any other party involved in the preparation of material contained in the *CS* represents or warrants that the information contained herein is in every respect accurate or complete, and they are not responsible for any errors or omissions or for the results obtained from the use of such material. Readers are encouraged to confirm the information contained herein with other sources.

Publisher

OAE Publishing Inc.
245 E Main Street ste 107, Alhambra, CA 91801, USA
Website: www.oaepublish.com

Contacts

E-mail: editorialoffice@chesynjournal.com
Website: https://www.oaepublish.com/cs

Chemical Synthesis

CONTENTS

Topic: 50 Years Selenium Organic Chemistry

Cheng *et al. Chem Synth* 2023;3:13
DOI: 10.20517/cs.2022.43

Chemical Synthesis

Research Article

Open Access

Dedicated to Professor Alain Krief on the occasion of his 80th Birthday

Luminescent alkynylplatinum(II) terpyridine-containing conjugated polymers: synthesis, characterization and photophysical studies

Heung-Kiu Cheng, Vivian Wing-Wah Yam*

Institute of Molecular Functional Materials and Department of Chemistry, The University of Hong Kong, Hong Kong 999077, China.

***Correspondence to:** Prof. Vivian Wing-Wah Yam, Institute of Molecular Functional Materials and Department of Chemistry, The University of Hong Kong, Pokfulam Road, Hong Kong 999077, China. E-mail: wwyam@hku.hk

How to cite this article: Cheng HK, Yam VWW. Luminescent alkynylplatinum(II) terpyridine-containing conjugated polymers: synthesis, characterization and photophysical studies. *Chem Synth* 2023;3:13. https://dx.doi.org/10.20517/cs.2022.43

Received: 29 Dec 2022 **First Decision:** 2 Feb 2023 **Revised:** 17 Feb 2023 **Accepted:** 23 Feb 2023 **Published:** 9 Mar 2023

Academic Editor: Bao-Lian Su **Copy Editor:** Ke-Cui Yang **Production Editor:** Ke-Cui Yang

Abstract

A series of alkynylplatinum(II) terpyridine complexes and alkynylplatinum(II) terpyridine-containing conjugated polymers with different polymer backbones has been synthesized, and their spectroscopic properties and Förster resonance energy transfer (FRET) processes has been investigated. The platinum(II)-containing polymers exhibit dual emissive features with emission maxima at *ca.* 416-465 nm and *ca.* 671-673 nm, which are assigned to be originated from singlet intraligand (^{1}IL) excited states from the polymer backbone and triplet metal-metal-to-ligand charge transfer (^{3}MMLCT) excited states from the platinum(II) pendants, respectively. The Förster radii (R_0) of the platinum(II)-containing conjugated polymers have been determined, and their distinctive thermo-responsive luminescence changes have also been observed. The present work has demonstrated the utilization of "click" reaction for the preparation of platinum(II)-containing conjugated polymers, which show unique photophysical and spectroscopic properties. Through the judicious design, this type of platinum(II)-containing polymer is found to be sensitive to temperature, resulting in ratiometric emission changes. This study has provided valuable insights into the preparation of metal-containing polymeric systems for different applications.

Keywords: Platinum(II) complexes, conjugated polymers, FRET

INTRODUCTION

Over the past few decades, conjugated polymers, which have been extensively studied with well-known examples such as poly(*p*-phenylene vinylene) (PPV)[1], polypyrrole (PPy)[2-4], polythiophene (PT)[5] and so on, represent important classes of organic macromolecules, and have found widespread applications in organic photovoltaic devices, light-emitting diodes, sensing materials, and others[6-11]. The prominence of conjugated polymers can be attributed to their unique properties of high planarity and extended π-electron delocalization, empowering them with rich photophysical and electrochemical functionalities for specific applications[6-11]. After the success in designing and synthesizing different kinds of conjugated polymers, attempts have been made to integrate conjugated polymers with transition metals, namely metallo-conjugated polymers, with a view to not only improving the physical properties of the parent organic polymers such as mechanical strength, thermal stability and carrier mobility but also enriching their photophysical properties such as harvesting energy from the triplet excited state and extending the absorption spectrum to the red or near-infrared (NIR) region[12-19]. Earlier examples include ruthenium(II)-containing conjugated polymers with poly(bpy-*co*-benzobisoxazole)s or poly(bpy-*co*-benzobisthiazole)s as the polymer backbones[20] and iridium(III)-containing conjugated polymers with polyfluorene as the polymer backbone and carbazole unit as the pendant[21]. Unlike most other commonly studied transition metal centers, including ruthenium(II), rhodium(III) and iridium(III), d^8 platinum(II) center favors coordination of a square-planar geometry, and their complexes, especially those bearing conjugated aromatic ligands capable of exhibiting π-π interactions, are well-known for their ability to self-assemble[22-26], forming aggregates[27-31] and providing remarkable photophysical properties associated with Pt···Pt and π-π interactions[32-35]. In light of their supramolecular assembly capability, it is envisaged that the introduction of platinum centers into conjugated polymers may provide an opportunity to further modulate the photophysical and morphological properties of the resulting metal–organic hybrid materials[36-38]. Although there were examples of platinum(II)-containing conjugated polymers such as platinum(II) polyynes[39-46] and cyclometalating bidentate ligand-containing platinum(II)-based conjugated polymers[47-49], none of these examples demonstrates supramolecular assembly properties or utilizes the system of tridentate *N*-donor ligands. In this work, a series of alkynylplatinum(II) terpyridine complexes (**1** and **2**) and alkynylplatinum(II) terpyridine-containing conjugated polymers with different polymer backbones (**3**-**5**) [Scheme 1] has been synthesized and their photophysical properties as well as FRET processes have been studied. With the aid of various spectroscopic techniques, the photophysical and spectroscopic properties of the organic polymers, platinum(II) precursor complexes and the newly synthesized platinum(II)-containing conjugated polymers have been investigated systematically. It was found that the choice of the polymer backbones would influence the intramolecular FRET efficiencies of the system of platinum(II)-containing polymers. Through the understanding of different factors affecting the spectroscopic properties and FRET processes of the platinum(II)-containing polymers, it is envisaged that the present study can provide further insights into the design and development of metal-containing polymers for the construction of different functional materials.

EXPERIMENTAL

Syntheses of conjugated polymers and complexes 1-5

The synthetic routes for platinum (II) precursor and reference complex are depicted in Supplementary Scheme 1. Alkynylplatinum (II) terpyridine precursor **1** for "click" reaction was prepared based on a modified procedure of copper(I)-catalyzed dehalogenation reaction (pp 9, Supplementary Materials)[50]. The alkynylplatinum (II) terpyridine reference complex **2** was obtained through copper(I)-catalyzed alkyne-azide cycloaddition ("click" reaction) by reacting **1**, 1-azidohexane, CuBr, PMDETA and sodium ascorbate in a saturated solution of ammonium triflate in DMF (pp S10, Supplementary Materials). **1** and **2** were obtained as orange and red solid, respectively. These complexes are found to be highly soluble in organic solvents such as dichloromethane, chloroform, acetone, methanol, THF, and others.

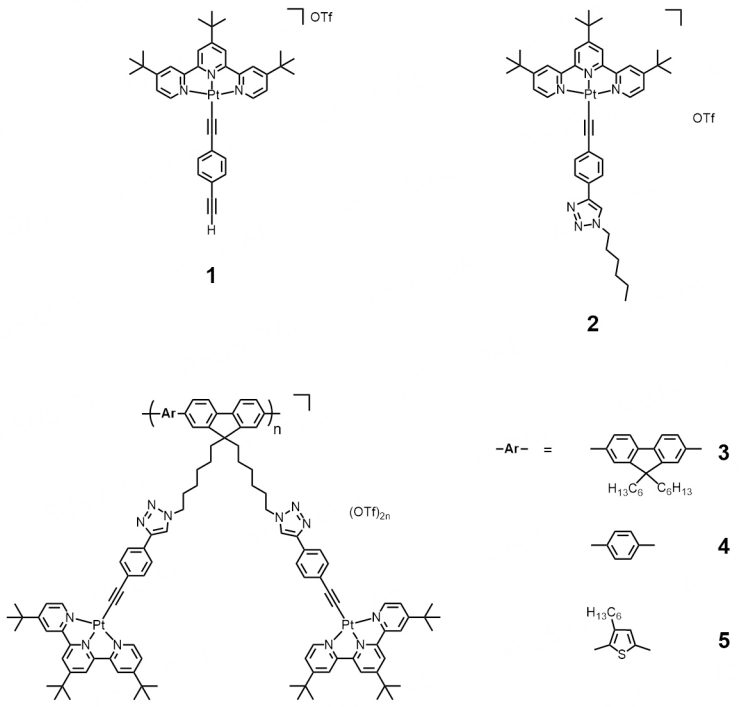

Scheme 1. Molecular structures of the platinum(II) complexes (**1** and **2**) and the platinum(II)-containing conjugated polymers (**3**-**5**).

The synthetic routes for the conjugated polymers are depicted in Supplementary Scheme 2. Detailed syntheses of the bromo-containing conjugated polymers, poly[fluorene($C_6H_{12}Br$)$_2$-*co*-fluorene(C_6H_{13})$_2$] (**PF-Br**), poly[fluorene($C_6H_{12}Br$)$_2$-*co*-phenylene](**PFP-Br**) and poly[fluorene($C_6H_{12}Br$)$_2$-*co*-thiophene(C_6H_{13})] (**PFT-Br**), and the corresponding azido-containing conjugated polymers (**PF-N$_3$**, **PFP-N$_3$** and **PFT-N$_3$**) are shown in pp S11-S14, Supplementary Materials. All the organic conjugated polymers were found to have good solubility in organic solvents such as chlorinated solvents, toluene, THF, and others. The identities of all of the organic conjugated polymers have been confirmed by ^{1}H NMR spectroscopy and GPC analysis.

The synthetic routes for the platinum(II)-containing conjugated polymers are depicted in Supplementary Scheme 3. The platinum(II)-containing conjugated polymers **3**-**5** were also obtained through copper(I)-catalyzed alkyne-azide cycloaddition of the corresponding azido-containing conjugated polymers and **1** in THF-DMF mixture in the presence of ammonium triflate (pp S15-S17, Supplementary Materials). The products were purified by precipitation in deionized water containing ammonium triflate. The platinum(II)-containing conjugated polymers were found to have fair solubility in acetonitrile, DMF and DMSO. Their limited solubility in methanol and THF has facilitated the purification by washing the precipitate with methanol and THF to further remove any unreacted starting materials.

Characterization

All the newly synthesized platinum(II) complexes **1** and **2** and platinum(II)-containing polymers **3**-**5** have been characterized by ^{1}H NMR and IR spectroscopy. In addition, **1** and **2** were also confirmed by positive-ion FAB mass spectrometry and showed satisfactory results in the elemental analyses. **3**-**5** were also confirmed by GPC analysis using DMF with 0.1 M KPF_6 as eluent. Representative GPC data of **5** is provided in Supplementary Figure 1.

From the IR measurements of **3-5** [Supplementary Figures 2-4], the disappearance of the strong absorption of the N=N=N stretch of the azide precursor at *ca.* 2095 cm^{-1}, the appearance of weak absorption of the C≡C stretch at 2110 cm^{-1} and strong absorption of the triflate counter-ion at *ca.* 1155 and 1030 cm^{-1} indicated the successful incorporation of the platinum(II) complexes onto the polymer *via* "click" reaction.

RESULTS AND DISCUSSION

The polymers, **PF-Br**, **PFP-Br** and **PFT-Br**, are soluble in dichloromethane and give high-energy absorption bands with a peak maxima at *ca.* 375-398 nm [Supplementary Figure 5 and Supplementary Table 1], which are assigned as the π→π* transitions along the polymer backbone, while these polymers show strong vibronic-structured emissions with peak maxima at *ca.* 410-462 nm upon photoexcitation [Supplementary Figures 6-9 and Supplementary Table 2], which are assigned as the singlet [π→π*] fluorescence of the conjugated polymer backbone.

For complexes **1-5**, they all give pale yellow solutions in acetonitrile. Their corresponding UV-vis absorption data and spectra in acetonitrile at 298 K are depicted in Table 1 and Figure 1, respectively. All the complexes exhibit intense absorption bands at *ca.* 285-341 nm with molar extinction coefficients in the order of 10^4 dm^3 mol^{-1} cm^{-1} and less intense low-energy absorption bands at *ca.* 420-466 nm with molar extinction coefficients in the order of 10^3 dm^3 mol^{-1} cm^{-1}. The higher-energy bands are ascribed to intraligand (IL) [π→π*] transitions of alkynyl and terpyridine ligands, while the lower-energy bands are assigned as an admixture of metal-to-ligand charge transfer (MLCT) [dπ(Pt)→π*(tpy)] and ligand-to-ligand charge transfer (LLCT) [π(alkynyl)→π*(tpy)] transitions. For the platinum(II)-containing conjugated polymers **3-5**, intense absorption bands at *ca.* 374-409 nm have been observed. With reference to the previous studies on the conjugated polymers[51-54] and the UV-vis absorption studies of the corresponding organic polymers [Supplementary Figure 5], these absorptions are tentatively assigned as the IL [π→π*] transitions of the polymer backbones. Interestingly, the lower-energy bands of **3-5** are extended to longer wavelengths when compared to the reference complex **2**. Since the molecular structures of the platinum(II) pendants in **3-5** are the same as that in **2**, the further red-shifted absorption tails suggest the existence of metal-metal-to-ligand charge transfer (MMLCT) character. As such, concentration-dependent UV-vis absorption studies have been performed. Based on the spectra [Supplementary Figures 10-14], the precursor platinum(II) complexes **1** and **2** and the platinum(II)-containing conjugated polymers **3-5** show good agreement with Beer's Law, suggesting that there are no significant intermolecular self-assembly properties of **1-5** upon increasing the concentration. However, the intramolecular self-assembly mode of having two platinum(II) pendants in each repeating unit, which are stabilized by the presence of intramolecular Pt···Pt and π-π interactions, may explain the presence of low-energy MMLCT bands for the platinum(II)-containing conjugated polymers **3-5**. In this regard, temperature-dependent UV-vis absorption experiments for **3-5** have been carried out. From the spectra [Figures 2-4], the low-energy band at *ca.* 450 nm shows a drop in absorbance accompanied by a blue shift of the high-energy band at *ca.* 400 nm upon increasing temperature, suggesting the occurrence of deaggregation process of both the platinum(II) terpyridine moieties and the polymer backbones, which corroborates with the disruption of intramolecular Pt···Pt and π-π interactions at high temperatures.

Complexes **1** and **2** are found to give phosphorescence in degassed solutions, while dual-emissive behaviors have been observed for the platinum(II)-containing conjugated polymers **3-5** in degassed solutions upon excitation. The luminescence data of all complexes have been summarized in Table 2. Upon photoexcitation at λ > 350 nm, **1** and **2** show Gaussian-shape emission bands centered at 596 nm and 630 nm in degassed acetonitrile [Supplementary Figure 15]. The large Stokes shifts and the long emission lifetimes in the microsecond regime indicate that these emissions are originated from a triplet parentage. Together with the

Table 1. UV-Vis absorption data for 1-5 at 298 K

Complex	Medium	Absorption λ/nm (ε/dm^3 mol^{-1} cm^{-1})
[Pt(^{t}Bu$_3$tpy)(C≡CC$_6$H$_4$C≡CH)]OTf (**1**)	CH_3CN	285 (52,030), 322 (18,620), 338 (19,130), 420 (6,660)
[Pt(^{t}Bu$_3$tpy)(C≡CC$_6$H$_4$C$_2$HN$_3$C$_6$H$_{13}$)]OTf (**2**)	CH_3CN	287 (49,290), 305 sh (35,150), 324 sh (16,330), 338 (15,980), 401 sh (15,980), 434 (5,560)
[PF-{N$_3$C$_2$H-C$_6$H$_4$C≡CPt(^{t}Bu$_3$tpy)}$_2$](OTf)$_{2n}$ (**3**)[a]	CH_3CN	288 (71,290), 308 sh (55,900), 341 (37,020), 383 (48,560), 445 sh (8,010)
[PFP-{N$_3$C$_2$H-C$_6$H$_4$C≡CPt(^{t}Bu$_3$tpy)}$_2$](OTf)$_{2n}$ (**4**)[a]	CH_3CN	287 (69,780), 308 sh (57,730), 341 (38,350), 374 (41,140), 451 sh (8,190)
[PFT-{N$_3$C$_2$H-C$_6$H$_4$C≡CPt(^{t}Bu$_3$tpy)}$_2$](OTf)$_{2n}$ (**5**)[a]	CH_3CN	289 (64,250), 308 sh (50,700), 340 sh (25,560), 409 (33,250), 466 sh (8,320)

[a]The molar extinction coefficients of the metallopolymers were approximated per repeating unit.

Table 2. Emission data for 1-5

Complex	Medium (T/K)	λ_{em}/nm (τ_o/μs)	Φ_{lum}[a]
[Pt(^{t}Bu$_3$tpy)(C≡CC$_6$H$_4$C≡CH)]OTf (**1**)	CH_3CN (298)	596 (1.09)	5.0 × 10^{-2b}
[Pt(^{t}Bu$_3$tpy)(C≡CC$_6$H$_4$-C$_2$HN$_3$C$_6$H$_{13}$)]OTf (**2**)	CH_3CN (298)	630 (0.14)	8.5 × 10^{-3b}
[PF-{N$_3$C$_2$H-C$_6$H$_4$C≡C-Pt(^{t}Bu$_3$tpy)}$_2$](OTf)$_{2n}$ (**3**)	CH_3CN (298)	416[c] (< 0.1), 671 (0.14)	1.2 × 10^{-3d} 2.6 × 10^{-3b}
[PFP-{N$_3$C$_2$H-C$_6$H$_4$C≡C-Pt(^{t}Bu$_3$tpy)}$_2$](OTf)$_{2n}$ (**4**)	CH_3CN (298)	417[c] (< 0.1), 673 (0.70)	9.0 × 10^{-4d} 1.4 × 10^{-2b}
[PFT-{N$_3$C$_2$H-C$_6$H$_4$C≡C-Pt(^{t}Bu$_3$tpy)}$_2$](OTf)$_{2n}$ (**5**)	CH_3CN (298)	465[c] (< 0.1), 673 (0.66)	8.4 × 10^{-4d} 1.7 × 10^{-3b}

[a]Data obtained with an uncertainty of 10 %; [b]the relative luminescence quantum yields were measured at room temperature using [Ru(bpy)$_3$]Cl$_2$ in degassed acetonitrile as a standard; [c]vibronic-structured band with vibrational progressional spacings of *ca.* 1150-1320 cm^{-1}; [d]the relative luminescence quantum yields were measured at room temperature using quinine sulfate in 0.5 M H_2SO_4 as a standard.

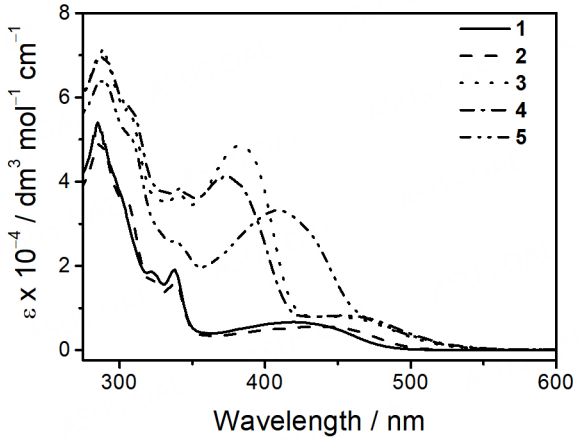

Figure 1. UV-Vis absorption spectra of **1-5** in acetonitrile at 298 K.

relatively short photoluminescence lifetimes in the range of 1 ms or lower, these emission bands are assigned to be originated from admixtures of ^{3}MLCT [dπ(Pt)→π(tpy)] and ^{3}LLCT [π(alkynyl)→π*(tpy)] excited states. On the other hand, platinum(II)-containing conjugated polymers **3-5** exhibit dual-emissive behaviors upon excitation [Figure 5]. The high-energy emission bands are vibronic-structured with emission maxima at *ca.* 416-465 nm, while the low-energy emissions are of Gaussian shape and centered at *ca.* 672 nm. Based on the previous studies[51-54] and the corresponding emission measurements of the organic

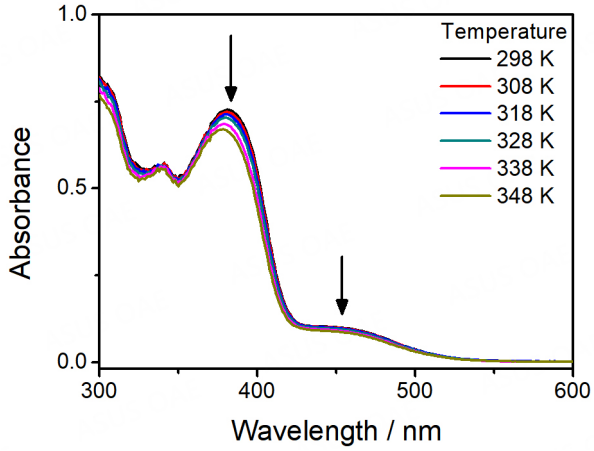

Figure 2. UV-Vis absorption spectral changes of [PF-{N_3C_2H-$C_6H_4C{\equiv}CPt(^tBu_3tpy)$}$_2$](OTf)$_{2n}$ (**3**) in acetonitrile with increasing temperature.

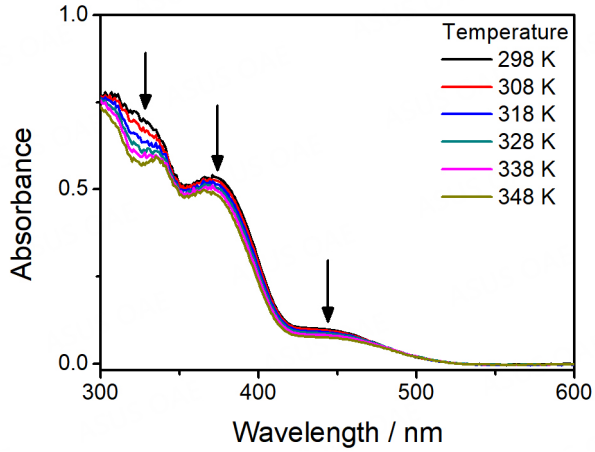

Figure 3. UV-Vis absorption spectral changes of [PFP-{N_3C_2H-$C_6H_4C{\equiv}CPt(^tBu_3tpy)$}$_2$](OTf)$_{2n}$ (**4**) in acetonitrile with increasing temperature.

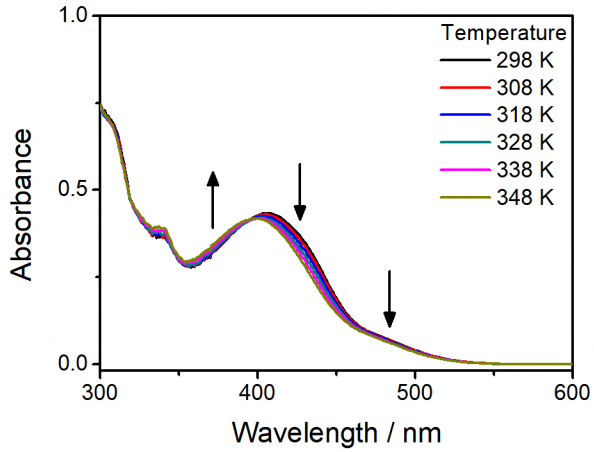

Figure 4. UV-Vis absorption spectral changes of [PFT-{N_3C_2H-$C_6H_4C{\equiv}CPt(^tBu_3tpy)$}$_2$](OTf)$_{2n}$ (**5**) in acetonitrile with increasing temperature.

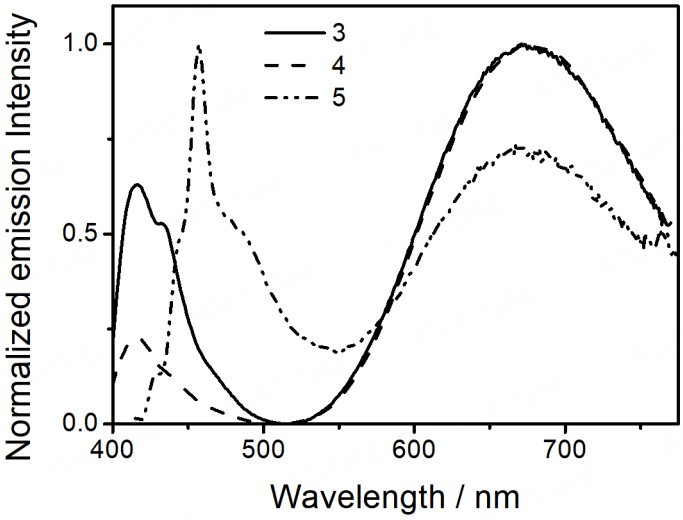

Figure 5. Normalized emission spectra of **3-5** in degassed acetonitrile at 298 K.

conjugated polymers, the high-energy emissions are ascribed to the singlet [$\pi\rightarrow\pi^*$] excited state of the polymer backbone, while the low-energy emissions of **3-5** are tentatively assigned to be originated from the ^{3}MMLCT excited states. To further validate the ^{3}MMLCT origin of these low-energy emissions, temperature-dependent emission studies have been performed [Supplementary Figures 16-18]. As a result, **3-5** exhibit a decrease in intensity of the low-energy emissions with significant blue shifts upon increasing temperature.

On the other hand, distinctive thermo-responsive emission changes have also been observed for the platinum(II)-containing conjugated polymers **3-5**. Upon increasing the temperature of the solution of **3**, the high-energy emission from the polymer backbone is found to increase in intensity [Figure 6]. The reason behind this can be attributed to the decrease in FRET efficiency from the polymer backbone to the platinum(II) moieties. From the variable-temperature UV-vis absorption spectral traces of **3** [Figure 2], there is a decrease in absorbance of the MMLCT band upon increasing temperature, leading to a decrease in the spectral overlap and the enhanced recovery of the polymer fluorescence [Figure 6]. Moreover, **4** is found to exhibit the largest recovery of the high-energy emission when compared to others upon increasing temperature, as shown in Figure 7. Since **4** bears the least number of alkyl chains in each repeating unit, it is believed that the energy would be less effectively dissipated through non-radiative decay pathways. As a result, the FRET process dominates in **4**, resulting in the greatest recovery of the polymer backbone emission. Furthermore, both emission bands of **5** are found to be diminished with increasing temperature [Figure 8], which can be attributed to the more dominating non-radiative process when compared to the recovery of the fluorescence of the polymer backbone. The corresponding ratiometric emission intensity plots of **3-5** have been depicted in Figure 9.

Due to the good spectral overlap between the absorption spectrum of the reference complex **2** and the emission spectra of the conjugated polymers (**PF-Br**, **PFP-Br** and **PFT-Br**) [Figure 10], it is believed that the intramolecular FRET process from the polymer backbone to the platinum(II) pendant would likely occur upon photoexcitation. Although the emissions from the conjugated polymer backbones could still be observed for **3-5**, they are already effectively quenched when compared to their corresponding organic polymers (Φ_{lum} of **PF-Br**, **PFP-Br** and **PFT-Br** = 0.45-0.92; Φ_{lum} of **3-5** = 8.4×10^{-4}-1.2×10^{-3}). It is worth noting that different extents of quenching efficiencies have been observed for **3-5**. For example, the emission

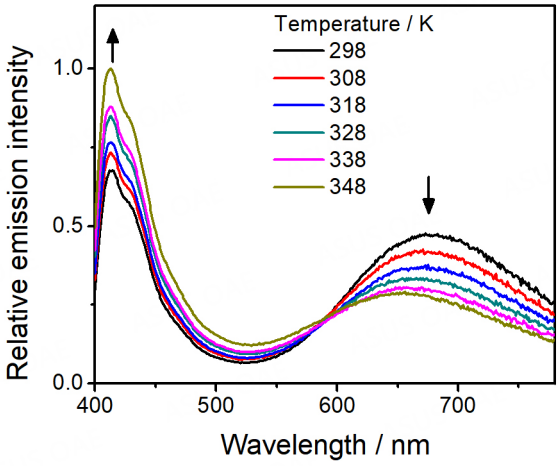

Figure 6. Emission spectra of [PF-{N_3C_2H-$C_6H_4C{\equiv}CPt(^tBu_3tpy)\}_2$](OTf)$_{2n}$ (**3**) in acetonitrile with increasing temperature.

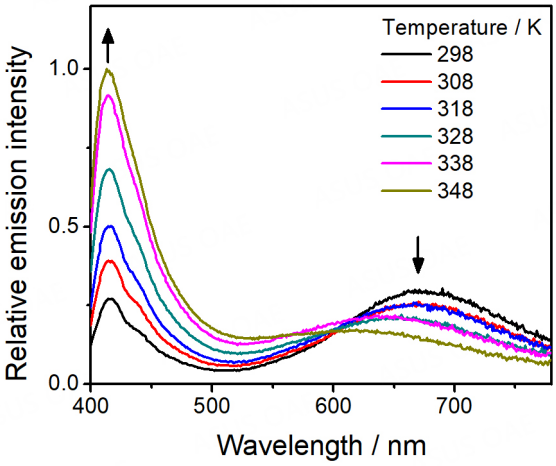

Figure 7. Emission spectra of [PFP-{N_3C_2H-$C_6H_4C{\equiv}CPt(^tBu_3tpy)\}_2$](OTf)$_{2n}$ (**4**) in acetonitrile with increasing temperature.

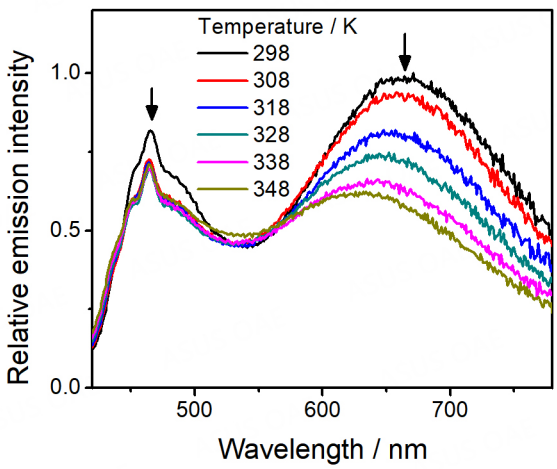

Figure 8. Emission spectra of [PFT-{N_3C_2H-$C_6H_4C{\equiv}CPt(^tBu_3tpy)\}_2$](OTf)$_{2n}$ (**5**) in acetonitrile with increasing temperature.

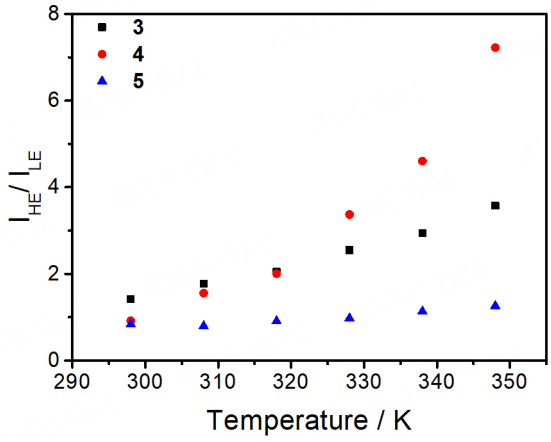

Figure 9. Ratiometric emission intensity plots of the high-energy (HE) and low-energy (LE) bands of **3**-**5** in acetonitrile with increasing temperature. I_{HE}/I_{LE} of **3** = I_{413nm}/I_{673nm}; I_{HE}/I_{LE} of **4** = I_{413nm}/I_{673nm}; I_{HE}/I_{LE} of **5** = I_{465nm}/I_{673nm}.

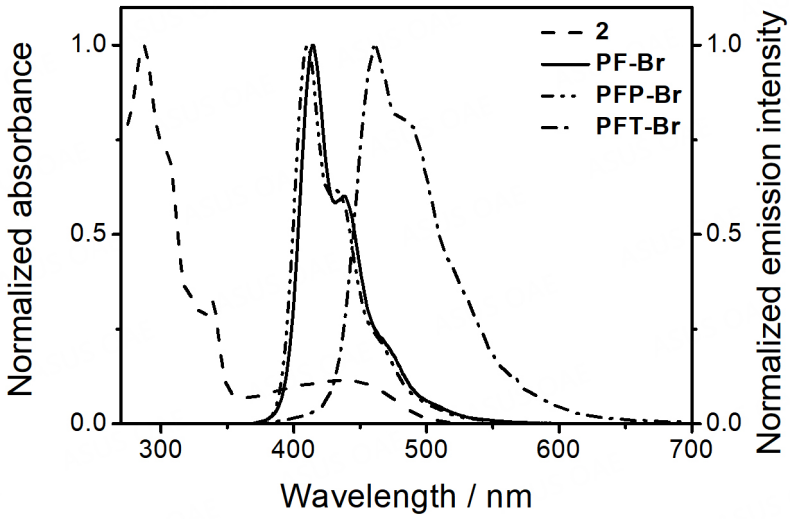

Figure 10. Normalized UV-vis absorption of [Pt(^{t}Bu$_3$tpy)(C≡CC$_6$H$_4$-C$_2$HN$_3$C$_6$H$_{13}$)]OTf (**2**) and emission spectra of **PF-Br**, **PFP-Br** and **PFT-Br** showing the spectral overlap between the emission spectra of the polymer energy donors and the UV-vis absorption spectrum of the platinum(II) complex **2** energy acceptor.

from the polymer backbone of **5** is found to be less effectively quenched when compared to that of **3** and **4**. The related parameters have been obtained and are summarized in Table 3. Since the platinum(II)-containing conjugated polymers **3**-**5** share similar molecular structures except for the polymer backbone, it is believed that the values of the relative orientation of the transition dipoles of the chromophores (κ) and the distance between the donor and the acceptor (r) should be almost the same. Therefore, the FRET efficiency is mainly governed by the emission quantum yield of the donor (Φ_D) and the spectral overlap integral of the absorption spectrum of the acceptor and emission spectrum of the donor ($J(\lambda)$), which are related to the Förster radius (R_0). It is found that the calculated R_0 value of **5** is the lowest, indicating that the FRET in **5** should be the least efficient, as reflected by the smallest decrease in emission quantum yield of the polymer backbone.

Table 3. Parameters obtained from the equation determining the Förster radius, R_0[a] of 3-5

Acceptor	Donor	Φ_D[b,c]	R_0/nm	Pt(II)-Polymer	Φ_{lum}[b,c,d]	Φ_{lum}/Φ_D
2	**PF-Br**	0.92	4.9	**3**	1.2×10^{-3}	1.30×10^{-3}
2	**PFP-Br**	0.90	4.9	**4**	9.0×10^{-4}	1.00×10^{-3}
2	**PFT-Br**	0.45	4.5	**5**	8.4×10^{-4}	1.87×10^{-3}

[a]$R_0 = 0.211[\kappa^2 n^{-4} \Phi_D J(\lambda)]^{1/6}$; [b]data obtained with an uncertainty of 10 %; [c]the relative luminescence quantum yields were measured at room temperature using quinine sulfate in 0.5 M H_2SO_4 as a standard; [d]the luminescence quantum yields of the polymer backbone.

CONCLUSION

Alkynylplatinum(II) terpyridine complexes (**1** and **2**) and alkynylplatinum(II) terpyridine-containing conjugated polymers with different polymer backbones (**3**-**5**) have been prepared, and their spectroscopic properties as well as FRET processes have been studied. The platinum(II)-containing polymers **3**-**5** are found to exhibit dual emissive features, in which the two emission bands correspond to ^{1}IL fluorescence from the polymer backbones and ^{3}MMLCT emissions from the platinum(II) pendants. Such unique luminescence behavior is attributed to the intramolecular Pt···Pt and/or π-π interactions between the platinum(II) pendants in the polymer molecules. The FRET processes between the conjugated polymer backbones and platinum(II) pendants have been studied systemically. It is found that **5** has the lowest Förster radii (R_0) among others, probably due to the lowest emission quantum yield of poly(fluorene-*co*-thiophene). Distinctive thermo-responsive ratiometric emission changes have been observed for **3** and **4**, in which an increase in intensity of the high-energy ^{1}IL emission originated from the polymer backbones and a decrease in intensity of the low-energy ^{3}MMLCT emission are found upon heating. The present work has demonstrated the utilization of "click" reaction for the convenient preparation of platinum(II)-containing conjugated polymers, which show unique photophysical and spectroscopic properties. Through the judicious design, ratiometric emission changes upon varying temperatures have been realized in this class of platinum(II)-containing polymers. This study may provide valuable insights into the preparation of metal-containing polymeric systems for different applications, such as thermochromic materials. Owing to the ease of structural modifications, various kinds of polymeric materials could be potentially fabricated, which could serve as thermochromic sensors for monitoring temperature in real time.

DECLARATIONS

Authors' contributions

Conducted the synthesis, characterization and photophysical measurements, analyzed the data and prepared the manuscript: Cheng HK

Initiated and designed the research, analyzed the data and prepared the manuscript: Yam VWW

Availability of data and materials

Not applicable.

Financial support and sponsorship

This work was supported by the Collaborative Research Fund (CRF) (C7075-21G) and the General Research Fund (GRF) from the Research Grants Council of the Hong Kong Special Administrative Region, People's Republic of China (HKU17303421), and the CAS-Croucher Funding Scheme for Joint Laboratory on Molecular Functional Materials for Electronics, Switching and Sensing. H.-K.C. acknowledges the receipt of a Postgraduate Studentship.

Conflicts of interest

All authors declared that there are no conflicts of interest.

Ethical approval and consent to participate

Not applicable.

Consent for publication

Not applicable.

REFERENCES

1. Burroughes JH, Bradley DDC, Brown AR, et al. Light-emitting diodes based on conjugated polymers. *Nature* 1990;347:539-41. DOI
2. Mcneill R, Siudak R, Wardlaw J, Weiss D. Electronic conduction in polymers. I. The chemical structure of polypyrrole. *Aust J Chem* 1963;16:1056-75. DOI
3. Bolto B, Weiss D. Electronic conduction in polymers. II. The electrochemical reduction of polypyrrole at controlled potential. *Aust J Chem* 1963;16:1076-89. DOI
4. Bolto B, Mcneill R, Weiss D. Electronic conduction in polymers. III. Electronic properties of polypyrrole. *Aust J Chem* 1963;16:1090-103. DOI
5. Mccullough RD. The chemistry of conducting polythiophenes. *Adv Mater* 1998;10:93-116. DOI
6. Sirringhaus H, Tessler N, Friend RH. Integrated optoelectronic devices based on conjugated polymers. *Science* 1998;280:1741-4. DOI PubMed
7. Ago H, Petritsch K, Shaffer MSP, Windle AH, Friend RH. Composites of carbon nanotubes and conjugated polymers for photovoltaic devices. *Adv Mater* 1999;11:1281-5. DOI
8. Friend RH, Gymer RW, Holmes AB, et al. Electroluminescence in conjugated polymers. *Nature* 1999;397:121-8. DOI
9. Sirringhaus H, Brown PJ, Friend RH, et al. Two-dimensional charge transport in self-organized, high-mobility conjugated polymers. *Nature* 1999;401:685-8. DOI
10. Mcgehee MD, Heeger AJ. Semiconducting (conjugated) polymers as materials for solid-state lasers. *Adv Mater* 2000;12:1655-68. DOI
11. Thomas SW 3rd, Joly GD, Swager TM. Chemical sensors based on amplifying fluorescent conjugated polymers. *Chem Rev* 2007;107:1339-86. DOI PubMed
12. Ho CL, Wong WY. Metal-containing polymers: facile tuning of photophysical traits and emerging applications in organic electronics and photonics. *Coord Chem Rev* 2011;255:2469-502. DOI
13. Gracia R, Mecerreyes D. Polymers with redox properties: materials for batteries, biosensors and more. *Polym Chem* 2013;4:2206. DOI
14. Liu S, Zhang K, Lu J, et al. High-efficiency polymer solar cells via the incorporation of an amino-functionalized conjugated metallopolymer as a cathode interlayer. *J Am Chem Soc* 2013;135:15326-9. DOI PubMed
15. Du M, Li C, Liu C, Fang S. Design and construction of coordination polymers with mixed-ligand synthetic strategy. *Coord Chem Rev* 2013;257:1282-305. DOI
16. Xu H, Chen R, Sun Q, et al. Recent progress in metal-organic complexes for optoelectronic applications. *Chem Soc Rev* 2014;43:3259-302. DOI PubMed
17. Winter A, Schubert US. Synthesis and characterization of metallo-supramolecular polymers. *Chem Soc Rev* 2016;45:5311-57. DOI PubMed
18. Ho CL, Yu ZQ, Wong WY. Multifunctional polymetallaynes: properties, functions and applications. *Chem Soc Rev* 2016;45:5264-95. DOI PubMed
19. Götz S, Zechel S, Hager MD, Newkome GR, Schubert US. Versatile applications of metallopolymers. *Prog Polym Sci* 2021;119:101428. DOI
20. Yu SC, Gong X, Chan WK. Synthesis and characterization of poly(benzobisoxazole)s and poly(benzobisthiazole)s with 2,2'-bipyridyl units in the backbone. *Macromolecules* 1998;31:5639-46. DOI
21. Chen X, Liao JL, Liang Y, Ahmed MO, Tseng HE, Chen SA. High-efficiency red-light emission from polyfluorenes grafted with cyclometalated iridium complexes and charge transport moiety. *J Am Chem Soc* 2003;125:636-7. DOI PubMed
22. Yam VWW, Wong KMC, Zhu N. Solvent-induced aggregation through metal···metal/π···π interactions: large solvatochromism of luminescent organoplatinum(II) terpyridyl complexes. *J Am Chem Soc* 2002;124:6506-7. DOI PubMed
23. Yam VWW, Chan KHY, Wong KMC, Zhu N. Luminescent platinum(II) terpyridyl complexes: effect of counter ions on solvent-induced aggregation and color changes. *Chem Eur J* 2005;11:4535-43. DOI PubMed

24. Yu C, Wong KMC, Chan KHY, Yam VWW. Polymer-induced self-assembly of alkynylplatinum(II) terpyridyl complexes by metal···metal/π···π interactions. *Angew Chem Int Ed* 2005;44:791-4. DOI PubMed
25. Yu C, Chan KHY, Wong KMC, Yam VWW. Single-stranded nucleic acid-induced helical self-assembly of alkynylplatinum(II) terpyridyl complexes. *Proc Natl Acad Sci USA* 2006;103:19652-7. DOI PubMed PMC
26. Leung SYL, Lam WH, Yam VWW. Dynamic scaffold of chiral binaphthol derivatives with the alkynylplatinum(II) terpyridine moiety. *Proc Natl Acad Sci USA* 2013;110:7986-91. DOI PubMed PMC
27. Wong KMC, Yam VWW. Luminescence platinum(II) terpyridyl complexes - From fundamental studies to sensory functions. *Coord Chem Rev* 2007;251:2477-88. DOI
28. Po C, Tam AYY, Wong KMC, Yam VWW. Supramolecular self-assembly of amphiphilic anionic platinum(II) complexes: a correlation between spectroscopic and morphological properties. *J Am Chem Soc* 2011;133:12136-43. DOI PubMed
29. Wong KMC, Yam VWW. Self-assembly of luminescent alkynylplatinum(II) terpyridyl complexes: modulation of photophysical properties through aggregation behavior. *Acc Chem Res* 2011;44:424-34. DOI PubMed
30. Cheung ASH, Leung SYL, Hau FKW, Yam VWW. Supramolecular self-assembly of amphiphilic alkynylplatinum(II) 2,6-bis(N-alkylbenzimidazol-2'-yl)pyridine complexes. *Chem Res Chin Univ* 2021;37:1079-84. DOI
31. Zheng X, Chan MHY, Chan AKW, et al. Elucidation of the key role of Pt···Pt interactions in the directional self-assembly of platinum(II) complexes. *Proc Natl Acad Sci USA* 2022;119:e2116543119. DOI PubMed PMC
32. Tam AYY, Wong KMC, Yam VWW. Unusual luminescence enhancement of metallogels of alkynylplatinum(II) 2,6-bis(N-alkylbenzimidazol-2'-yl)pyridine complexes upon a gel-to-sol phase transition at elevated temperatures. *J Am Chem Soc* 2009;131:6253-60. DOI
33. Yam VWW, Au VKM, Leung SYL. Light-emitting self-assembled materials based on d^8 and d^{10} transition metal complexes. *Chem Rev* 2015;115:7589-728. DOI PubMed
34. Yam VWW, Chan AKW, Hong EYH. Charge-transfer processes in metal complexes enable luminescence and memory functions. *Nat Rev Chem* 2020;4:528-41. DOI
35. Chan MHY, Yam VWW. Toward the design and construction of supramolecular functional molecular materials based on metal-metal interactions. *J Am Chem Soc* 2022;144:22805-25. DOI PubMed
36. Chan K, Chung CYS, Yam VWW. Conjugated polyelectrolyte-induced self-assembly of alkynylplatinum(II) 2,6-bis(benzimidazol-2'-yl)pyridine complexes. *Chem Eur J* 2015;21:16434-47. DOI PubMed
37. Chan K, Chung CYS, Yam VWW. Parallel folding topology-selective label-free detection and monitoring of conformational and topological changes of different G-quadruplex DNAs by emission spectral changes via FRET of mPPE-Ala-Pt(II) complex ensemble. *Chem Sci* 2016;7:2842-55. DOI PubMed PMC
38. Chan CWT, Chan K, Yam VWW. Induced self-assembly and disassembly of alkynylplatinum(II) 2,6-bis(benzimidazol-2'-yl)pyridine complexes with charge reversal properties: "proof-of-principle" demonstration of ratiometric förster resonance energy transfer sensing of pH. *ACS Appl Mater Interfaces* 2022;Online ahead of print. DOI PubMed
39. Sonogashira K, Takahashi S, Hagihara N. A new extended chain polymer, poly[trans-bis(tri-*n*-butylphosphine)platinum 1,4-butadiynediyl]. *Macromolecules* 1977;10:879-80. DOI
40. Takahashi S, Kariya M, Yatake T, Sonogashira K, Hagihara N. Studies of poly-yne polymers containing transition metals in the main chain. 2. Synthesis of poly[trans-bis(tri-*n*-butylphosphine)platinum 1,4-butadiynediyl] and evidence of a rodlike structure. *Macromolecules* 1978;11:1063-6. DOI
41. Beljonne D, Wittmann HF, Köhler A, et al. Spatial extent of the singlet and triplet excitons in transition metal-containing poly-ynes. *J Chem Phys* 1996;105:3868-77. DOI
42. Younus M, Köhler A, Cron S, et al. Synthesis, electrochemistry, and spectroscopy of blue platinum(II) polyynes and diynes. *Angew Chem Int Ed Engl* 1998;37:3036-9. DOI PubMed
43. Chawdhury N, Köhler A, Friend RH, et al. Evolution of lowest singlet and triplet excited states with number of thienyl rings in platinum poly-ynes. *J Chem Phys* 1999;110:4963-70. DOI
44. Rogers JE, Cooper TM, Fleitz PA, Glass DJ, Mclean DG. Photophysical characterization of a series of platinum(II)-containing phenyl−ethynyl oligomers. *J Phys Chem A* 2002;106:10108-15. DOI
45. Liu Y, Jiang S, Glusac K, Powell DH, Anderson DF, Schanze KS. Photophysics of monodisperse platinum-acetylide oligomers: delocalization in the singlet and triplet excited states. *J Am Chem Soc* 2002;124:12412-3. DOI PubMed
46. Schanze KS, Silverman EE, Zhao X. Intrachain triplet energy transfer in platinum-acetylide copolymers. *J Phys Chem B* 2005;109:18451-9. DOI PubMed
47. Clem TA, Kavulak DFJ, Westling EJ, Fréchet JMJ. Cyclometalated platinum polymers: synthesis, photophysical properties, and photovoltaic performance. *Chem Mater* 2010;22:1977-87. DOI
48. Thomas III SW, Yagi S, Swager TM. Towards chemosensing phosphorescent conjugated polymers: cyclometalated platinum(II) poly(phenylene)s. *J Mater Chem* 2005;15:2829. DOI
49. Wang P, Liu S, Lin Z, et al. Design and synthesis of conjugated polymers containing Pt(II) complexes in the side-chain and their application in polymer memory devices. *J Mater Chem* 2012;22:9576. DOI
50. Lu W, Law YC, Han J, et al. A dicationic organoplatinum(II) complex containing a bridging 2,5-bis-(4-ethynylphenyl)-[1,3,4]oxadiazole ligand behaves as a phosphorescent gelator for organic solvents. *Chem Asian J* 2008;3:59-69. DOI PubMed
51. Liu B, Yu W, Lai Y, Huang W. Blue-light-emitting fluorene-based polymers with tunable electronic properties. *Chem Mater*

2001;13:1984-91. DOI

52. Vamvounis G, Schulz GL, Holdcroft S. Enhanced blue-violet emission from poly(fluorene-*co*-thiophene) host-guest systems. *Macromolecules* 2004;37:8897-902. DOI
53. Grell M, Bradley DDC, Ungar G, Hill J, Whitehead KS. Interplay of physical structure and photophysics for a liquid crystalline polyfluorene. *Macromolecules* 1999;32:5810-7. DOI
54. Lim E, Jung B, Shim H. Synthesis and characterization of a new light-emitting fluorene-thieno[3,2-*b*]thiophene-based conjugated copolymer. *Macromolecules* 2003;36:4288-93. DOI

Dang *et al. Chem Synth* 2023;3:14
DOI: 10.20517/cs.2022.33

Chemical Synthesis

Review

Open Access

Selenium nanomaterials enabled flexible and wearable electronics

Chao Dang[1], Mingyang Liu[1], Zhiwei Lin[1], Wei Yan[1,2,3,*]

[1]School of Electrical and Electronic Engineering, Nanyang Technological University, Singapore 639798, Singapore.
[2]School of Materials Science and Engineering, Nanyang Technological University, Singapore 639798, Singapore.
[3]State Key Laboratory for Modification of Chemical Fibers and Polymer Materials, College of Materials Science and Engineering, Donghua University, Shanghai 201620, China.

***Correspondence to:** Prof./Dr. Wei Yan, School of Electrical and Electronic Engineering, Nanyang Technological University, 50 Nanyang Avenue, Singapore 639798, Singapore. E-mail: wei.yan@ntu.edu.sg

How to cite this article: Dang C, Liu M, Lin Z, Yan W. Selenium nanomaterials enabled flexible and wearable electronics. *Chem Synth* 2023;3:14. https://dx.doi.org/10.20517/cs.2022.33

Received: 23 Oct 2022 **First Decision:** 26 Dec 2022 **Revised:** 2 Feb 2023 **Accepted:** 7 Mar 2023 **Published:** 20 Mar 2023

Academic Editors: Aicheng Chen, Bao-Lian Su **Copy Editor:** Ying Han **Production Editor:** Ying Han

Abstract

Selenium (Se), as an intriguing chalcogenide semiconductor, has traditionally been used for solar energy harvesting. The recent development of nanoscience and nanotechnology has enabled a myriad of Se nanomaterials with compelling structures and unique features. Compared with other chalcogens, Se nanomaterials possess anisotropic crystalline structure, intrinsic chirality, and high reactivity, as well as unique optical, electrical, photoconductive, and piezoelectrical properties. The integration of these Se nanomaterials with technologically important materials, such as conductors and semiconductors, over flexible, bendable, stretchable, and highly curved substrates offer a new generation of Se nanomaterial-based flexible and wearable electronics. In this mini review, we survey the recent scientific and technological breakthroughs in Se nanomaterials-enabled flexible and wearable electronics. We highlight the synthesis, fabrication, morphologies, structure, and properties (optical, electrical, optoelectrical, photovoltaic, and piezoelectric) of Se nanomaterials as well as their integration into innovative functional devices that deliver higher forms of applications across smart sensing, health care, and energy domains. We conclude with a critical analysis of existing challenges and opportunities that will trigger the continued progress of the field.

Keywords: Selenium, Nanomaterials, Flexible electronics, Wearable electronics, Functional fibers

INTRODUCTION

Flexible and wearable electronics capable of continuous monitoring of physiological signals[1-5], minimally invasive interrogation of neural circuitry[6-10], and performing diagnostic and therapeutic treatment[11-15] are offering unprecedented value to society and our everyday lives[16-20]. Functional materials that are responsive to stimuli (such as photons[21-25], stress[26-30], and chemicals[31-34]) are the core part of flexible and wearable electronics[35-37]. The incorporation of semiconducting materials with excellent electrical and optical properties into flexible and wearable electronics enables innovative smart devices and systems with powerful potential in personalized healthcare, precision medical surgery and large-area energy harvesting and storage[38-40]. Selenium (Se) is a trace element of group VI with a direct bandgap at room temperature[41]. Due to its unique band structure and crystal structure, Se, in its bulky form, shows attractive optical, electrical, electronic and piezoelectric properties opening up interesting applications in photodetection and solar energy harvesting[42-44]. Compared with typical semiconductors in electronic industry (such as silicon and germanium) that require sophisticated micro- and nanofabrication conditions, Se can be physically, thermally or chemically processed in simple, low-cost and robust manners, which makes its integration with flexible and wearable electronics straightforward, thereby enabling versatile devices and applications[45,46].

Thanks to the remarkable progress in nanofabrication and nanotechnology, bulky Se can be scaled down to tunable nanostructures ranging from zero-dimensional (0D) nanoparticles to two-dimensional (2D) nanosheets. Benefiting from the "nano-size" effect, Se nanomaterials exhibit distinct physical and chemical properties that cannot be found in their bulky counterparts, featuring improved mechanical, electrical, thermal, optical and piezoelectric performance[47-49]. Compared with other functional semiconducting nanomaterials such as Si nanowires, Ge nanowires and ZnSe nanowires employed in flexible electronics[50], Se nanomaterials show the distinctive advantage of processability. They can be easily integrated with traditional conductors and semiconductors over the flexible, bendable, stretchable, and highly curved substrates to fabricate innovative functional devices in the form factors of two-dimensional large-area films and patches as well as one-dimensional indefinitely long fibers as we elaborated in the section of "APPLICATIONS OF SELENIUM NANOMATERIALS IN FLEXIBLE AND WEARABLE ELECTRONICS". This allows for the development of a new generation of Se nanomaterial-based flexible and wearable electronics. This mini review highlights the recent advances in Se nanomaterials enabled flexible and wearable electronics. We will first briefly review the typical morphologies and crystal structure of Se nanomaterials that directly determine their properties and subsequent applications. We will then present the synthesis and fabrication methodologies of Se nanostructures, namely the "bottom-up" and "top-down" strategies that have been widely exploited in the nanofabrication field. In the next section, we will discuss the physical properties of Se nanomaterials, focusing on optical, electrical, optoelectrical, photovoltaic, and piezoelectric behaviors that are of great importance for their functional applications in flexible and wearable electronics. Finally, we will discuss how Se nanomaterials can be integrated with substrates that are flexible, bendable, large-area and highly curved and how these innovative devices open up interesting opportunities in photosensing, mechanical deformation sensing, physiological sensing and energy storage. The review concludes with some key remaining challenges and perspectives that will be of value for future advances and breakthroughs in the field.

MORPHOLOGIES AND CRYSTAL STRUCTURES OF SELENIUM NANOMATERIALS

The morphologies, sizes and crystal structure of materials determine their properties and applications. We begin with a brief introduction to the morphologies and structure of Se nanomaterials.

Generally, nanostructured Se can be categorized into zero-dimensional (0D), one-dimensional (1D), and two-dimensional (2D) form factors, as shown by the microscopic images in Figure 1 and Table 1. 0D Se

Table 1. Summary of some representative synthesis methods, structures, properties, and applications of the Se nanomaterials

Se morphology	Crystal structures	Synthesis methods	Precursors	Reaction conditions	Properties	Applications	Refs.
0D nanoparticles	Hexagonal structure	Chemical reduction	Sodium selenite	Water, 2 ± 8 °C, 72 h	Anti hydroxyl radical property	Anti-oxidative stress drugs	[52]
0D nanoparticles	Hexagonal structure	Solvent-thermal method	Selenous acid	Ethanol and distilled water, 150 °C, 24 h	Fluorescence property	Fluorescence sensors	[64]
0D nanoparticles	Hexagonal structure	Laser-ablation method	Solide Se	Water, radiation wavelength of 1060 to 1070 nm, pulse repetition rate of 20 kHz, pulse duration of 80 ns	NA	Biological therapy	[65]
0D nanoparticles	Hexagonal structure	Ball Milling and heating	Se bulk	Ball milling, 72 h, heating, 260 °C, 20 h, argon gas atmosphere	Electrical/Electrochemical properties	Li-Se batteries	[104]
1D nanowires	Trigonal structure	Thermally-drawn assisted method	Se core	260 °C, air atmosphere	Optoelectrical property	Fluorescence imaging fibers	[39]
1D nanowires	Trigonal structure	Chemical reduction	SeO_2	Water, room temperature	Electrical property	Li-Se batteries	[53]
1D nanorods	Hexagonal structure	Microwave-polyol method	SeO_2	195 °C, 30 min, microwave heating	NA	NA	[54]
1D nanotubes	Trigonal structure	Hydrothermal method	Sodium selenite	Water, 100 °C, 25 h	NA	NA	[55]
1D nanobelts	Trigonal structure	Chemical reduction	Sodium selenite	Acid condition, 50 °C, 3 h	Optical property	Optical detector	[56]
1D nanowires	Trigonal structure	Self-seeding solution-phase method	Selenious acid	Ice water	Optical/Photoconductivity property	Electronic, optical or mechanical nanodevices	[68]
1D nanowires	Trigonal structure	Plasma-assisted selenization method	Se tank	300 °C, plasma, heating	Optoelectrical property	Flexible photodetectors	[69]
1D nanowire /nanotube	Trigonal structure	Thermally-drawn assisted method	Se rod	260 °C, 30 min	Photoconductivity property	Optoelectronic detectors	[70]
1D nanowires	Trigonal structure	Solvent-thermal method	SeO_2	Water and ethanol, 160 °C, 20 h	Piezoelectric property	Piezoelectric nanogenerators	[85]
1D nanobelts	Trigonal structure	Thermal evaporation method	Se powder	250 °C, 1 h, argon gas atmosphere	Electrical/ Photoconductivity property	Visible light photodetector	[94]
2D nanosheets	Trigonal structure	Physical vapor deposition method	Se powder	210 °C, 60 min argon atmosphere	Photoelectrical property	Phototransistors	[57]
2D nanolayers	Hexagonal structure	Chemical vapor transport synthesis	Se powder	Liquid phase, hydrogen and argon gas atmosphere	NA	NA	[71]
2D nanoflakes	Trigonal structure	Sonication liquid-phase exfoliation method	Bulk Se powder	IPA, 9 h, energy power of 600 W	Fluorescence property	Photoluminescence	[58]

nanomaterials include Se nanospheres and Se nanoparticles[51,52]. The synthesis method, surfactant or additive, reaction temperature, or reaction time influences their morphologies and properties. 1D Se nanomaterials have attracted lots of research interest recently because of their unique optical and electrical properties as well as potential employment in flexible electronics. A number of well-established techniques, mostly derived from "top-down" and "bottom-up" strategies, have been adopted to produce 1D nanostructures, including nanowires, nanorods, nanotubes, and nanobelts[53-56]. Compared with 1D metal nanomaterials, 1D Se nanomaterials show competitive advantages in terms of synthesis methodologies,

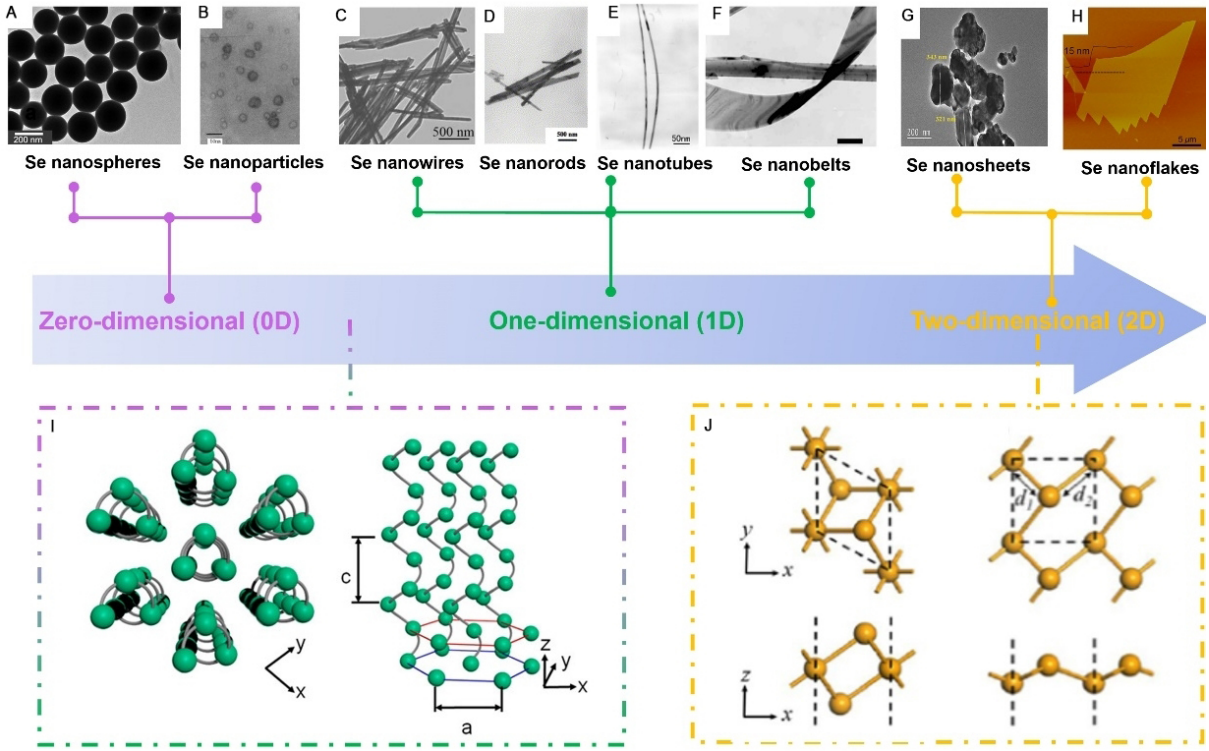

Figure 1. (A) TEM image of Se nanosphere[51]; Copyright 2014, Elsevier. (B) TEM image of Se nanoparticles[52]; Copyright 2002, Wiley-VCH. (C) TEM image of Se nanowires[53]; Copyright 2015, Elsevier. (D) TEM image of Se nanorods[54]; Copyright 2004, Elsevier. (E) SEM image of Se nanotube[55]; Copyright 2006, American Chemical Society. (F) TEM image of Se nanobelts[56]; Copyright 2005, American Chemical Society. (G) TEM image of Se nanosheets[57]; Copyright 2017, American Chemical Society. (H) AFM topography image of Se nanoflakes[58]; Copyright 2017, Wiley-VCH. (I) Hexagonal structure existed in 0D and 1D Se nanomaterials[57]; Copyright 2002, Wiley-VCH. (J) 1T-MoS_2-like structure and square structure existed in 2D Se nanomaterials[60]; Copyright 2022, Springer.

structural and morphological tunability, and volumetric dispersion. Considerable efforts have been made to develop 2D Se nanomaterials since the emergence of Se nanoflakes in 2017[57]. 2D nanostructures have been demonstrated to be crucial and more suitable for device applications thanks to their high specific surface area, carrier capacity, energy storage ability, conversion efficiency, and environmental stability[58,59]. 2D Se nanomaterials offer a huge number of active sites on the surface for storing and transporting ions, thus acting as active electrode materials in energy storage systems[59].

Se has six allotropic forms that can be classified as either crystalline or amorphous in the solid state based on its molecular structure[60,61]. There are five types of crystalline phases, including hexagonal Se with thermodynamic stability, a, b, c-monoclinic Se, rhombohedral Se, orthorhombic Se, and a and b-cubic Se. Non-crystalline allotropes of Se can be classified as amorphous and vitreous forms. The red and black amorphous Se is formed based on Se_8 rings and Se_8 chains, respectively, while vitreous Se is established on Se_8 chains[62]. The chain arrangement greatly affects the electronic structure of Se[63]. For instance, monoclinic, amorphous, or another metastable Se is insulating. In contrast, trigonal Se is semiconducting. The atoms in trigonal Se are covalently bonded into spiral chains oriented along the c-axis, while the adjacent chains are weakly connected via van der Waals interactions and run along their radical directions, leading to a hexagonal structure [Figure 1I], which can facilitate electronic conduction[57]. The hexagonal structure exists in a wide range of 0D and 1D Se nanomaterials, enabling them to be promising semiconductors for optoelectronics and piezoelectronics. Because of the intrinsic anisotropy of the atomic structure, Se is prone to form 0D and 1D nanostructures, while 2D Se nanomaterials are relatively difficult

to fabricate. It is reported that 2D Se nanomaterials have relatively complex structures based on crystal search computations. Besides the hexagonal and trigonal structure, two other stable structures including 1T-MoS_2-like structure (*T*-Se) and square structure (*S*-Se) may exist [Figure 1J][63].

SYNTHESIS STRATEGIES AND FABRICATION TECHNIQUES OF SELENIUM NANOMATERIALS

The synthesis strategies and fabrication techniques greatly dictate the morphologies and structures of the resulting Se. So far, numerous protocols for synthesizing Se nanomaterials, such as chemical reduction, chemical vapor transfer synthesis, and thermally drawn-assisted synthesis, have been reported [Table 1]. The following section analyzes some representative synthesis and fabrication strategies of Se nanomaterials, including nanospheres, nanoparticles, nanotubes, nanowires, and nanosheets.

0D Se nanomaterial

Due to the low cost, biocompatibility, and outstanding electrical properties, 0D Se nanomaterials have been brought into focus in chemical and material communities. Chemical reduction is one of the most common strategies for the synthesis of 0D Se. This approach involves reducing Se salts with various reducing chemicals. Se nanoparticles with a hollow structure synthesized by using A (Pr), sodium selenite, and mercaptothion as a template, Se sources, and reducing agents have been reported [Figure 2A][52]. TEM characterization revealed the hollow structures at the edges and centers. However, the obtained Se nanoparticles contain impurities, transferring these nanoscale materials is complicated, and breaking the serious aggregation remains challenging. All these issues restrict the practical application of these nanoparticles. The emergence of solvothermal synthesis successfully solves the problems, resulting in nanoparticles of high purity, uniform morphologies, and slight aggregation [Figure 2B][64]. Additionally, this method is facile to enable super-small nanoparticles. One example shown in Figure 2B (ii) shows nanoparticles with radii of 3-8 nm. In addition, laser ablation of solid bulky Se at the solid-liquid interface could also be harnessed to produce Se nanoparticles [Figure 2C][65]. With this "top-down" strategy, colloidal Se nanoparticles with sizes of below 100 nm are fabricated in pure water. Such Se nanoparticles are expected to be useful for biological applications. However, some issues that impede the practical application of 0D Se are also reported in these studies. For example, the collision and aggregation of Se nanoparticles frequently occurred, which easily led to serious surface oxidation and degradation. The research on oxidation and degradation will be at the center of the solvothermal synthesis of 0D Se nanomaterials.

1D Se nanomaterials

1D Se nanomaterials such as nanowires, nanorods, nanotubes, and nanobelts have elicited significant interest because of their outstanding optical and electrical properties. Two strategies, namely the "top-down" and "bottom-up" approaches, have been generally employed for the synthesis of 1D formats. Specifically, the "top-down" strategy relies on selective removal of material from a solid bulky Se in a subtractive manner, while the "bottom-up" strategy utilizes individual atoms as the building blocks to realize structure assembling in an additive fashion[66,67].

1D Se nanomaterials are commonly fabricated with the "bottom-up" approach because the atomic composition, size, and shape can be tailorable and controllable. This approach typically involves the decomposition of Se-based compound via chemical reactions either at room or an elevated temperature [Figure 3A]. The resulting nanowires are highly uniform, large-area and of high aspect ratio [Figure 3A (i)][68]. Their lateral dimensions are controllable depending on the process parameters [Figure 3A (ii)]. However, Se nanowires prepared by this approach can be easily contaminated by the used chemical reagents. In addition, the relatively poor crystallinity and high density of defects further frustrate

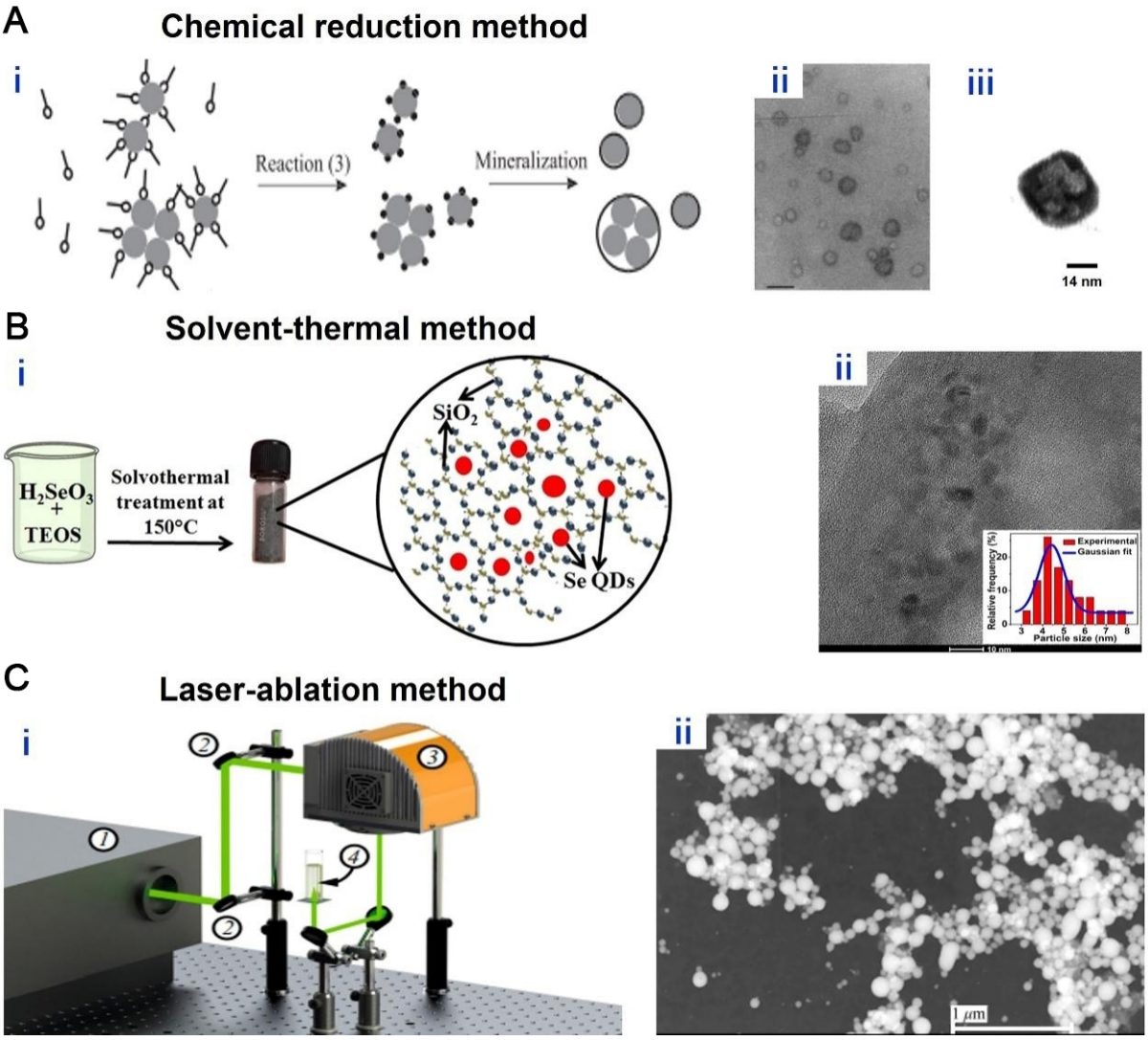

Figure 2. (A) (i) Schematic illustration of the chemical reduction method[52]; (ii) TEM image of hollow sphere Se nanoparticles; (iii) HRTEM image of a hollow sphere Se nanoparticle; Copyright 2002, Wiley-VCH. (B) Scheme illustration of the solvent-thermal method[64]; (i) Large-area HRTEM image and the particle size distribution of Se nanoparticles; (ii) HRTEM image of Se nanoparticles showing *d* spacings; Copyright 2021, American Chemical Society. (C) (i) Schematic of the laser-ablation method[65]; (ii) TEM image of selenium nanoparticles; Copyright 2019, Springer.

the device application. In contrast, chemical vapor deposition (CVD), which involves chemical reaction, vapor evaporation, and decomposition, enables the production of defect-free, trigonal Se nanowires. For example, Chen *et al.* developed a reliable strategy for Se nanowires synthesis in a selenization furnace with the aid of plasma [Figure 3B][69]. Upon reaching its vaporization point at 300 °C, the Se tank emitted Se vapor, which flowed towards the plasma coil, creating ionized Se, which is then grown into Se nanowires on an oxidized silicon substrate [Figure 3B (i)]. As displayed by the SEM and TEM images, a forest of Se nanowires was synthesized, and high-quality crystallinity was achieved [Figure 3B (ii)].

Although the bottom-up approach allows the massive production of Se nanowires at a low cost and in an efficient manner, the manipulation of the entangled nanowire mesh and their integration into devices remains challenging. Very recently, an impressive "top-down" route that exploits the thermal drawing

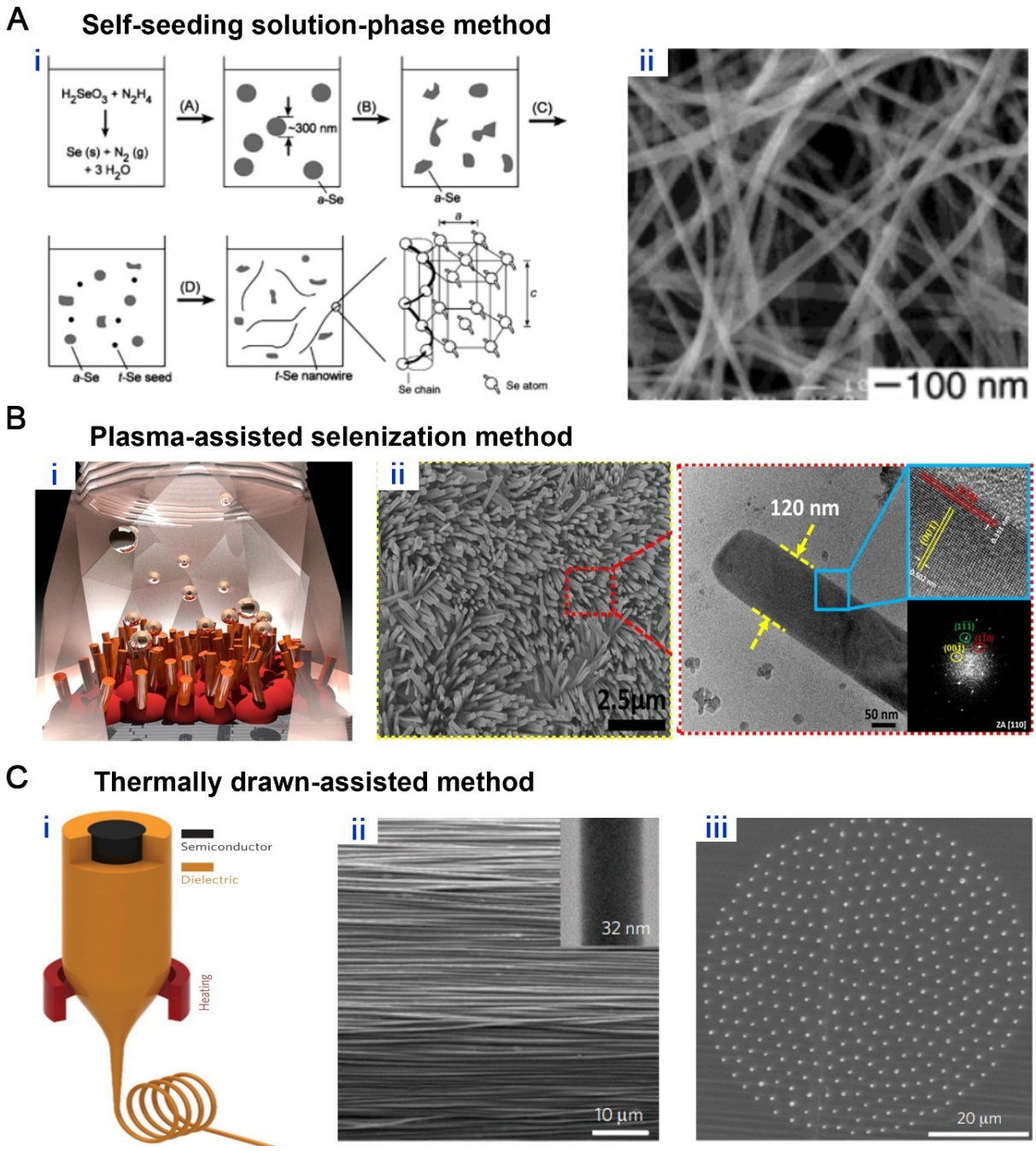

Figure 3. (A) (i) Schematic illustration of self-seeding solution-phase method[68]; (ii) SEM image of Se nanowires; Copyright 2002, Wiley-VCH. (B) (i) Schematic of the plasma-assisted selenization process[69]; (ii) A top view SEM image of Se nanowires and a magnified TEM image of single Se nanowire with the lattice spacings of 0.351 nm of (110) and 0.502 nm of (001); Copyright 2018, American Chemical Society. (C) (i) Schematic illustration of thermally drawn-assisted method[70]; (ii) SEM image of Se nanowire arrays and inset is TEM image of a single nanowire with 32 nm thickness; (iii) Cross-sectional SEM micrograph of Se nanowires; Copyright 2011, Nature Publishing Group.

approach has been developed to fabricate well-ordered, highly uniform Se nanowires and nanotubes [Figure 3C (i)][70]. This method involves multistep iterative co-drawing of Se embedded in a polymeric cladding that supports most of the stress resulting from thermal drawing. Starting with a Se macroscopic

rod that was sealed in a thermoplastic matrix, the first draw scaled down the lateral feature size of Se to a few millimeters. Assembling a bundle of first-drawn fibers and embedding them into a second polymer matrix that was re-drawn reduced the feature size to a few micrometers. A third step finally enabled nanowires and nanotubes with diameters of a few tens of nanometers [Figure 3C (ii)-(iii)]. The nanostructures are radially and axially uniform, axially parallel and indefinitely long, unachieved with any other approaches. Most strikingly, it is very easy to handle these nanostructures and interface them with external electrodes forming flexible electronic devices.

2D Se nanomaterials

2D nanomaterials have attracted exponentially increased academic attention since graphene was discovered. The unique physicochemical properties of 2D nanomaterials make them suitable for use in optoelectronics, electronics, energy storage, and catalysts. Due to Se's intrinsic anisotropic atomic structure, the fabrication of 2D Se nanomaterials remains challenging as opposed to the 0D and 1D Se nanomaterials.

Physical vapor deposition (PVD), a thin-film coating process in which solid materials are vaporized under vacuum conditions and then deposited onto a substrate, has been considered as a promising technique for 2D Se nanomaterials fabrication. Se nanoflakes featured with thicknesses of 5 nm have been fabricated on a Si wafer substrate via depositing Se vapor generated from bulky Se powders [Figure 4A (i)][57]. The nanoflakes were irregularly shaped and zigzagged [Figure 4A (ii)]. Structural characterization reveals the helical atomic chains as well as lattice fringe spacing of typical trigonal structure [Figure 4A (iii)]. Chemical vapor transport (CVT) has also been emerging as one of the promising techniques for 2D Se nanomaterials fabrication[71]. CVT utilizes reversible chemical reactions to trigger crystal growth in different directions at different temperatures. The source materials are easy to obtain, and chemical reactions can be controlled. More importantly, the reactant composition can be easily tailored, thus enabling control over the characteristics of the targeted 2D Se nanomaterials. With this technique, Se nanosheets with typical trigonal crystals have been fabricated [Figure 4B (i)]. The thickness of the monolayer is 0.75 nm [Figure 4B (ii)-(iii)][71].

However, stringent conditions such as ultrahigh vacuum and high temperature frustrate the large-scale production and potential applications of those 2D Se nanomaterials. Exploring more facile and green strategies and techniques is the mainstream direction for future development. Due to their strong in-plane chemical covalent bonds and weak out-of-plane van der Waals interactions, 2D Se nanomaterials can be readily fabricated by the well-established "top-down" methods, such as exfoliating from Se bulk materials in liquid phase. However, it is important to note that the processing temperature should be maintained at 0-10 ℃ in an ice bath, which can prevent the serious oxidation of Se nanostructures. Se nanosheets with ultrathin nanolayered structure have thus been fabricated in an isopropanol solution with probe sonication and centrifugation [Figure 4C (i)][58]. Under a low centrifugation speed, Se nanosheets showed average thicknesses of between 10 and 27 nm, whereas ultrathin features with average thicknesses of 3-6 nm were observed at high centrifugation speeds. TEM characterization revealed the lattice fringe spacings of 0.38, 0.22, and 0.29 nm, which correspond to the crystal plane spacings of (100), (110), and (101) planes [Figure 4C (ii)-(iii)].

PROPERTIES OF SELENIUM NANOMATERIALS

As shown in Table 1, several unique properties of Se nanomaterials, including optical, optoelectronic and piezoelectric properties, and the morphologies and structure-properties relationship are briefly discussed in this section.

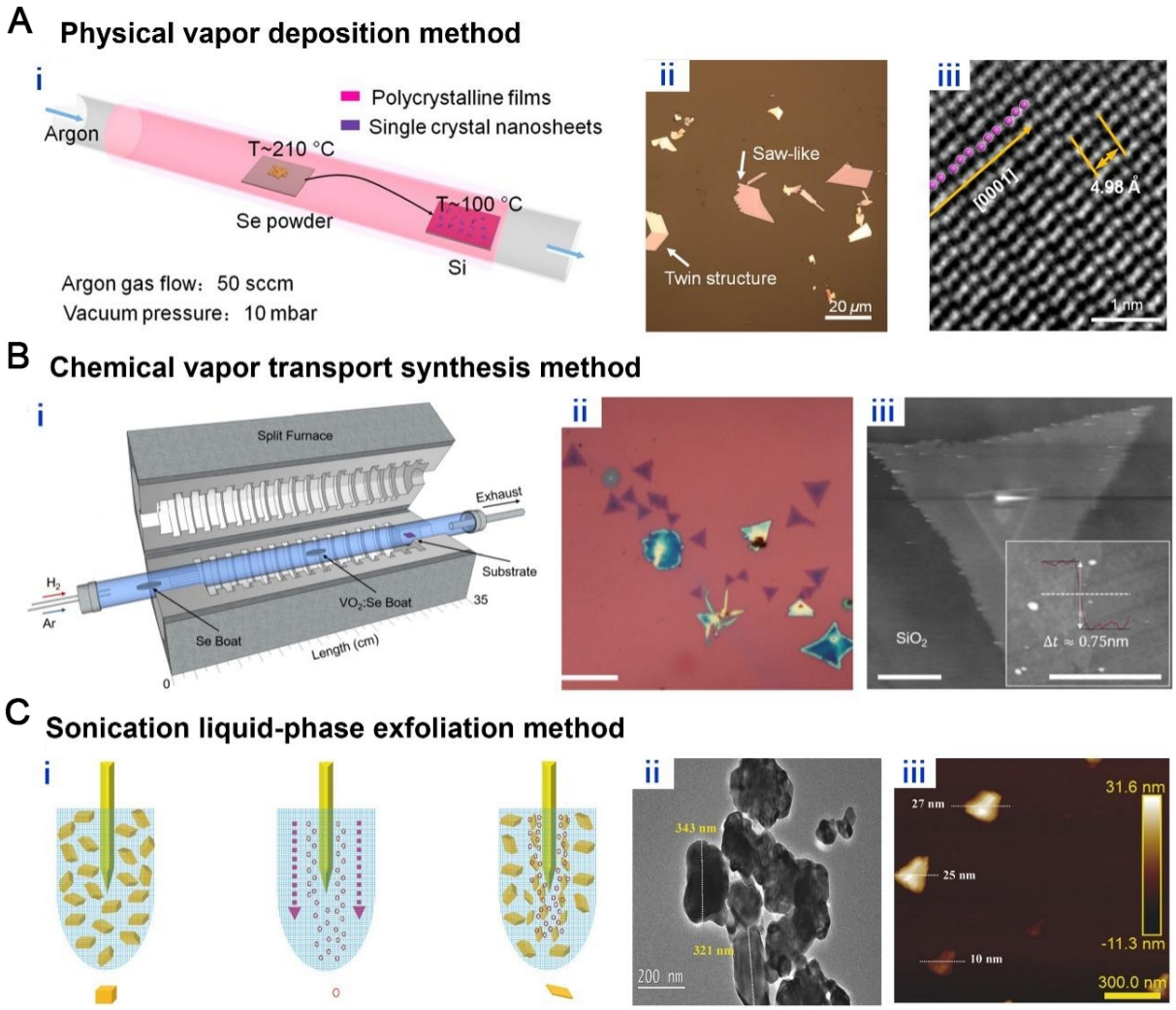

Figure 4. (A) (i) Schematic diagram of the PVD method[57]; (ii) AFM height profile of a twin structure nanosheet; (iii) HAADF-STEM image of Se nanosheets; Copyright 2017, American Chemical Society. (B) (i) Schematic of the CVT method[71]; (ii) Optical microscope image of Se nanoflakes; (iii) AFM image of a Se nanoflake; Copyright 2018, © TÜRKİYE. (C) (i) Schematic demonstration of sonication liquid-phase exfoliation method[58]; (ii) TEM images of Se nanosheets; (iii) AFM images of Se nanosheets; Copyright 2017, Wiley-VCH.

One of the attractive features is tunable and controllable optical properties caused by the quantum confinement effect. The optical properties of Se are of great importance for its photoconductive, photovoltaic and rectifying behaviors and, thus, its device application. Filippo *et al.* found that the UV-vis absorption spectrum of Se microtubes with nanoscale walls consisted of many bands that were typically observed in Se nanowires and some other distinct bands that could be attributed to the interchain interactions perpendicular to the c-axis [Figure 5A][72]. The optical properties of the nanostructured tubes are very different from those of the bulky Se powder source. Moreover, Xing *et al.* found that the optical properties of Se nanoflakes could be modulated through sonication treatments that affected the concentration of the formed Se nanoflakes, as demonstrated by the tunable optical absorbance versus sonication time [Figure 5B (i)][58]. Because of the fluorescence quenching effect and the equilibration of lateral sizes of Se nanoflakes, a new fluorescence emission peak appeared at 367 nm after 3.5 h sonication [Figure 5B (ii)]. The bandgap of Se nanoflakes ranged from 1.8 to 2.2 eV, making it a promising transition semiconductor. Based on electronic structure calculations, it is found that Se nanoflakes with 1T-MoS_2-like structure and tiled helical-chain structure had an indirect bandgap of 1.11 eV and 2.64 eV, respectively[60].

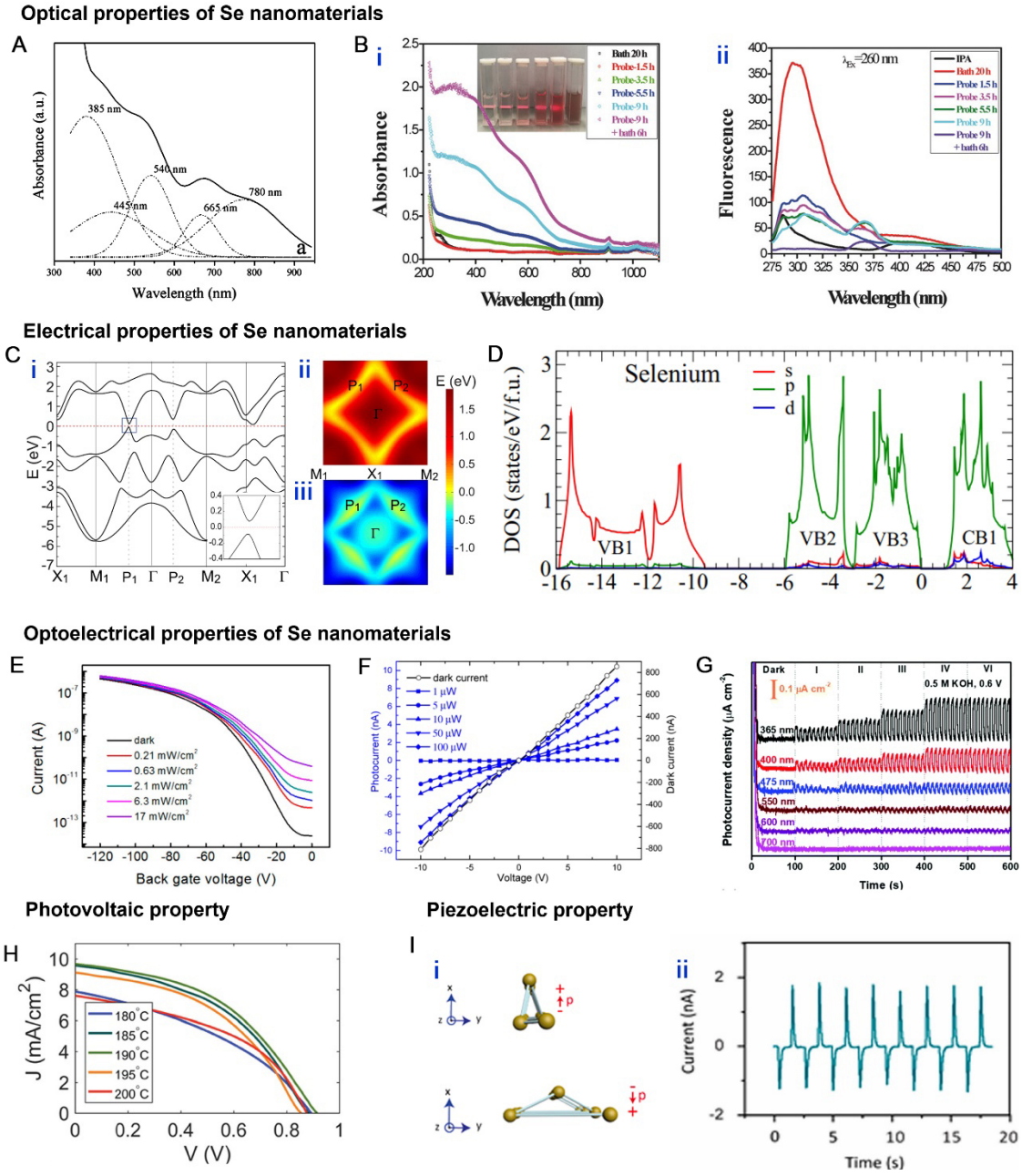

Figure 5. (A) Room temperature UV-vis absorption spectrum[72]; Copyright 2010, American Chemical Society. (B) (i) UV-vis absorption spectrum; (ii) Fluorescence spectra with an excitation wavelength of 260 nm[58]; Copyright 2017, Wiley-VCH. (C) (i) Band structure; (ii) and (iii) Band contour for the bottom conduction band (upper panel) and the top valence band (lower panel) in the first Brillouin zone[61]; Copyright 2019; IOP Publishing. (D) Total and orbital-projected density of states (DOS) for Se[73]; Copyright 2019, American Physical Society. (E) Transfer curves of a Se nanosheet phototransistor measured under various laser irradiation powers at V_{ds} = 3 V[57]; Copyright 2017, American Chemical Society. (F) Photocurrent as a function of laser illumination power measured from voltage of -10 V to 10 V[77]; Copyright 2017, Optical publishing group. (G) Photo response behaviors under lasers with various wavelengths and various laser power densities of dark and levels in 0.5 M KOH at a bias voltage of 0.6 V[78]; Copyright 2020, Royal society of chemistry. (H) *J-V* curves of Se-devices annealed at different specific temperatures[81]; Copyright 2019, Wiley-VCH. (I) (i) Schematic showing the deformed Se nanowire chain and the origin of the piezoelectric polarization; (ii) Short-circuit current (I_{sc}) of Se-PENGs[85]; Copyright 2015, Elsevier.

Moreover, Se nanoflakes presented a centrosymmetric structure possessing a spontaneous in-plane ferroelectric polarization of about 2.68 × 10^{-10} cm^{-1} per layer, which is favorable in nanoscale electronic devices. First-principles calculations revealed that two-dimensional layered Se structure exhibited two gapped semi-Dirac cones in the square Brillouin zone, indicating that they were topological insulators with nontrivial topological properties[61]. The Brillouin zone had Dirac-cone-like dispersion at P1. However, these band distributions showed significant anisotropy at the band contours around P1 [Figure 5C (i)-(iii)]. A density-functional-theory method was conducted to calculate the total and orbital projected densities of states of the trigonal Se[73]. As shown in Figure 5D, the lowest valence band ranging from -15.9 to -9.5 eV can be found in the VB1 region. VB2/VB3 and CB1 regions can also be observed in upper valence bands and lower conduction bands, respectively. A great deal of potential for the development and application of trigonal Se in linear electro-optic devices has thus been suggested.

Taking advantages of high photoconductivity, electrical anisotropy, and nonlinear optical properties, Se nanomaterials show great potential in optoelectrical applications[73-77]. Figure 5E shows the optoelectronic property of a phototransistor based on Se nanosheets[57]. The current-gate voltage curves show a gate tunability, where a photocurrent of up to 54 nA is generated even at a low illumination power of 0.21 mW cm^{-2}. This result indicates an excellent photoresponsivity of Se nanosheets. Control over the grain size of Se can further increase the optoelectronic performance. For example, a laser-based annealing approach enabled a polycrystalline domain where the grain size was a few micrometers in the direction perpendicular to the electric field while the grain size was much smaller in the direction of illumination, which led to a super-sensitive photodetector with performance on par with some planar nanoscale devices [Figure 5F][77]. Besides 2D and 3D Se nanomaterials, 0D Se nanomaterials, such as Se quantum dots, also show excellent optoelectronic properties. As shown by Figure 5G, the photocurrent is detected in Se quantum dots under an applied bias voltage of 0.6 V[78]. Notably, the potential gradient generated within Se quantum dots promoted the separation of electrons and holes, thus enabling a higher photocurrent density (1.80 μA cm^{-2}) than photodetectors based on Se nanosheets or Se nanowires.

Since its deployment in solar cells about 140 years ago, Se has been acting as a promising semiconducting material for the fabrication of photovoltaic devices[79,80]. Modulating crystalline structure can be an approach to improving solar cell efficiency. The relationship between solar cell performance and Se crystalline structure was investigated by Hadar *et al.*[81]. The presence of small crystal grains in Se's structure, as shown in Figure 5H, contributed to the low short-circuit current density (J_{sc}), which could be explained by the low orientation order of the crystals. In addition, another efficient strategy to improve high solar cell efficiency is incorporating Se with other metal elements, such as germanium (Ge), copper (Cu), and indium (In)[82-84].

Piezoelectric properties are also discovered in Se nanomaterials. Se nanowires exhibit strong piezoelectric properties due to the anisotropic crystal structure of the trigonal phase [Figure 5I][85]. When longitudinal stress is applied along the x-axis, the Se atoms undergo internal displacement and the electronic charge is displaced against the Se cores, resulting in piezoelectric polarization parallel to the x-axis. When Se nanowires are stretched (compressed) vertically, piezoelectric polarization pointing upward (downward) is generated [Figure 5I (i)]. As a result, short-circuit current (I_{sc}) is generated by compressing the Se nanowires along the alignment direction, showing a good perspective for piezoelectric nanogenerators [Figure 5I (ii)].

APPLICATIONS OF SELENIUM NANOMATERIALS IN FLEXIBLE AND WEARABLE ELECTRONICS

Several recent studies have demonstrated that Se nanomaterials represent an intriguing class of functional materials in flexible and wearable electronics because of their anisotropic structure, quantum confinement effects, large surface areas, and interesting optical, electrical, optoelectronic, electrochemical, photovoltaic,

and piezoelectric properties. This section summarizes and discusses the fabrication and application of Se nanomaterials-based flexible or wearable electronics, including flexible and wearable sensors for photedetection, mechanical deformation sensing and physiological sensing, and flexible batteries.

Flexible and wearable sensors for biomedicine and healthcare

Selenium is an intriguing optoelectronic material, and its bulk form has been used for a myriad of optoelectronic applications in xerography, ultrasensitive imaging, chemical detection and photodiodes[86-89]. Selenium nanowires with a trigonal phase offer more appealing optoelectronic properties over their bulky form[90,91]. The integration of trigonal selenium nanowires into flexible devices is bringing novel opportunities for smart sensing, surgical tools and optogenetics[92,93]. The iterative thermal drawing discussed in the previous section enabled ultralong Se nanowire array to align along the fiber length. Interfacing the nanowires at the two extremities of the fiber with external electrodes formed a fiber-based photodetector that was sensitive to visible light[70]. However, the in-fiber selenium exhibited either an amorphous or a polycrystalline structure. The disorganized atomic arrangement and crystal defects like grain boundaries act as recombination centers for charge carriers, hindering the charge collection and reducing the photosensitivity and photoresponsivity. Yan *et al.* have recently devised a novel method that combines thermal drawing and sonochemical synthesis to create flexible fiber-based optoelectronic devices made of single-crystal semiconducting nanowires [Figure 6A][39]. The bulk in-fiber Se underwent a transformation into a dense array of nanowires through the manipulation of the anisotropy in the surface energy of the crystal's crystal planes. The growth of single crystal nanowires from the amorphous bulk in 1-propanol resulted in the formation of in-fiber optoelectronic devices with built-in electrodes in intimate contact. These fiber devices showcased exceptional optical and optoelectronic performances, including high photoresponsivity and photosensitivity, low dark current, low noise-equivalent power, and ultrafast response speed, which rivaled many wafer-based devices. Notably, this innovative approach enabled high-throughput integration of nanowires into devices on an ultra-large scale, eliminating the need for intricate clean room contacting procedures. This was demonstrated through the growth of high-performance nanowire-based devices along the fiber length. The integration of multiple Se nanowire-based photodetectors and an optical fiber resulted in a hybrid fiber [Figure 6B][70]. The unique capability of this technology for fluorescent bioimaging based on the single multimodal fiber exhibiting simultaneous efficient optical guidance and excellent photodetection performance was demonstrated. The outstanding performance of the Se nanowires was analyzed to uncover the underlying mechanism. Ultrafast transient absorption spectroscopy, nanosecond flash photolysis, and time-resolved terahertz spectroscopy were used to study the charge carrier dynamics and mobility of Se nanowire meshes[11,31]. These noninvasive, contact-free methods uncovered a picosecond lifetime for free carriers and a microsecond lifetime for trapped carriers, both limited by trap-assisted recombination. Additionally, a high free carrier mobility of approximately 3.0 $cm^2 V^{-1} s^{-1}$ was discovered.

Due to their flexibility, small cross-section and high aspect ratio, fiber-shaped selenium nanowire optoelectronics are particularly useful for minimally invasive bioimaging, and remote and distributed photodetection. In addition to the fiber form factor, the selenium nanomaterials can also be integrated into large-area planar devices. Luo *et al.* reported fabrication of a thin film-based photodetector with full transparency and flexibility, in which the individual Se nanobelts were deposited on a flexible polyethylene terephthalate (PET) matrix [Figure 6C][94]. A number of characteristics were demonstrated to be impressive, including excellent transparency and flexibility, high light sensitivity, and stable response under various bending conditions.

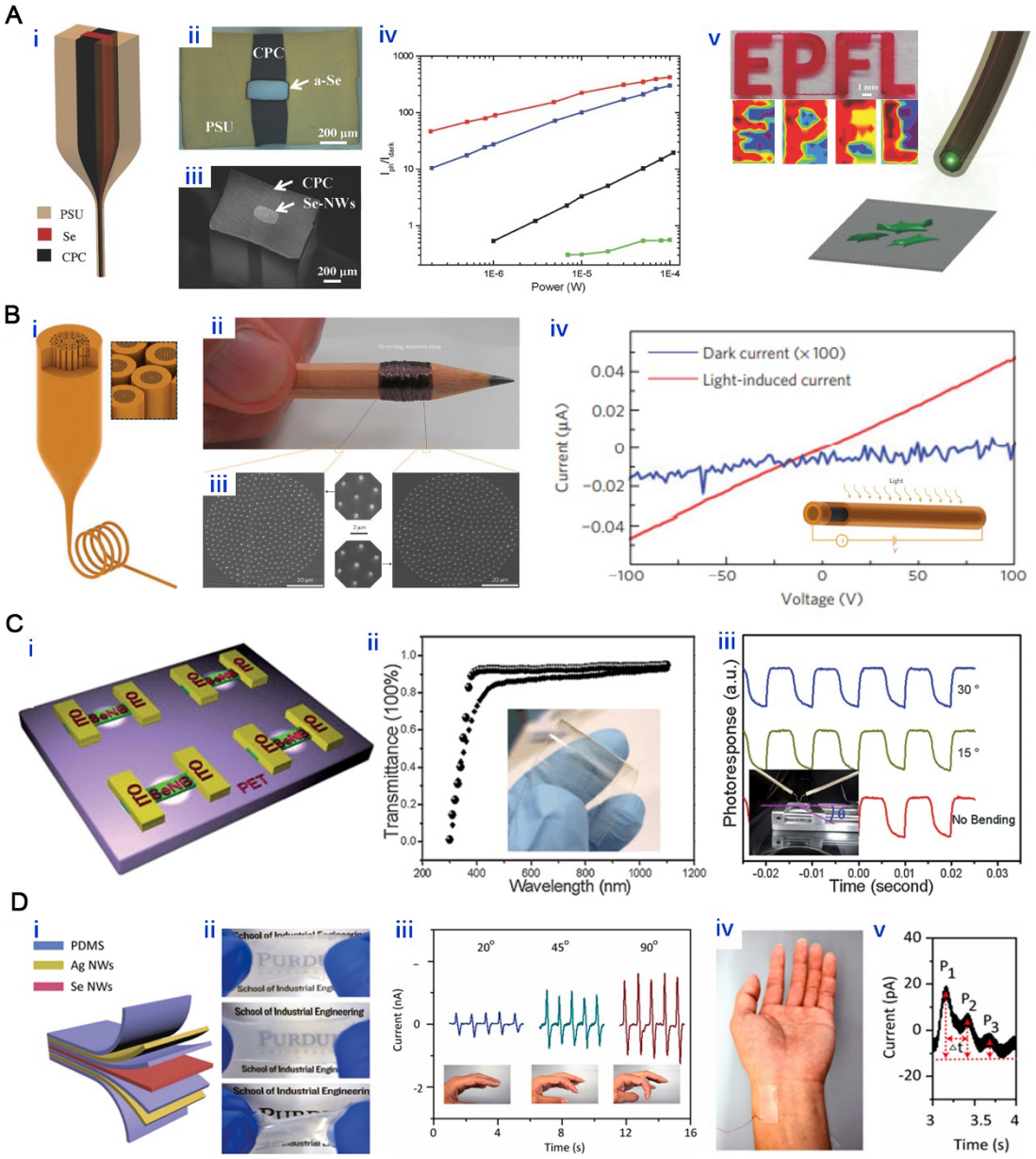

Figure 6. (A) (i) Schematic of multimaterials thermal drawing; (ii) Optical photograph of the cross section of the as-drawn fiber; (iii) SEM image of the fiber cross section after Se-nanowire formation;) Ratio I_{ph}/I_{dark} versus power for the same fibers;) Schematic of the fluorescence imaging system. Top: photograph of the "EPFL" logo filled with dye Rhodamine B dissolved in ethanol; bottom: fluorescent image obtained with the hybrid fiber device[39]; Copyright 2017, Wiley-VCH. (B) (i) Fabrication technique based on iterative size reduction to produce ordered, indefinitely long nanowire and nanotube arrays; (ii) A polymer-embedded nanowire array rolled around a pencil; (iii) Cross-sectional SEM micrographs from both sides of a 10-m-long polymer fibre that contains hundreds of nanowires; (iv) The photoconductance from a selenium nanowire in the dark and on white-light illumination[70]; Copyright 2011, Nature Publishing Group. (C) (i) Schematic illustration of the Se nanobelts photodetectors on transparent and flexible PET film; (ii) Optical transmittance spectra of Se nanobelts photodetector, the inset shows a picture of the photodetectors on PET film; (iii) Photoresponse of the photodetector a PET substrate with different bending angles, the inset shows a picture of the bending setup[94]; Copyright 2012, Royal society of chemistry. (D) (i) 3D illustration of the Se-PENG device; (ii) Optical images of the device in the original state, being stretched and twisted, respectively; (iii) The output current of the Se-PENG attached on the human fingers and bent with different angles; (iv) and (v) The real-time artery pulse signal monitored by the Se-PENG[85]; Copyright 2015, Elsevier.

By leveraging the piezoelectric property, selenium nanomaterials serve as excellent wearable sensors for mechanical deformation and physiological diagnosis. Wu *et al.* developed a Se nanowire-based piezoelectric nanogenerator (PENG) that consisted of PDMS layers, electrodes derived from Ag nanowires, and piezoelectric Se nanowires, as presented in Figure 6D[85]. Here, the PDMS layer serves two purposes: one is to act as the insulating layer between the Se and Ag nanowires, and the other is to encapsulate the Se and Ag nanowires to prevent oxidation and performance deterioration [Figure 6D (i)]. This device was flexible, stretchable, and robust enough to withstand mechanical deformation without breaking. Therefore, PENGs could be adhered to the skin of the human body to detect very faint deformations such as finger bending. The piezoelectric output voltage increases with the bending angle, allowing the finger movement to be recognized. Moreover, the nanogenerator could also be attached to a human wrist to detect the pulses of the radial artery in real time. Three distinct peaks are observed in the piezoelectric current output curve for the cardiac cycle. The P1, P2, and P3 represent the early systolic peak pressure, late systolic augmentation shoulder, and diastolic pulse waveform, respectively. These peaks can be valuable indicators to quantify the physiological information about the cardiovascular system of the wearer.

Flexible batteries

Recent studies have also demonstrated the huge potential of Se nanomaterials for high-performance electrodes in energy storage devices. Typical lithium-sulfur (Li-S) batteries show high theoretical specific capacities and energy densities. However, two major issues have hindered their practical application. First, sulfur is not a preferable electrode material because of its low electronic and ionic conductivity. Second, electrolyte-soluble polysulfide intermediate products are dissolvable in liquid electrolytes when a battery is working, leading to the significant shuttle effect and capacity loss[95-98].

Se is an alternative to sulfur and has been used as a potential electrode material for Li-Se batteries[99-101]. However, bulky Se cathodes exhibit poor cycle performance and low Coulombic efficiency in comparison with S cathodes[102]. One strategy to overcome this issue is to incorporate Se into a 3D interconnected mesoporous carbon nanofibers (CNFs)[103]. This nanostructured Se/CNF enabled high-performance electrodes [Figure 7A]. The resulting Li-Se batteries can deliver a reversible capacity of 516 mAh g^{-1} after 900 cycles without any capacity loss at 0.5 A g^{-1}.

Moreover, self-standing nanostructured graphene-Se@CNT film electrodes for Li-Se batteries have been synthesized[104]. The electrode displays high flexibility and bendability, as shown in Figure 7B. The flexible film cathode delivers a high reversible discharge capacity of 400 mAh g^{-1} that is slightly reduced to 315 mAh g^{-1}, as well as a stable Coulombic efficiency above 96% even after 100 charging-discharging cycles. Nanostructured Se has also been integrated into Na-Se batteries for improved performance. For example, impregnating Se into microporous multichannel carbon nanofibers (MCNF) forms a self-standing cathode film in a Na-Se battery [Figure 7C] that exhibits an extraordinary discharge capacity (596 mA h g^{-1} at the 100th cycle at 0.1 A g^{-1}), excellent rate capability (379 mA h g^{-1} at 2 A g^{-1}), and long-time capacity durability over 300 charging-discharging cycles[105]. With more advances in performance, flexible batteries based on nanostructured Se might constitute a powerful platform for powering flexible and electronic devices and systems instead of using conventional heavy and rigid counterparts.

CONCLUSION AND OUTLOOK

Se nanomaterials are experiencing a flourishing research momentum. Advances in materials synthesis and fabrication, control over morphologies and structure, fundamental understanding of structure-properties relationship, and methodologies of devices integration offer a new class of Se nanomaterial-based flexible and wearable electronics, with wide-ranging applications in smart sensing, health care and energy. While the translation of nanoscale materials into macroscopic real devices is truly exciting, some challenges relevant to fundamental and applied science still exist.

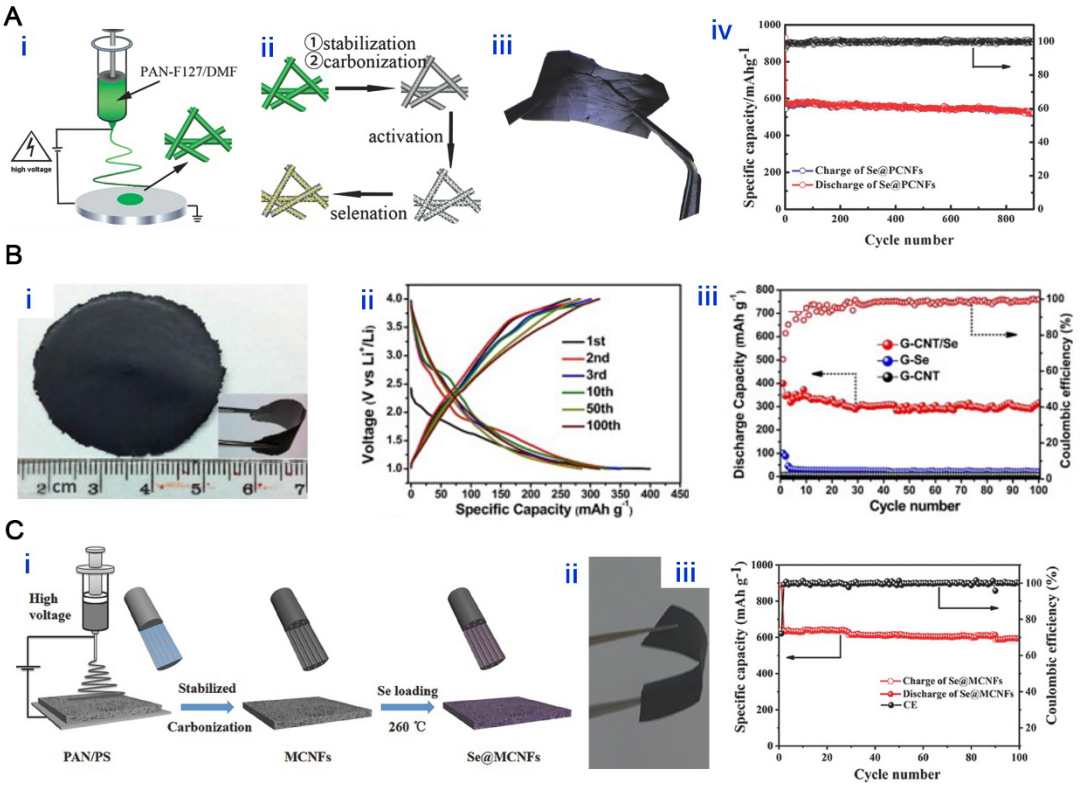

Figure 7. (A) (i) and (ii) Schematic illustration of the synthesis process of the Se@PCNFs electrode; (iii) Photograph of free-standing and flexible Se@PCNFs electrode; (iv) Long-term cycling performance of Se@PCNFs electrode in Li-ion batteries at 0.5 A g^{-1} for 900 cycles[103]; Copyright 2015, Wiley-VCH. (B) (i) Digital photo of the flexible self-standing graphene-Se@CNT composite film; (ii) Charge/discharge profiles of the graphene-Se@CNT composite film with cycles at 0.1 C current rate; (iii) Cycling performance of the self-standing graphene-Se@CNT at 0.1 C[104]; Copyright 2014, Elsevier. (C) (i) Schematic illustration of the synthesis process for Se@MCNF electrode; (ii) photograph of flexible and freestanding Se@MCNF electrode; (iii) Cyclic performances of the Se@MCNF electrode at a current density of 0.1 A g^{-1} and coulombic efficiency during cycling[105]; Copyright 2017, Wiley-VCH.

Synthesis and fabrication: The fabrication of high-performance Se nanomaterial-based flexible and wearable electronic devices relies on the precise positioning and alignment of Se nanomaterials. Most existing approaches to Se nanomaterials synthesis are built upon solution-based processes that involve complex chemical reactions, producing Se nanomaterials with irregular positioning and agglomeration or entanglement. The fabrication of well-ordered, highly uniform Se nanomaterials remains a significant challenge. Moreover, the solution-based approaches, for the most part, exploit noxious raw materials such as Na_2SeO_3 and H_2SeO_3. Their inappropriate handling poses a significant threat to the environment. While solution-free methods such as PVD and CVT only process bulky Se, fulfilling the requirements of high temperature, high-vacuum environment, and highly purified gases demands high operation costs, which undermines the possibility of large-scale production. More controllable, effective, and eco-friendly synthesis and fabrication methods are heavily needed. The recent innovation in harnessing the multimaterial thermal drawing platform has demonstrated a unique and powerful platform for manufacturing periodic arrays of Se nanomaterials in an unprecedentedly green, sustainable and scalable manner[70,76,106-108]. The research along this direction has just begun and is expected to be an exciting paradigm for next-generation Se nanomaterial-based flexible and wearable electronics.

Structure-properties correlation: Se nanomaterials exhibit many intriguing optical, electrical, optoelectronic, photovoltaic, and piezoelectric properties. However, a deep understanding of the structure-properties correlation is still very limited. Harnessing sophisticated characterization techniques such as ultrafast transient absorption spectroscopy, nanosecond flash photolysis and time-resolved terahertz spectroscopy has paved a novel way toward this research direction[31]. This would allow us, on the one hand, to unravel the working principles of Se nanomaterial-based devices and, on the other hand, conversely tune the material structure to further improve performance.

Materials assembly and device integration: Most existing Se nanomaterials suffer from agglomeration or entanglement. Therefore, it requires a stringent post-synthesis process for materials alignment, assembly and device integration. Even though thermal drawing produces well-aligned and exquisitely controllable in-fiber nanomaterials, their monolithic integration with other functional materials such as electrodes for the fabrication of flexible and wearable electronic devices remains challenging. The difficulty is twofold: the co-drawing of Se with other functional materials is challenging because of their incompatible rheological properties; handling materials at the nanoscale is complicated. Nevertheless, an initial step with innovative advances in in-fiber nanowire self-assembly and simultaneous integration with built-in electrodes offers an appealing inspiration for us to further break through the roadblock[39]. More simpler and robust strategies for Se nanomaterials assembly and device integration are desirable for future real-world applications.

Se nanomaterial-based flexible and wearable electronics represent a class of technology with innovative potentials in smart sensing, health care and energy. With continued and concerted efforts in synthesis and fabrication, control over morphologies and structure, device assembly and integration, more advanced flexible and wearable electronics with more sophisticated functionalities and practical applications will emerge.

DECLARATIONS

Authors' contributions

Made substantial contributions to the conception and design of the study: Dang C, Yan W
Writing-original draft preparation and review editing: Dang C, Liu M, Lin Z, Yan W

Availability of data and materials

Not applicable.

Financial support and sponsorship

Yan W acknowledges the Nanyang Technological University (Start-up Grant 021850-00001: Yan W) and the National Natural Science Foundation of China (Grant No. 52202167).

Conflicts of interest

All authors declared that there are no conflicts of interest.

Ethical approval and consent to participate

Not applicable.

Consent for publication

Not applicable.

REFERENCES

1. Yan W, Noel G, Loke G, et al. Single fibre enables acoustic fabrics via nanometre-scale vibrations. *Nature* 2022;603:616-23. DOI PubMed
2. Yan W, Dong C, Xiang Y, et al. Thermally drawn advanced functional fibers: new frontier of flexible electronics. *Mater Today* 2020;35:168-94. DOI
3. Zeng W, Shu L, Li Q, Chen S, Wang F, Tao XM. Fiber-based wearable electronics: a review of materials, fabrication, devices, and applications. *Adv Mater* 2014;26:5310-36. DOI PubMed
4. Leber A, Dong C, Chandran R, Das Gupta T, Bartolomei N, Sorin F. Soft and stretchable liquid metal transmission lines as distributed probes of multimodal deformations. *Nat Electron* 2020;3:316-26. DOI
5. Song W. A smart sensor that can be woven into everyday life. *Nature* 2022;603:585-6. DOI PubMed
6. Du M, Huang L, Zheng J, et al. Flexible fiber probe for efficient neural stimulation and detection. *Adv Sci (Weinh)* 2020;7:2001410. DOI PubMed PMC
7. Weng W, Yang J, Zhang Y, et al. A route toward smart system integration: from fiber design to device construction. *Adv Mater* 2020;32:e1902301. DOI PubMed
8. Loke G, Alain J, Yan W, et al. Computing fabrics. *Matter* 2020;2:786-8. DOI
9. Liu M, Lin Z, Wang X, et al. Focused rotary jet spinning: a novel fiber technology for heart biofabrication. *Matter* 2022;5:3576-9. DOI
10. Jiang S, Patel DC, Kim J, et al. Spatially expandable fiber-based probes as a multifunctional deep brain interface. *Nat Commun* 2020;11:6115. DOI PubMed PMC
11. Xu B, Ma S, Xiang Y, et al. In-fiber structured particles and filament arrays from the perspective of fluid instabilities. *Adv Fiber Mater* 2020;2:1-12. DOI
12. Pan S, Zhu M. Nanoprocessed silk makes skin feel cool. *Adv Fiber Mater* 2022;4:319-20. DOI
13. Wang H, Zhang Y, Liang X, Zhang Y. Smart fibers and textiles for personal health management. *ACS Nano* 2021;15:12497-508. DOI PubMed
14. Zhang T, Li K, Zhang J, et al. High-performance, flexible, and ultralong crystalline thermoelectric fibers. *Nano Energy* 2017;41:35-42. DOI
15. Martin-monier L, Gupta TD, Yan W, Lacour S, Sorin F. Nanoscale controlled oxidation of liquid metals for stretchable electronics and photonics. *Adv Funct Mater* 2021;31:2006711. DOI
16. Pan S, Zhu M. Fiber electronics bring a new generation of acoustic fabrics. *Adv Fiber Mater* 2022;4:321-3. DOI
17. Qian S, Liu M, Dou Y, Fink Y, Yan W. A 'Moore's law' for fibers enables intelligent fabrics. *Natl Sci Rev* 2023;10:nwac202. DOI PubMed PMC
18. Loke G, Khudiyev T, Wang B, et al. Digital electronics in fibres enable fabric-based machine-learning inference. *Nat Commun* 2021;12:3317. DOI PubMed PMC
19. Kim J, Jia X. From space to battlefield: a new breed of multifunctional fiber sheets for extreme environments. *Matter* 2020;3:602-4. DOI
20. Cao Y, Wu H, Allec SI, Wong BM, Nguyen DS, Wang C. A highly stretchy, transparent elastomer with the capability to automatically self-heal underwater. *Adv Mater* 2018;30:e1804602. DOI PubMed
21. Hou C, Jia X, Wei L, et al. Crystalline silicon core fibres from aluminium core preforms. *Nat Commun* 2015;6:6248. DOI PubMed
22. Wei L, Hou C, Levy E, et al. Optoelectronic fibers via selective amplification of in-fiber capillary instabilities. *Adv Mater* 2017;29:1603033. DOI PubMed
23. Qu Y, Nguyen-Dang T, Page AG, et al. Superelastic multimaterial electronic and photonic fibers and devices via thermal drawing. *Adv Mater* 2018;30:e1707251. DOI PubMed
24. Yan W, Burgos-caminal A, Das Gupta T, Moser J, Sorin F. Direct synthesis of selenium nanowire mesh on a solid substrate and insights into ultrafast photocarrier dynamics. *J Phys Chem C* 2018;122:25134-41. DOI
25. Chin AL, Jiang S, Jang E, et al. Implantable optical fibers for immunotherapeutics delivery and tumor impedance measurement. *Nat Commun* 2021;12:5138. DOI PubMed PMC
26. Dong C, Leber A, Das Gupta T, et al. High-efficiency super-elastic liquid metal based triboelectric fibers and textiles. *Nat Commun* 2020;11:3537. DOI PubMed PMC
27. Cao Y, Morrissey TG, Acome E, et al. A Transparent, self-healing, highly stretchable ionic conductor. *Adv Mater* 2017;29:1605099. DOI PubMed
28. Yan W, Richard I, Kurtuldu G, et al. Structured nanoscale metallic glass fibres with extreme aspect ratios. *Nat Nanotechnol* 2020;15:875-82. DOI PubMed
29. Nguyen-dang T, de Luca AC, Yan W, et al. Controlled sub-micrometer hierarchical textures engineered in polymeric fibers and microchannels via thermal drawing. *Adv Funct Mater* 2017;27:1605935. DOI
30. Zhang Y, Li X, Kim J, et al. Thermally drawn stretchable electrical and optical fiber sensors for multimodal extreme deformation

sensing. *Adv Optical Mater* 2021;9:2001815. DOI

31. Jiang S, Song J, Zhang Y, et al. Nano-optoelectrodes integrated with flexible multifunctional fiber probes by high-throughput scalable fabrication. *ACS Appl Mater Interfaces* 2021;13:9156-65. DOI PubMed
32. Das Gupta T, Martin-Monier L, Yan W, et al. Self-assembly of nanostructured glass metasurfaces via templated fluid instabilities. *Nat Nanotechnol* 2019;14:320-7. DOI PubMed
33. Kim J, Zhao Y, Yang S, et al. Laser machined fiber-based microprobe: application in microscale electroporation. *Adv Fiber Mater* 2022;4:859-72. DOI
34. Dong C, Page AG, Yan W, Nguyen-dang T, Sorin F. Microstructured multimaterial fibers for microfluidic sensing. *Adv Mater Technol* 2019;4:1900417. DOI
35. Grena B, Alayrac JB, Levy E, Stolyarov AM, Joannopoulos JD, Fink Y. Thermally-drawn fibers with spatially-selective porous domains. *Nat Commun* 2017;8:364. DOI PubMed PMC
36. Sun H, Xie S, Li Y, et al. Large-area supercapacitor textiles with novel hierarchical conducting structures. *Adv Mater* 2016;28:8431-8. DOI PubMed
37. Khudiyev T, Lee JT, Cox JR, et al. 100 m long thermally drawn supercapacitor fibers with applications to 3D printing and textiles. *Adv Mater* 2020;32:e2004971. DOI PubMed
38. Zhang J, Zhang T, Zhang H, et al. Single-crystal snse thermoelectric fibers via laser-induced directional crystallization: from 1d fibers to multidimensional fabrics. *Adv Mater* 2020;32:e2002702. DOI PubMed
39. Yan W, Qu Y, Gupta TD, et al. Semiconducting nanowire-based optoelectronic fibers. *Adv Mater* 2017;29:1700681. DOI PubMed
40. Hou C, Jia X, Wei L, et al. Direct atomic-level observation and chemical analysis of ZnSe synthesized by in situ high-throughput reactive fiber drawing. *Nano Lett* 2013;13:975-9. DOI PubMed
41. Zhang H, li L, Zheng D, et al. Broadband photodetector based on vapor-deposited selenium self-supporting films. *Ceramics International* 2022;48:27750-7. DOI
42. Shalaev VM. Physics Transforming light. *Science* 2008;322:384-6. DOI PubMed
43. Hu K, Chen H, Jiang M, Teng F, Zheng L, Fang X. Broadband photoresponse enhancement of a high-performance *t* -Se microtube photodetector by plasmonic metallic nanoparticles. *Adv Funct Mater* 2016;26:6641-8. DOI
44. Kumar M, Dubey A, Adhikari N, Venkatesan S, Qiao Q. Strategic review of secondary phases, defects and defect-complexes in kesterite CZTS-Se solar cells. *Energy Environ Sci* 2015;8:3134-59. DOI
45. Wang S, Liu X, Zhou P. The road for 2D semiconductors in the silicon age. *Adv Mater* 2022;34:e2106886. DOI PubMed
46. Kang SK, Park G, Kim K, et al. Dissolution chemistry and biocompatibility of silicon- and germanium-based semiconductors for transient electronics. *ACS Appl Mater Interfaces* 2015;7:9297-305. DOI PubMed
47. Khalid A, Tran PA, Norello R, Simpson DA, O'Connor AJ, Tomljenovic-Hanic S. Intrinsic fluorescence of selenium nanoparticles for cellular imaging applications. *Nanoscale* 2016;8:3376. DOI PubMed
48. Ramírez-montes L, López-pérez W, González-hernández R, Pinilla C. Large thermoelectric figure of merit in hexagonal phase of 2D selenium and tellurium. *Int J Quantum Chem* 2020:120. DOI
49. Qin JK, Zhou F, Wang J, Chen J, et al. Anisotropic signal processing with trigonal selenium nanosheet synaptic transistors. *ACS Nano* 2020;14:10018-26. DOI PubMed
50. Huang W, Wang M, Hu L, Wang C, Xie Z, Zhang H. Recent advances in semiconducting monoelemental selenium nanostructures for device applications. *Adv Funct Mater* 2020;30:2003301. DOI
51. Kumar A, Sevonkaev I, Goia DV. Synthesis of selenium particles with various morphologies. *J Colloid Interf Sci* 2014;416:119-123. DOI PubMed
52. Gao X, Zhang J, Zhang L. Hollow sphere selenium nanoparticles: their *in-vitro* anti hydroxyl radical effect. *Adv Mater* 2002;14:290-3. DOI
53. Zhang J, Xu Y, Fan L, Zhu Y, Liang J, Qian Y. Graphene-encapsulated selenium/polyaniline core-shell nanowires with enhanced electrochemical performance for Li-Se batteries. *Nano Energy* 2015;13:592-600. DOI
54. Zhu Y, Hu X. Preparation of powders of selenium nanorods and nanowires by microwave-polyol method. *Mater Lett* 2004;58:1234-6. DOI
55. Xi G, Xiong K, Zhao Q, Zhang R, Zhang H, Qian Y. Nucleation-dissolution-recrystallization: a new growth mechanism for *t* -selenium nanotubes. *Crystal Growth & Design* 2006;6:577-82. DOI
56. Ma Y, Qi L, Shen W, Ma J. Selective synthesis of single-crystalline selenium nanobelts and nanowires in micellar solutions of nonionic surfactants. *Langmuir* 2005;21:6161-4. DOI PubMed
57. Qin J, Qiu G, Jian J, et al. Controlled growth of a large-size 2D selenium nanosheet and its electronic and optoelectronic applications. *ACS Nano* 2017;11:10222-9. DOI PubMed
58. Xing C, Xie Z, Liang Z, et al. 2D Nonlayered selenium nanosheets: facile synthesis, photoluminescence, and ultrafast photonics. *Adv Optical Mater* 2017;5:1700884. DOI
59. Shi Z, Zhang H, Khan K, Cao R, Xu K, Zhang H. Two-dimensional selenium and its composites for device applications. *Nano Res* 2022;15:104-22. DOI
60. Liu C, Hu T, Wu Y B, et al. 2D selenium allotropes from first principles and swarm intelligence. *J Phys Condens Matter* 2019;31:235702. DOI PubMed
61. Xian L, Pérez Paz A, Bianco E, Ajayan PM, Rubio A. Square selenene and tellurene: novel group VI elemental 2D materials with

nontrivial topological properties. *2D Mater* 2017;4:041003. DOI

62. Degtyareva O, Gregoryanz E, Somayazulu M, Mao H, Hemley RJ. Crystal structure of the superconducting phases of S and Se. *Phys Rev B* 2005;71:214104. DOI
63. Cherin P, Unger P. The crystal structure of trigonal selenium. *Inorg Chem* 1967;6:1589-91. DOI
64. Anupama K, Paul T, Mary KAA. Solid-state fluorescent selenium quantum dots by a solvothermal assisted sol-gel route for curcumin sensing. *ACS Omega* 2021;6:21525-33. DOI PubMed PMC
65. Ayyyzhy KO, Voronov VV, Gudkov SV, Rakov II, Simakin AV, Shafeev GA. Laser fabrication and fragmentation of selenium nanoparticles in aqueous media. *Phys Wave Phen* 2019;27:113-8. DOI
66. Salazar-alvarez G, Muhammed M, Zagorodni AA. Novel flow injection synthesis of iron oxide nanoparticles with narrow size distribution. *Chem Eng Sci* 2006;61:4625-33. DOI
67. Basak S, Chen D, Biswas P. Electrospray of ionic precursor solutions to synthesize iron oxide nanoparticles: modified scaling law. *Chem Eng Sci* 2007;62:1263-8. DOI
68. Gates B, Mayers B, Cattle B, Xia Y. Synthesis and characterization of uniform nanowires of trigonal selenium. *Adv Funct Mater* 2002;12:219. DOI
69. Chen YZ, You YT, Chen PJ, et al. Environmentally and mechanically stable selenium 1D/2D hybrid structures for broad-range photoresponse from ultraviolet to infrared wavelengths. *ACS Appl Mater Interfaces* 2018;10:35477-86. DOI PubMed
70. Yaman M, Khudiyev T, Ozgur E, et al. Arrays of indefinitely long uniform nanowires and nanotubes. *Nat Mater* 2011;10:494-501. DOI PubMed
71. Kasirga TS. Chemical vapor transport synthesis of a selenium-based two-dimensional material. *Turk J Phys* 2018:42. DOI
72. Filippo E, Manno D, Serra A. Characterization and growth mechanism of selenium microtubes synthesized by a vapor phase deposition route. *Crystal Growth & Design* 2010;10:4890-7. DOI
73. Cheng M, Wu S, Zhu Z, Guo G. Large second-harmonic generation and linear electro-optic effect in trigonal selenium and tellurium. *Phys Rev B* 2019:100. DOI
74. Jun SW, Jeon S, Kwon J, Lee J, Kim C, Hong SW. Full-color laser displays based on optical second-harmonic generation from the thin film arrays of selenium nanowires. *ACS Photonics* 2022;9:368-77. DOI
75. Gumennik A, Stolyarov AM, Schell BR, et al. All-in-fiber chemical sensing. *Adv Mater* 2012;24:6005-9. DOI PubMed
76. Deng DS, Orf ND, Abouraddy AF, et al. In-fiber semiconductor filament arrays. *Nano Lett* 2008;8:4265-9. DOI PubMed
77. Yan W, Nguyen-dang T, Cayron C, et al. Microstructure tailoring of selenium-core multimaterial optoelectronic fibers. *Opt Mater Express* 2017;7:1388. DOI
78. Jiang X, Huang W, Wang R, et al. Photocarrier relaxation pathways in selenium quantum dots and their application in UV-Vis photodetection. *Nanoscale* 2020;12:11232-41. DOI PubMed
79. Shin D, Zhu T, Huang X, Gunawan O, Blum V, Mitzi DB. Earth-abundant chalcogenide photovoltaic devices with over 5% efficiency based on a Cu_2 $BaSn(S,Se)_4$ absorber. *Adv Mater* 2017;29:1606945. DOI PubMed
80. Jayswal NK, Rijal S, Subedi B, et al. Optical properties of thin film Sb_2Se_3 and identification of its electronic losses in photovoltaic devices. *Solar Energy* 2021;228:38-44. DOI
81. Hadar I, Song T, Ke W, Kanatzidis MG. Modern processing and insights on selenium solar cells: the world's first photovoltaic device. *Adv Energy Mater* 2019;9:1802766. DOI
82. Liu SC, Dai CM, Min Y, et al. An antibonding valence band maximum enables defect-tolerant and stable GeSe photovoltaics. *Nat Commun* 2021;12:670. DOI PubMed PMC
83. Seo Y, Lee B, Jo Y, et al. Facile microwave-assisted synthesis of multiphase $CuInSe_2$ nanoparticles and role of secondary cuse phase on photovoltaic device performance. *J Phys Chem C* 2013;117:9529-36. DOI
84. Ulaganathan RK, Yadav K, Sankar R, Chou FC, Chen Y. Hybrid InSe nanosheets and MoS_2 quantum dots for high-performance broadband photodetectors and photovoltaic cells. *Adv Mater Interfaces* 2019;6:1801336. DOI
85. Wu M, Wang Y, Gao S, et al. Solution-synthesized chiral piezoelectric selenium nanowires for wearable self-powered human-integrated monitoring. *Nano Energy* 2019;56:693-9. DOI
86. Harkin JM, Dong A, Chesters G. Elevation of selenium levels in air by xerography. *Nature* 1976;259:204-5. DOI PubMed
87. Zhu B, Wu L, Wang Y, et al. A highly selective and ultrasensitive ratiometric far-red fluorescent probe for imaging endogenous peroxynitrite in living cells. *Sensor Actuat B-Chem* 2018;259:797-802. DOI
88. Manjare ST, Kim Y, Churchill DG. Selenium- and tellurium-containing fluorescent molecular probes for the detection of biologically important analytes. *Acc Chem Res* 2014;47:2985-98. DOI PubMed
89. Triet Ho LT, Mukherjee A, Vasileska D, et al. Modeling dark current conduction mechanisms and mitigation techniques in vertically stacked amorphous selenium-based photodetectors. *ACS Appl Electron Mater* 2021;3:3538-46. DOI PubMed PMC
90. Liao ZM, Hou C, Liu LP, Yu DP. Temperature dependence of photoelectrical properties of single selenium nanowires. *Nanoscale Res Lett* 2010;5:926-9. DOI PubMed PMC
91. Luo LB, Jie JS, Chen ZH, et al. Photoconductive properties of selenium nanowire photodetectors. *J Nanosci Nanotechnol* 2009;9:6292-8. DOI PubMed
92. Akiyama N. A sensor array based on trigonal-selenium nanowires for the detection of gas mixtures. *Sensor Actuat B-Chem* 2016;223:131-7. DOI
93. Yan W, Page A, Nguyen-Dang T, et al. Advanced multimaterial electronic and optoelectronic fibers and textiles. *Adv Mater*

2019;31:e1802348. DOI PubMed

94. Luo L, Yang X, Liang F, et al. Transparent and flexible selenium nanobelt-based visible light photodetector. *CrystEngComm* 2012;14:1942. DOI
95. Ji L, Rao M, Zheng H, et al. Graphene oxide as a sulfur immobilizer in high performance lithium/sulfur cells. *J Am Chem Soc* 2011;133:18522-5. DOI PubMed
96. Bruce PG, Freunberger SA, Hardwick LJ, Tarascon JM. Li-O_2 and Li-S batteries with high energy storage. *Nat Mater* 2011;11:19-29. DOI PubMed
97. Luo C, Xu Y, Zhu Y, et al. Selenium@mesoporous carbon composite with superior lithium and sodium storage capacity. *ACS Nano* 2013;7:8003-10. DOI
98. Guo J, Xu Y, Wang C. Sulfur-impregnated disordered carbon nanotubes cathode for lithium-sulfur batteries. *Nano Lett* 2011;11:4288-94. DOI PubMed
99. Abouimrane A, Dambournet D, Chapman KW, Chupas PJ, Weng W, Amine K. A new class of lithium and sodium rechargeable batteries based on selenium and selenium-sulfur as a positive electrode. *J Am Chem Soc* 2012;134:4505-8. DOI PubMed
100. Liu L, Hou Y, Wu X, et al. Nanoporous selenium as a cathode material for rechargeable lithium-selenium batteries. *Chem Commun (Camb)* 2013;49:11515-7. DOI PubMed
101. Yang CP, Xin S, Yin YX, Ye H, Zhang J, Guo YG. An advanced selenium-carbon cathode for rechargeable lithium-selenium batteries. *Angew Chem Int Ed Engl* 2013;52:8363-7. DOI PubMed
102. Zhang Z, Zhang Z, Zhang K, Yang X, Li Q. Improvement of electrochemical performance of rechargeable lithium-selenium batteries by inserting a free-standing carbon interlayer. *RSC Adv* 2014;4:15489-92. DOI
103. Zeng L, Zeng W, Jiang Y, et al. A flexible porous carbon nanofibers-selenium cathode with superior electrochemical performance for both Li-Se and Na-Se batteries. *Adv Energy Mater* 2015;5:1401377. DOI
104. Han K, Liu Z, Ye H, Dai F. Flexible self-standing graphene-Se@CNT composite film as a binder-free cathode for rechargeable Li-Se batteries. *J Power Sources* 2014;263:85-9. DOI
105. Yuan B, Sun X, Zeng L, Yu Y, Wang Q. A Freestanding and long-life sodium-selenium cathode by encapsulation of selenium into microporous multichannel carbon nanofibers. *Small* 2018;14:1703252. DOI PubMed
106. Marion JS, Gupta N, Cheung H, Monir K, Anikeeva P, Fink Y. Thermally drawn highly conductive fibers with controlled elasticity. *Adv Mater* 2022;34:e2201081. DOI PubMed
107. Deng DS, Nave JC, Liang X, Johnson SG, Fink Y. Exploration of in-fiber nanostructures from capillary instability. *Opt Express* 2011;19:16273-90. DOI PubMed
108. Esposito W, Martin-Monier L, Piveteau PL, Xu B, Deng D, Sorin F. Controlled filamentation instability as a scalable fabrication approach to flexible metamaterials. *Nat Commun* 2022;13:6154. DOI PubMed PMC

Cerri. *Chem Synth* 2023;3:18
DOI: 10.20517/cs.2022.37

Chemical Synthesis

Opinion

Open Access

Information, knowledge, and human learning for chemistry: the visionary contribution of Professor Alain Krief

Stefano A. Cerri[1,2]

[1]LIRMM, Laboratory of Informatics, Robotics and Microelectronics of Montpellier, University of Montpellier, Montpellier F-34095, France.
[2]Digital Knowledge Technologies Services (DKTS) SRL, Via Ampère 61/a, Milan 20131, Italy.

Correspondence to: Prof. Stefano A. Cerri. LIRMM, Laboratory of Informatics, Robotics and Microelectronics of Montpellier, University of Montpellier, 161 Rue Ada, Montpellier F-34095, France. E-mail: cerri@lirmm.fr; VP. Digital Knowledge Technologies Services (DKTS) SRL, Via Ampère 61/a, Milan 20131, Italy. E-mail: sacerri@didaelkts.it

How to cite this article: Cerri SA. Information, knowledge, and human learning for chemistry: the visionary contribution of Professor Alain Krief. *Chem Synth* 2023;3:18. https://dx.doi.org/10.20517/cs.2022.37

Received: 29 Nov 2022 **First Decision:** 9 Mar 2023 **Revised:** 21 Mar 2023 **Accepted:** 22 Mar 2023 **Published:** 10 Apr 2023

Academic Editor: Bao-Lian Su **Copy Editor:** Ke-Cui Yang **Production Editor:** Ke-Cui Yang

Abstract

This is not a paper about the current state of chemistry but rather the author's perspective on a strategy for the future of chemistry and other scientific and technical disciplines. This future vision is based on synergies of natural sciences and technical disciplines on one side and the science of information, i.e., informatics, on the other. It relates the author's interactions during 2003-2023 in professional collaborations with Alain Krief, now Emeritus Professor at the University of Namur. It is argued that the scientific value of Prof. Krief's work - particularly related to his well-known interest in "chemical knowledge transfer" - extends beyond the scientific-technical domain of chemistry to include a much broader area of natural sciences and associated technologies. Prof. Krief's signal contribution has resulted from his profound interest in information, knowledge, and human learning, which has been at the core of our exchanges during the last 20 years.

Keywords: Information, knowledge, human learning, interaction, agents, collective intelligence

THE EMERGENCE OF INFORMATICS AS A NATURAL SCIENCE

Natural sciences can and should seek to answer questions about the essential elements (components,

properties, functions) of natural phenomena, to understand them and to forecast their evolutions as much as possible. Each of the traditional disciplines (e.g., physics, chemistry, biology) answers questions about one of the components/properties of natural phenomena. The primary concern of physics is energy; for chemistry, the goal is to understand matter; and for biology, it is to understand life.

In ancient times, these areas were regarded as part of philosophy. Aristoteles, for example, wrote about physics (*περί φύσεως* means *about nature)*, with philosophy considered to be a general reflection on nature. These disciplines were originally part of philosophy and emerged as distinctive subjects; furthermore, each continues to split with increasing speed and acceleration today. For example, we may now speak about nanotechnologies as a technical offshoot of modern physics and chemistry or genetics as an offshoot of contemporary biology.

Disciplines also fuse with one another: biochemistry and bioinformatics are examples. Their interactions are increasingly perceived, measured, and controlled, so no scientist wishing to be taken seriously may admit to ignoring these interactions if they want to be regarded as credible in understanding nature. This evolving picture illustrates a recognition of the extreme complexity of nature itself and an acknowledgment of the diverse and sometimes paradoxically contradictory qualities of real scientists, including ambition and modesty. Scientists should be ambitious to explore the complexity of natural phenomena but also modest because no single competence may comprehend the subtleties of interactions among all significant factors. This limitation may justify a strong interest in multidisciplinary studies supported by collective intelligence - but the reality is far from theory, as we all know.

The emergence of sciences over many centuries was marked, in the 19th century, by significant progress in understanding "what is energy" (physics) and "what is matter" (chemistry), and in the 20th century by progress in the "what is life" (biology). Another crucial property, steering all natural phenomena (and enabling our ability to study them), was only gradually emerging to be identified, isolated, and studied in this later period: information.

The invention of the computer had a similar triggering effect on the construction of knowledge as had been the case for the printing press centuries earlier. Indeed, essential computer scientists from 1940 to 1960 (e.g., Turing, Wiener, Shannon) paved the way for a foundational new discipline. A well-known aphorism reminds us that computer science is not more about computers than astronomy is about telescopes. In the second half of the 20th century, informatics became recognized as the science of information, a property of nature of the same importance as energy, matter, and life, the four being in perpetual interaction in all natural phenomena. Examples of extreme complexity and significance in the human body are the brain and the immune system (see, for example, debates on the meaning of informatics: https://en.wikipedia.org/wiki/Informatics). Being the computer programs (i.e., the control) stored in the same memory as data, programs are able to treat program code as data. Therefore the invented artefact - the computer - is much more than a machine, it is rather a meta machine, i.e.: a machine capable of learning, i.e.: able to produce totally different machines as a function of the course of interactions with the environment. This phenomenon is very clear and popular today, with the emergence of machine learning in deep neural nets with big data and large language models and consequently the emergence of interactive, generative artificial intelligence systems such as ChatGPT.

As colleagues at the University of Edinburgh (https://www.ed.ac.uk/informatics/about/what-is-informatics) have synthesized the subject, informatics, the science of information, consists of computer science (the components of modern computers, including robots), cognitive science (how animals, individually and

collectively, perceive, understand, reason, decide and act) and artificial intelligence, which links the two complementary disciplines. This vision of informatics includes

1. Technical/mathematical components, such as logic, complexity theory, algorithms, software, databases, hardware, and networks typical of computer science; the anatomy of artificial systems.

2. Functional processes, such as perception, reasoning, communication in natural language, and action: the physiology of natural systems typical of cognitive science.

3. The synergy between artificial and natural systems typical of artificial intelligence, for instance, in the approach called "multi-agent systems" pioneered by Norbert Wiener in his book on Cybernetics: (https://en.wikipedia.org/wiki/Cybernetics:_Or_Control_and_Communication_in_the_Animal_and_the_Machine).

4. And, in recent years, emotions and social studies.

In other words, information and knowledge are essential elements of "agents," whether the latter are living or artificial, engaged collectively in collaboration and competition (see, e.g., evidence of these processes in the development of species produced by Darwin), as has long been recognized as the case for animals, from single cells to complex heterogeneous living societies.

In this vein, the author will revisit his interactions with Prof. Krief over the last 20 years to demonstrate that the latter's vision merits profound interest regarding the future of chemistry and natural sciences more broadly and, consequently, of related technologies.

THE ENCORE PROJECT: KNOWLEDGE CONSTRUCTION AND USE BY INTERACTIONS

Around 2003, the author met Prof. Krief, who was interested in our work and considered it somewhat different from other computer scientists he had encountered previously. At the time, Prof. Krief wanted to devote his experience, competence, and reputation to an enterprise that was attractive and simultaneously daunting - the EnCOrE project.

EnCOrE is an acronym for Encyclopedie Chimie Organique Electronique. The idea was to build a repository (an encyclopedia) in the domain of organic chemistry that could help scientists and students "understand and forecast" natural phenomena in organic chemistry (e.g., reactions).

As an informatician, the author was enthusiastic about the project, which could be a very concrete, compelling, and valuable testbed for constructing a series of interactive, knowledge-based systems but recognizing that critical bottlenecks would include using such systems once they existed and the construction itself. By 2005, we could include EnCOrE in the European Union (EU) 6th Framework Programme Project E-LeGI (European Learning Grid Infrastructure https://cordis.europa.eu/project/id/002205). The proposal convinced the EU that the interactions necessary for constructing and using EnCOrE were significant for human learning. As one of the critical application testbeds (or SEES: Service Elicitation Exploitation Scenarios), EnCOrE won part of a significant support gained by E-LeGI (€10 million for 23 partners) from the EU for a period of four years.

To express the needs adequately, the following is a paragraph quoting remarks by Prof. Krief, founder of EnCOrE, which he made when addressing the E-LeGI consortium during its meeting in Brazil in 2004[1,2]. The author highlights a few issues and phrases that he finds particularly valuable:

"*Currently, the information is only delivered flat according to a* ***single point of view*** *dictated by tradition of 'book organization' following the 'Johannes Gutenberg age' (ca.1400-1468). In fact, chemists' brains work differently, and the usual delivery message is* ***context-oriented****. There is a huge number of different contexts which are covered, and it is impossible using a book or even a lecture to describe them all (experimental-oriented, starting material-oriented, product-oriented, mechanism-oriented, stereochemical-oriented, calculation-oriented...)... Not only methods and tools needed for each context are different (flasks, molecular models, heavy calculation), but* ***even the words used in each of these contexts are not properly defined****.*"

"*The construction of the EnCOrE Dictionary is extremely important for our project. It will fix the language and the related ideas and will play an important role in questioning EnCOrE. Its production is an act of power. If this power is not well understood, the chemists will ignore it. For that purpose, it is extremely important that chemists accept and use it. For that purpose, it should be elaborated through a* ***collaborative work*** *implying discussions, contextualization, and consensus between the chemist's community. We want to* ***archive the discussions*** *in order to keep the dictionary always alive by* ***reactivating the discussions*** *on a single word from time to time according to new needs. We believe that the times where confirmed chemists, sent by their respective governments, were gathering in palaces sponsored by IUPAC (Union of Pure and Applied Chemistry, https://iupac.qmul.ac.uk/) to build the compendium of chemical terms in a non contextual manner, is over.*"

The two fundamental messages from Prof. Krief were 1. the importance of words, language, and agreements about the semantics and 2. the strong dependence of these on the context. Both concerns remain at the core of modern informatics, thus encouraging a joint project. Prof. Krief's vision of the future of chemistry was one of a pioneer, without any doubt.

A crucial point concerns the difference between "information" and "knowledge." We were perfectly aware that it would be possible to build a repository of information, a kind of electronic library of concepts, properties of concepts, and relations among concepts and their properties, often called "ontologies." There are many databases, particularly in chemistry; however, the goal of EnCOrE was much more ambitious. Prof. Krief explained that he wanted to identify and implement a process of construction and use of chemical *knowledge*, not merely chemical *information*.

For years, we discussed the difference between information and knowledge. We proposed a simple definition: knowledge is information necessary and sufficient in the context of a decision. Prof. Krief agreed, but simultaneously, problems emerged: the "context" where knowledge is exploited depends heavily on the individual and their previous knowledge, goals, strategies, and tactics, in the case of an expert chemist constructing the encyclopedia and when the knowledge is being exploited, whether by a student or an expert.

After months of work on a small subset of chemical concepts (e.g., chemical equation, chemical structure, element, functional group, named reaction, pure substance, retro-synthesis scheme, segment, reaction vessel), a small encyclopedia was built; nevertheless, many different points of view remained unresolved among the contributing senior chemists. However, the participants all progressed significantly in "learning," as described below. In retrospect, this failure led us to revise our plans: Prof. Krief and the chemists were

encouraged to investigate more deeply the tools, methods, and initiatives dedicated to human learning and dissemination of scientific knowledge, particularly in chemistry, while the informaticians started another project (ViewpointS) which continues (see, e.g., Refs.[2-6]). This latter project is the best testimony of the influence of the experience we gathered previously working with Prof. Krief in EnCOrE.

A synthesis view (2) of the interactive process is presented in Figure 1, in which the agents reach a consensus even in the presence of different points of view about the world.

HUMAN LEARNING AS A SIDE EFFECT OF INTERACTIONS

The E-LeGI project in which Prof. Krief participated with EnCOrE was meant to build a European infrastructure - based on GRID services[7] - that would support human learning. The technical progress of the infrastructure was based on two primary aspects:

1. GRID infrastructures, i.e., network-based predecessors of the cloud, distributed/centralized repositories of information accessible via middleware/web; and

2. GRID services (unlike web services) are "stateful" ones, i.e., they retain a memory of the history of interactions, an essential element for the personalization of teaching-learning processes as well as any other significant interaction. Thanks to these stateful services, one may realize the goal of Prof. Krief when he wanted to store and retrieve the history of conversations that justify any decision about the Encyclopedia.

Both these critical technical aspects were discussed with Prof. Krief, whose enthusiasm and engagement were unlimited. He adopted and reinforced the author's own vision of the requirements for successful learning and for successful progress in science - in fact, we agreed that learning, discovering, and inventing are human activities strongly related to each other (see, for instance, the subsequent work in Refs.[4-6]).

Below are a few snapshots of the work undertaken with Prof. Krief, fully described in the papers and deliverables for the EU.

The Grid Shared Desktop was the interface of a system called AGORA, which enabled the definition and exploitation of Agents (human and eventually software agents), Groups (sets of Agents), Organizations (the structure of rights and duties of groups), Resources (computational and communication resources), and activities (the processes activated within the system). AGORA interactions run on Grid middleware (i.e., worldwide on the web) services (processes activated by software) were stateful, i.e., with memory, enabling the storage and retrieval of histories of the interactions.

In Figure 2, from a 2012 presentation in Brazil by the author, we see six persons connected to the system. In addition to Prof. Krief, who was in Namur, Belgium, participants included a junior chemist (Catherine Colaux-Castillo: at the time, a student of Prof. Krief) from Paris, a senior chemist (Claude Laurenco, Ecole de Chimie, Montpellier) from Montpellier, and two senior informaticians (Philippe Lemoisson and Pascal Dugénie) from different labs in Montpellier. The "conductor" of the interaction was Monica Crubezy, the author of the interface of Protégé[8] from Stanford University, who actively supported the project. Protégé is (even now) one of the most successful editors for ontologies worldwide. The session aimed to define the concepts and relations (ontology) concerning the synthesis of the natural product carpanone. The session involved the use of different shared applications such as Flashmeeting (http://flashmeeting.open.ac.uk/) for communication (courtesy of the Open University, Knowledge Media Institute, UK: Prof. Marc Eisenstadt, one of our partners), ChemDraw (a standard software for drawing chemical elements), Resyn Assistant (a

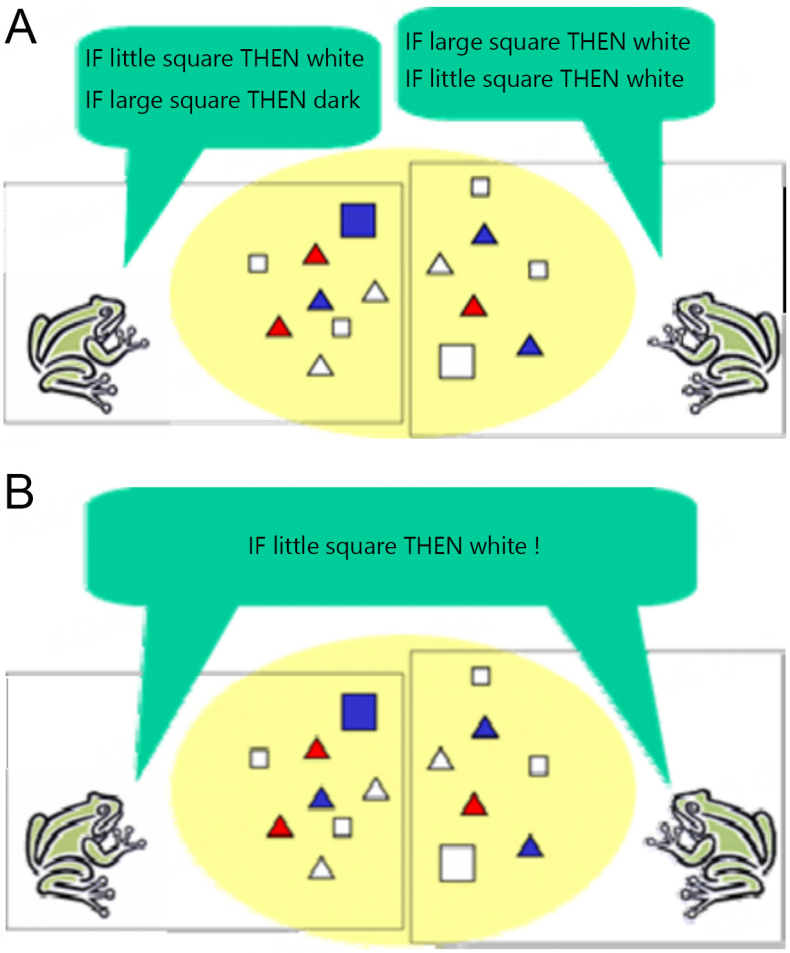

Figure 1. Building a consensus in presence of different viewpoints. (A) Each agent makes his own abduction, according to his local horizon; (B) each agent takes into account the other's abduction and proceeds to a revision of one's theory.

research tool developed by Dr. Laurenco and seldom shown outside his laboratory), and Microsoft PowerPoint (operated by Prof. Krief during a "classical" lecture at a distance).

The duties and rights of the five components of AGORA, the core software behind its interface, the Grid Shared Desktop, were set previously to coordinate the reasoned exploitation of the collaborative processes during the interactions at a distance. To the author, no other software tool currently offers the same robust control and communication functionalities.

Human learning in these experiments occurred in many ways because of the interactions. Each participant "learned" continuously from the others and the whole experience. Two examples highlight how this experiment was an exceptional source of human learning at a distance.

The first was linked to Prof. Krief, a senior scientist learning to use complex software. Previously, he had never been in a situation where he could build an ontology, i.e., a written, formal symbolic representation of concepts, properties, and relations, that software could use to infer new concepts/properties/relations. His profound knowledge of chemistry was indispensable for the success of the enterprise. No other (younger) scientist - probably better acquainted with the tool - could replace him. Therefore, he needed to

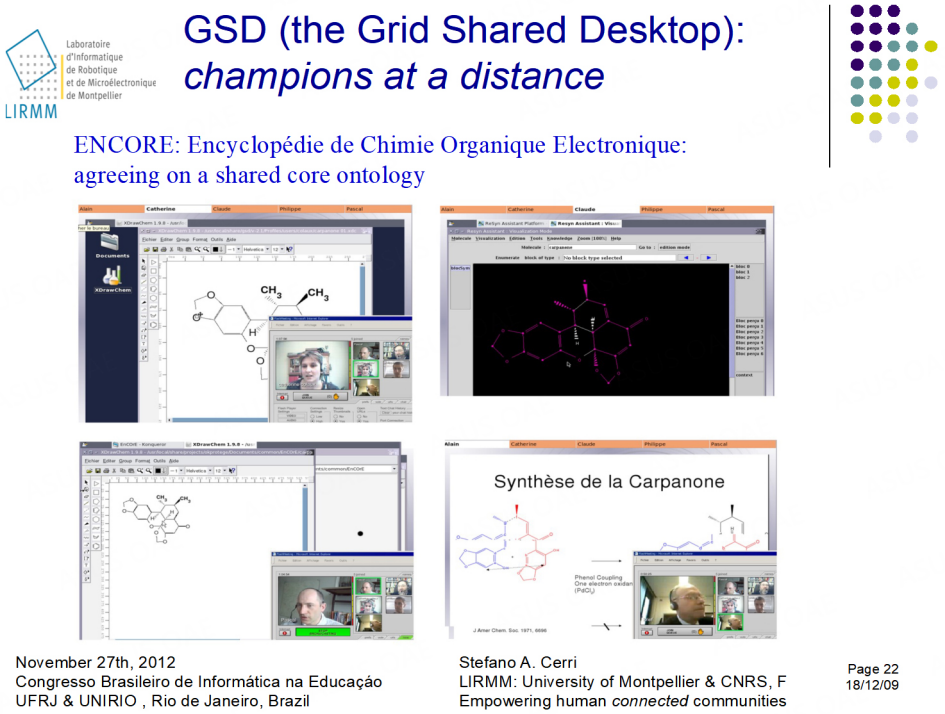

Figure 2. Working and learning at a distance.

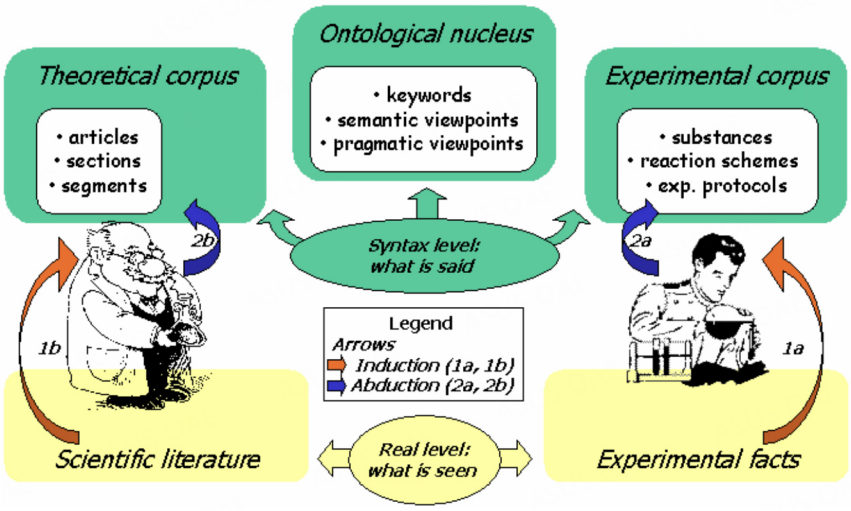

Figure 3. Information, knowledge, and human learning in the EnCOrE project.

"understand and exploit" the powerful, complex Protégé tool. Monica Crubezy, the author of the interface, helped him (at a distance) to become familiar with Protégé in the context of knowledge construction.

The second was related to Claude Laurenco, a senior chemist learning how to teach others to use complex software. Having never previously shown his Resyn Assistant tool, which he had developed over the years, outside his laboratory, he had to learn how to communicate its functionalities to other participants and disseminate its operation and value at a distance.

In experiences from 2005 to 2007, the power of technology then being put into action suggested what today appears normal for people working and learning at a distance. At the time, however, it was not yet widely exploited in its complete spectrum of capacities to the extent true within EnCOrE. We were convinced of the importance of our progress and began to propose to several agencies to advance the work. Unfortunately, none understood the interest of working on the "collective brain"[4,6] put into action at a distance, and the projects proposed were not considered research in either chemistry or informatics (computer science or artificial intelligence) that merited long-term support. Inter- and multi-disciplinarity and the power of information and communication technologies for science construction did not attract those evaluating the submitted research proposals.

Later, information technology companies (e.g., Zoom or Microsoft and many others) presented tools that were apparently similar but realistically were incomplete concerning the one we had demonstrated years ago. Despite what is often declared, the lesson learned is that interdisciplinary progress is rarely sponsored because advances are all too often expected as a side effect of pure disciplinary research plans. Of course, this policy can be understood but does not fit with the observation - supported by many historical examples - that most new discoveries and inventions occurred serendipitously (see, e.g., Ref.[5]) within projects involving high risk, not planned in detail according to the current state of the art. This reality was embedded in the construction of EnCOrE as an encyclopedia supporting information, knowledge, and human learning (Figure 3, from Ref.[1]).

CONCLUSION

One of Prof. Krief's essential attributes is his invaluable curiosity for innovative concepts, methods, and tools, even when they seem far from his previous experience. This ambition to master advances from other disciplines (concerning our collaboration: computer science, cognitive science, artificial intelligence) by interacting with experts has always been related to a profound modesty, witnessing his character as a genuinely modern scientist.

The author, who has known several colleagues with different expertise who have been interested in his approach to informatics, considers Prof. Krief one of the few able to establish a true partnership between our two very different disciplines. If modern scientists are expected to be ambitious and modest, he is such a person. It has always been a pleasure to accompany Prof. Krief in explorations regarding the future of chemistry based on information, knowledge, and human learning, the three components we have long identified as necessary, if not sufficient, for the progress of the discipline and, in general, for the advancement of science. The author is confident that the future will acknowledge the pioneering work of Prof. Krief for his various achievements in organic chemistry, documented by several contributions in this journal issue, and especially for his broad and telescopic vision of the conditions fostering the advancement of science by collective knowledge, such as those he has demonstrated to the author in the last 20 years.

DECLARATIONS

Authors' contributions

The author contributed solely to the article.

Availability of data and materials

Not applicable.

Financial support and sponsorship
None.

Conflicts of interest
The author declared that there are no conflicts of interest.

Ethical approval and consent to participate
Not applicable.

Consent for publication
Not applicable.

REFERENCES

1. Lemoisson P, Untersteller E, Netto Nunes MAS, Cerri SA, Krief A, Paraguaçu F. Interactive construction of EnCOrE (learning by building and using an encyclopedia). Available from: https://hal-lirmm.ccsd.cnrs.fr/lirmm-00108797 [Last accessed on 3 Apr 2023].
2. Lemoisson P, Cerri S. Interactive knowledge construction in the collaborative building of an encyclopedia. *Appl Artif Intell* 2005;19:933-66. DOI
3. Lemoisson P, Cerri SA, Douzal V, Dugénie P, Tonneau JP. Collective and informal learning in the ViewpointS interactive medium. *Information* 2021;12:183. DOI
4. Lemoisson P, Cerri SA. ViewpointS: a collective brain. In: Frasson C, Bamidis P, Vlamos P, editors. Brain function assessment in learning. Cham: Springer International Publishing; 2020. pp. 34-44. DOI
5. Cerri SA, Lemoisson P. Serendipitous learning fostered by brain state assessment and collective wisdom. In: Frasson C, Bamidis P, Vlamos P, editors. Brain function assessment in learning. Cham: Springer International Publishing; 2020. pp. 125-36. DOI
6. Cerri SA, Lemoisson P. Sovereignty by personalization of information search: a collective wisdom may influence my knowledge. In: Cristea AI, Troussas C, editors. Intelligent Tutoring Systems. Cham: Springer International Publishing; 2021. pp. 376-83. DOI
7. Foster I, Kesselman C, Tuecke S. The anatomy of the grid: enabling scalable virtual organizations. *Int J High Perform Comput Appl* 2001;15:200-22. DOI
8. Noy NF, Crubézy M, Fergerson RW, et al. Protégé-2000: an open-source ontology-development and knowledge-acquisition environment. *AMIA Annu Symp Proc* 2003;2003:953. PubMed PMC

Li *et al. Chem Synth* 2023;3:30
DOI: 10.20517/cs.2023.16

Chemical Synthesis

Research Article

Open Access

Pore structure unveiling effect to boost lithium-selenium batteries: selenium confined in hierarchically porous carbon derived from aluminum based MOFs

Hong-Yan Li[1,2,#], Chao Li[1,2,#], Ying-Ying Wang[1,2], Wen-Da Dong[3], Xi-Kun Zhang[1,2], Ming-Hui Sun[1,2], Yu Li[3,*], Bao-Lian Su[1,2,3,*]

[1]Laboratory of Inorganic Materials Chemistry (CMI), University of Namur, Namur B-5000, Belgium.
[2]Namur Institute of Structured Matter (NISM), University of Namur, Namur B-5000, Belgium.
[3]State Key Laboratory of Advanced Technology for Materials Synthesis and Processing, Wuhan University of Technology, Wuhan 430074, Hubei, China.
[#]These authors contributed equally.

*__Correspondence to:__ Prof. Bao-Lian Su, Laboratory of Inorganic Materials Chemistry (CMI), University of Namur, Rue de Bruxelles 61, Namur 5000, Belgium. E-mail: bao-lian.su@unamur.be/baoliansu@whut.edu.cn; Prof. Yu Li, State Key Laboratory of Advanced Technology for Materials Synthesis and Processing, Wuhan University of Technology, 122 Luoshi Road, Wuhan 430074, Hubei, China. E-mail: yu.li@whut.edu.cn

How to cite this article: Li HY, Li C, Wang YY, Dong WD, Zhang XK, Sun MH, Li Y, Su BL. Pore structure unveiling effect to boost lithium-selenium batteries: selenium confined in hierarchically porous carbon derived from aluminum based MOFs. *Chem Synth* 2023;3:30. https://dx.doi.org/10.20517/cs.2023.16

Received: 19 Mar 2023 **First Decision**: 07 Apr 2023 **Revised**: 10 May 2023 **Accepted**: 22 May 2023 **Published:** 9 Jun 2023

Academic Editors: Xiangdong Yao, Aicheng Chen **Copy Editor:** Dan Zhang **Production Editor:** Dan Zhang

Abstract

Lithium-selenium (Li-Se) batteries have attracted much attention in recent years because of their high volumetric capacity (3253 mA h cm^{-3}) compared to the current commercial Li-ion battery. The shuttle effect and large volume variation during the electrochemical reactions limit its practical applications. The widely accepted strategy to reduce these drawbacks is confining selenium (Se) in porous carbon materials. However, how to boost electrochemical kinetics, reduce the shuttle effect and accommodate volume expansion for maximized battery performance still remains highly challenging. Herein, we synthesized three kinds of hierarchically porous carbon materials by facile pyrolysis of aluminum-based metal-organic frameworks (MOFs) with different porous networks. The large surface area and high pore volume can ensure the excellent polyselenides adsorption while tailoring the ratio between micropores and mesopores of the hierarchically porous hosts can highly enhance electrolyte and electron transportation, leading to excellent electrochemical performance with a capacity as high as 530.1 mA h g^{-1} (Se@MIL-68-800) after 200 cycles, an excellent rate capability of 307 mA h g^{-1} at 5 C, and a high

reversible capacity of 544 mA h g^{-1} when current density returns to 0.1 C. The present invention not only provides a facile way to obtain hierarchically porous carbon materials from MOFs but also gives insights on tailoring micropores and mesopores proportion to maximize Li-Se battery performance for their practical industrial implementation.

Keywords: Metal-organic frameworks (MOFs), hierarchically porous carbon host, lithium-selenium (Li-Se) battery, physical adsorption

INTRODUCTION

Selenium (Se), from the same group as sulfur (S), has much higher electronic conductivity (1×10^{-3} S m^{-1}) compared with S (5×10^{-28} S m^{-1}) and comparable volumetric capacity (3253 mA h cm^{-3})[1,2]. This makes Li-Se one of the most promising candidates and has attracted growing attention. However, the soluble intermediates lithium polyselenides (Li_2Se_n, $4 \leq n \leq 8$) in Li-Se battery still induce shuttle effects; in addition, the Se particles undergo volume expansion, and the final lithium selenide (Li_2Se) products are not conductive, leading to quick capacity decay, poor cycle performance, and low Coulombic efficiency (CE).

Confining Se in porous carbon materials is the most widely adopted and very efficient strategy to address these drawbacks. The porous carbon materials have significant influences on the final battery performances via highly improved conductivity of the electrode and increased reaction areas to adsorb the soluble polyselenides to relieve the shuttle effect and the volume expansion[3-5]. The porous carbon materials with diverse morphologies and architectures, such as spheres[6], 1D nanotubes[7], 2D graphene[8], 3D hierarchical structures[9], hollow nanostructures[10], and core-shell structures[11], have been applied and shown improved performance of Li-Se batteries. According to the theoretical calculations using density functional theory (DFT), the size of the cyclo-Se_8 is determined to be 0.726 nm[12]. The pores around this size are necessary for effectively accommodating and maintaining the loaded active Se in a well-infiltrated short chain-like amorphous state. Therefore, tailoring the pore size of porous carbon materials plays an important role in Li-Se batteries. Xin *et al.* reported microporous carbon coated on carbon nanotube (CNT) (CNT@MPC) composite consisting of numerous short-range-ordered slit pores of approximately 0.5 nm to confine Se in order to only form active small Se molecules[13]. The electrochemical behavior of these confined Se chains revealed a reversible one-step reaction with lithium (Li) to yield highly active small Se molecules after the initial discharge. This significantly reduces the shuttle effect in the battery. Liu *et al.* prepared a microporous carbon polyhedral with a pore size of 1.1 nm to confine Se[14]. The enlarged microporous carbon nanospheres with a pore size of around 1.3 nm were also utilized to confine Se[6]. Excellent cycling stability has been observed because the micropores are beneficial for efficient polyselenides adsorption during the reaction. In a study on the effect of pore size on Li-S battery, Hippauf *et al.* experimentally demonstrated that the ultramicropores (less than 0.7 nm), supermicropores (between 0.7 and 2 nm), and mesopores behave quite differently to polysulfide adsorption in liquid phase with the help of UV/vis absorption spectroscopy[15]. They reported that the ultramicroporous materials are up to eight times more efficient than mesoporous ones in adsorbing polysulfide. However, the solely microporous carbon is limited to the high proportion of Se loading, while it is detrimental to fast electrolyte diffusion. The typical ordered mesoporous carbon CMK-3 with a pore size of 3 nm and a high pore volume (1.276 $cm^3 g^{-1}$) was proposed to confine Se[16,17]. The mesoporous carbon can confine a higher amount of Se and promote quick electrolyte penetration. However, the cycling performance fades quickly because of polyselenides formation and easy dissolution in mesoporous carbons. Moreover, Liu *et al.* synthesized mesoporous carbon microspheres with different average pore sizes of 3.8, 5, 6.5, and 9.5 nm, using resorcinol-formaldehyde as a carbon precursor and silica sol as a hard template. The battery cycling performance decreases with increasing sizes of mesopores, and they proved that the size of mesoporous carbon host plays a key role in Se

immobilization[18].

It is obvious that neither a microporous nor mesoporous structure alone could meet the requirements of a superior Li-Se battery with a high amount of Se and recycling stability performance at the same time. Other studies have focused on the bimodal or hierarchically porous carbons to combine the advantages of both micropores and mesopores, and such works have been reported[19-21]. Park *et al.* introduced a self-sacrificed MOF template on polyacrylonitrile to obtain mesopores by direct carbonization and micropores by further chemical activation. They proved that the obtained porous carbon-containing simultaneously micropores and mesopores can achieve high cycling stability because the microporous part facilitates polyselenides trapping and high capacity, while the mesoporous part is beneficial for Se loading and electrolyte filtration[19]. Our group also designed various hierarchically porous carbon, such as single ZIF-8 derived micro-meso-macropores carbon[22], MWCNTs weaved MOF[23], 3D hierarchically ordered porous carbon[24], etc.[25,26] All of them achieved good electrochemical performance. This demonstrates again that combining micropores and mesopores in a carbon host could be a good method to achieve high Se loading and enhance the adsorption of the polyselenides, leading to high cycle stability with a high energy density Li-Se battery. Proper pore size distribution of the host materials is critical to achieving good electrochemical performance of the battery. However, tailoring the ratio of the different size ranges of pores in porous carbon materials to get good cooperation needs to be deeply researched. It is thus highly valuable to investigate porous carbon materials with not only the best pores composition but also the optimized pore sizes ratio to maximize the synergy effects between different size pores.

MOFs have attracted increasing attention in the field of batteries because of their high surface area, uniform pore size, and chemical structure diversity[27-30]. However, the low electrical conductivity of MOFs resulting in low capacity impedes their practical application. The pyrolysis of MOFs leads to much improved conductivity while keeping their defined porosity[31-35]. The widely used MOFs for Li-Se batteries are based on zinc clusters, such as MOF-5 and ZIF-8. The zinc atoms can be conveniently removed during pyrolysis[14,36]. However, the low boiling point of zinc tends to break the original order of micropores. Whereas for Co-MOF, Ni-MOF, and Fe-MOF, the formation of pores by the pyrolysis process will not be influenced by metal evaporation, and the remaining atoms of Co, Ni, and Fe have been proven to catalyze the discharge/charge reaction[37-40]. In addition to the advantages same as Co-, Ni-, and Fe-MOF, aluminum-based MOFs are promising because they can form various MOFs with diverse morphologies with the same or different ligands in different synthesis conditions.

In this work, three kinds of hierarchically micro-mesoporous carbon materials have been successfully fabricated by facile aluminum-based MOF carbonization. The three aluminum-based MOFs originally are composed of the same metal cluster and similar ligands but with fully different pore configurations and volumes under different synthesis conditions. The obtained hierarchically micro-mesoporous carbon materials derived from these aluminum-based MOFs with large surface area and pore volume, interconnected pores, and the different proportions of micropores and mesopores. It is observed that the different ratios of micropores and mesopores can strongly impact the electrochemical properties of Li-Se batteries, leading to different charge-discharge capacities, rate capabilities, and recycling stability. By tailoring the ratio of micropores and mesopores, outstanding properties such as high loading of Se, high volume variation resistance during the electrochemical reaction, excellent fixing capacity of polyselenides, fast electrolyte, and electron transportation can be achieved, leading to a capacity as high as 530.1 mA h g^{-1} after 200 cycles and excellent rate performance around 307 mA h g^{-1} at 5 C. This work sheds light on a generic strategy to boost the electrochemical kinetics and to reduce the shuttle effect by tailoring the ratio of micropores and mesopores for Se confinement toward the practical implementation of Li-Se battery.

EXPERIMENTAL

Preparation of MIL-53 (Al)

MIL-53 (Al) was successfully synthesized through a hydrothermal reaction[41]. In detail, aluminum nitrate nonahydrate [$Al(NO_3)_3.9H_2O$, VWR, 3.9 g], terephthalic acid (TPA, VWR, 0.864 g), and deionized water (15.3 mL) were transferred into 50 mL Teflon-lined stainless steel autoclaves. The mixtures were then stirred for 30 mins and kept at 220 °C in an oven for three days for reaction. Afterward, the mixture was filtered, washed three times with deionized water and ethanol, and dried at 80 °C. The resulting white product was then purified in a muffle furnace (280 °C, three days). This high temperature can make sure complete removal of unreacted TPA species and the occluded TPA molecules within the structure. Finally, the light yellow powdery MIL-53(Al) was obtained.

Preparation of MIL-68 (Al)

The synthesis of MIL-68 (Al) was carried out following the reported work[42,43]. Typically, TPA (VWR, 5 g) and aluminum chloride hexahydrate ($AlCl_3.6H_2O$, VWR, 4.88 g) were dissolved in 300 mL of N, N-dimethylformamide (DMF, VWR). The mixture was then stirred for 2 h and transferred into autoclaves with Teflon insets, where it was kept at 130 °C for 18 h. Afterward, the mixture was cooled down to room temperature and collected by filtration. To remove any free acid that may still remain in the pores, the as-synthesized product was dispersed in 50 mL of DMF under stirring three times at room temperature. To further remove the DMF from the pores, the same procedure was repeated four times using 50 mL of methanol instead of DMF.

Preparation of MIL-100 (Al)

The synthesis of MIL-100 (Al) follows the reported protocol[44,45]. In detail, 0.75 g $Al(NO_3)_3.9H_2O$ and 0.37 g trimesic acid (H_3BTC, VWR) were mixed in a deionized water (10 mL) solution (pH = 1.9-2.0). More importantly, 0.192 g of DMF was added dropwise into this solution, and the quantity of DMF was 2.63 mmol based on their double CH_3 groups (pH = 1.9). After heating the mixture solution to 200 °C for about 4 h, a light yellow sample was obtained after filtration. Then, washing the powder three times with DMF and methanol, respectively, the purified MIL-100 (Al) was obtained after drying at 60 °C for 6-10 h.

Preparation of selenium@porous carbon composites

Each of the as-synthesized MIL-53 (Al), MIL-68 (Al), and MIL-100 (Al) was calcinated at 700, 800, and 900 °C, respectively, with a heating rate of 5 °C min^{-1} for 4 h in an argon (Ar) atmosphere. To remove the aluminum species, the resulting black powder was immersed in a 4 M HCl aqueous solution at room temperature for 12 h. After washing with deionized water to remove any remaining acid, the products were dried in a vacuum oven overnight. The porous carbon materials derived from Al-MIL were labeled as MIL-53-700, MIL-53-800, MIL-53-900, MIL-68-700, MIL-68-800, MIL-68-900, and MIL-100-700, MIL-100-800, MIL-100-900, respectively. The Se-porous carbon composites were synthesized by a two-step melt-diffusion procedure. As all the samples calcined at 800 °C gave the highest surface area and highest pore volume, only the samples calcined at 800 °C were selected for the study on Se confinement. For example, with a weight ratio of 2:1, bulk Se (Sigma-Aldrich) and MIL-53-800 were thoroughly mixed by ball milling (labeled as Se-MIL-53-800). The mixture was then heated to 260 °C and maintained for 16 h, followed by heating to 300 °C for 4 h in a tube furnace filled with flowing Ar to obtain the composites. The final products were labeled as Se@MIL-53-800. The same procedures were carried out with MIL-68-800 and MIL-100-800, leading to the fabrication of Se@MIL-68-800 and Se@MIL-100-800, respectively.

Materials characterization

X-ray diffraction (XRD) patterns were obtained on a Panalytical with Cu Kα radiation (λ = 0.15406 nm) with 45 kV and 30 mA. The scanning electron microscopy (SEM) observation was carried out using a JEOL

7500 F field-emission SEM. Transmission electron microscopy (TEM) images of the samples were recorded on microgrid copper mesh by using a TECNAI 10 at an acceleration voltage of 200 kV. Nitrogen (N_2) adsorption–desorption isotherms were obtained using an ASAP 2420 surface area & porosity analyzer at 77 K. The specific surface area was calculated by the Brunauer-Emmett-Teller (BET). The pore size distribution was calculated by the Barrett–Joyner–Halenda (BJH) method and the nonlocal density functional theory (NLDFT) analysis method. Thermogravimetric analysis (TGA) was carried out using a thermal analyzer (Setaram Labsys Evo) under a flow of N_2 with a temperature ramp of 5 °C min^{-1}. X-ray photoelectron spectroscopy (XPS) characterization was carried out in a Thermo Fisher ESCALAB 250 Xi instrument with a monochromatic Al Kα x-ray source (1486.6 eV). Raman spectra were collected by an Invia Refl (Renishaw, UK) under ambient conditions, from 2000 to 200 cm^{-1} with 632.8 nm laser light.

Electrochemical measurements

The electrochemical measurements were carried out at room temperature using CR2032 coin-type cells. The cathodes were prepared with a conventional slurry coating method[40]. The slurry was prepared by mixing the active material, Super-P carbon (Timcal), and sodium alginate (SA, Sigma-Aldrich) at the weight ratio of 80:10:10 in deionized water. The reference pure Se cathode slurry was prepared by mixing commercial Se, Super-P carbon, and SA with a weight ratio of 60:30:10. The resulting slurry was coated onto an aluminum foil and dried in a vacuum at 60 °C one night. The coated aluminum foil was cut into discs with a diameter of 14 mm to obtain the Se cathode. The mass loading of Se on the cathode is approximately 1.5 mg cm^{-2}. The coin-type cells were assembled in an Ar-filled glovebox with moisture and oxygen concentrations lower than 1 ppm, using Li metal as the counter/reference electrode, glass fiber membrane as the separator, and 1 M Lithium bis(trifluoromethanesulfonyl)imide (LiTFSI, Solvay) in a mixture of dioxolane (DOL, Sigma-Aldrich) and dimethoxygethane(DME, Sigma-Aldrich) (1:1 in volume) with 1% $LiNO_3$ (Sigma-Aldrich) as the electrolyte. The galvanostatic discharge and charge experiments were performed on a battery tester (LAND) with a voltage window of 1.75-2.6 V *vs.* Li^+/Li at different current rates of 0.1, 0.2, 0.5, 1, 2, and 5 C (1 C = 75 mA g^{-1}). Cyclic voltammetry (CV) study (1.75-2.6 V *vs.* Li^+/Li, 0.1 mV s^{-1}) was performed using an electrochemical workstation Princeton VersaSTAT 3, beginning with discharge at 2.6 V. Electrochemical impedance spectroscopy (EIS) measurement was also conducted using Princeton VersaSTAT 3 with a frequency range between 100 kHz and 10 mHz with an AC voltage amplitude of 5 mV at open circuit voltage.

RESULTS AND DISCUSSION

Structural analysis

Scheme 1 illustrates the preparation process to (A) MIL-53 (Al), (B) MIL-68 (Al), and (C) MIL-100 (Al) and then to MIL-53-800, MIL-68-800, and MIL-100-800. MIL-53 (Al) (A) and MIL-68 (Al) (B) were synthesized with the same ligand (TPA) but with different solvents and temperatures, while MIL-100 (Al) (C) was synthesized with trimesic acid. These three MOFs exhibit fully different pore networks. In the case of MIL-53 (Al), only one 1D-rhombic type of pore with a size of 0.85 nm is found [Scheme 1A][46], while MIL-68 (Al) exhibits two different types of channels (triangular and hexagonal) with pore sizes of 0.5-0.85 nm and 1.6-1.7 nm, respectively [Scheme 1B][47]. As for MIL-100 (Al), its framework is formed by channels of micropores and mesopores of around 0.6 and 2.5-2.9 nm in diameter, respectively [Scheme 1C][48]. The MOF-derived porous carbon materials were obtained by the calcination of MOFs at high temperature in Ar, followed by an acid wash to remove aluminum.

The successful synthesis of aluminum-based MOFs, including MIL-53 (Al), MIL-68 (Al), and MIL-100 (Al), can be confirmed by the powder XRD patterns shown in Supplementary Figure 1. The representative peaks of MIL-53 (Al), MIL-68 (Al), and MIL-100 (Al) are the same as the simulated peaks, which are consistent with the previous reports[41-44]. Following the pyrolysis, porous carbon materials are synthesized.

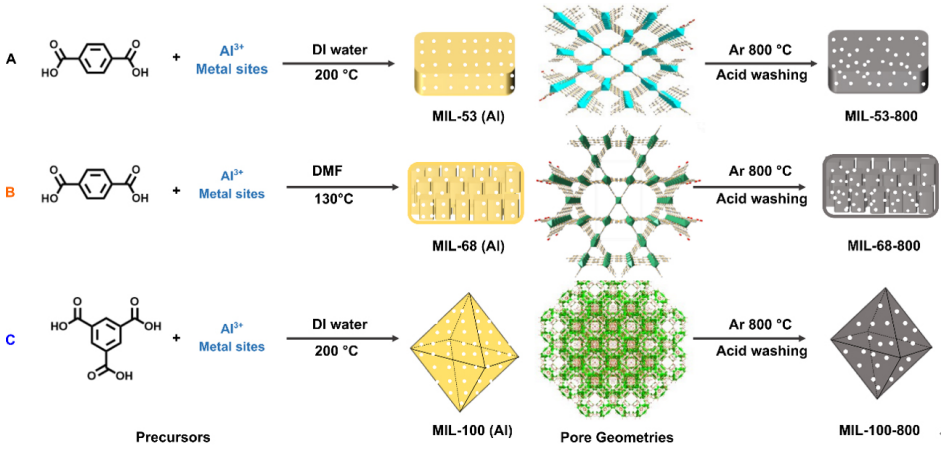

Scheme 1. Synthesis routes to (A) MIL-53 (Al); (B) MIL-68 (Al); and (C) MIL-100 (Al) with different precursors and thus to MIL-53-800, MIL-68-800, and MIL-100-800 by pyrolysis at 800 °C.

Supplementary Table 1 and Supplementary Figure 2 summarize the surface area and pore volume information of samples before and after pyrolysis at 700, 800, and 900 °C. Notably, the surface area and pore volume of MIL-53 (Al) and MIL-68 (Al) decrease after pyrolysis at 700 °C due to the collapse of ordered micropores[49]. However, the surface area and pore volume of MIL-100 (Al) increase owing to the stable trimesic acid ligand that could relieve the collapse of the MIL-100 (Al) structure. By increasing the pyrolysis temperature from 700 to 800 °C, the Al-MIL-derived porous carbon materials achieve higher surface area and pore volume for the reason of the gasification of carbon atoms. When the temperature rises to 900 °C, the surface area of MIL-53-900 and MIL-68-900 drops from 1566 to 413 and 1053 to 240 $m^2 g^{-1}$, and pore volume from 2.33 to 0.68 and 2.16 to 0.26 $cm^3 g^{-1}$, respectively. The sharp decrease in the surface area and pore volume reflects the high collapse of the particle structure[50-52]. The MIL-100-900 also shows a decrease in surface area and pore volume, but not as high as MIL-53-900 and MIL-68-900. That is because the trimesic acid ligands in the spatial configuration of MIL-100 (Al) help to resist high temperature to keep structural stability, which is commonly observed during the pyrolysis of ZIF series materials[19,53]. To obtain enough pore space for Se loading and high surface area for electrochemical reactions, the samples from three Al-MOFs calcined at 800 °C showing the highest BET surface area and the pore volume were selected for Se confinement.

The morphologies of MOF-derived porous carbon materials are examined by SEM and TEM [Figure 1]. The morphology of MIL-53-800 remained intact after calcination compared with MIL-53 (Al) [Supplementary Figure 3A]and shows a massive porous structure with particle size ranging from several hundred nanometers to several micrometers [Figure 1A]. The TEM image [Figure 1B and its inset] presents the particle size and some empty space surrounded by carbon, which is consistent with the SEM result. Figure 1C confirmed the continuous amorphous carbon network with a microporous structure. The morphology of MIL-68-800 shows that the pyrolysis generates a highly porous structure [Figure 1D and E]. Compared with the original TEM morphology of MIL-68 (Al) in Supplementary Figure 3B, the big particle size of MIL-68-800 was composed of small carbon aggregates of 10-20 nm, where exists an interparticle mesopores structure. The micropores of MIL-68-800 can be observed in Figure 1F. MIL-100 (Al) showed a typical octahedron crystal structure with a size of 200-500 nm [Supplementary Figure 3C], and this morphology is still maintained after pyrolysis at 800 °C [Figure 1G]. Both mesopores and micropores were observed in Figure 1H and I. Consequently, the original morphologies can still be maintained after the pyrolysis of MOFs under appropriate conditions.

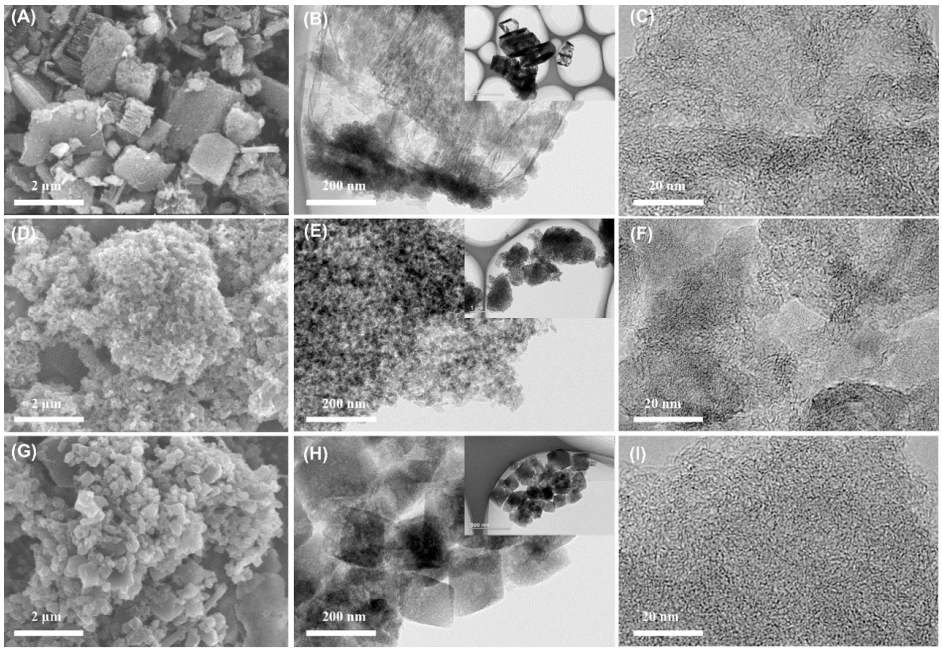

Figure 1. (A) SEM images and (B) (C) TEM images of MIL-53-800; (D) SEM images and (E) (F) TEM images of MIL-68-800; and (G) SEM images and (H) (I) TEM images of MIL-100-800.

The detailed pore size and cumulative pore volume distribution of these three selected MOF-derived porous carbon materials were measured by N_2 desorption-adsorption. The sharp increase of N_2 adsorption at low relative pressures ($p/p_0 < 0.01$) and hysteresis loop in the N_2 adsorption isotherms [Figure 2A] demonstrate that all three MOF-derived porous carbon materials contain micropores and mesopores[54]. Compared with MIL-53-800 and MIL-68-800, MIL-100-800 has much more micropores but fewer mesopores. The cumulative pore size distribution of MIL-53-800, MIL-68-800, and MIL-100-800, calculated by the method of NLDFT, is shown in Figure 2B and converted into a histogram with four size zones in Figure 2C. All three samples show hierarchically porous structures with various pore sizes at different length scales. Four kinds of pores can be observed: ultramicropore (< 0.7 nm), supermicropore (0.7-2 nm), small mesopore (2-10 nm), and big mesopore (10-50 nm). Considering the ultramicropores (< 0.7 nm), the pore volume in this range of MIL-53-800 is 0.15 $cm^3 g^{-1}$, which is similar to that of MIL-100-800 (0.16 $cm^3 g^{-1}$) while four times higher than that of MIL-68-800 (0.04 $cm^3 g^{-1}$). For the supermicropores (0.7-2 nm), the pore volume of MIL-53-800 (0.15 $cm^3 g^{-1}$) is comparable to that of MIL-68-800 (0.12 $cm^3 g^{-1}$) and half of that of MIL-100-800 (0.33 $cm^3 g^{-1}$). For the small mesopores (2-10 nm), the volume of MIL-53-800 is the biggest (1.21 $cm^3 g^{-1}$), which is two and six times higher than that of MIL-68-800 and MIL-100-800, respectively. The big mesoporous volume (10-50 nm) of MIL-53-800, MIL-68-800, and MIL-100-800 is 0.82, 1.41, and 0.14 $cm^3 g^{-1}$, respectively. Due to the three-dimensional trimesic acid ligand, MIL-100-800 shows higher stability with more micropores, which represents 60% of the total volume. The harsh pyrolysis temperature and acid wash lead to the formation of high quantities of mesopores in MIL-53-800 and MIL-68-800. The detailed pore information of these three MIL-(53, 68, and 100)-800, including micropores and mesopores, is shown in Figure 2D-F. The pore size distribution and value of the pore volume are well consistent with the above-mentioned results.

For Se@MIL-(53, 68, 100)-800, the composites of Se and corresponding prepared porous carbon materials with a weight ratio of 2:1 were ball-milled and heated in Ar at 260 °C. The Se was confined by the metal diffusion method, in which the commercial Se particles were melted to liquid that diffused from micropores

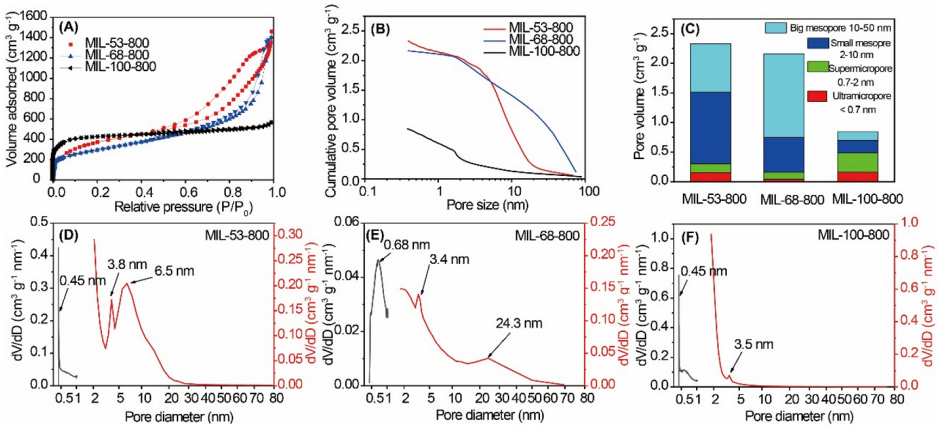

Figure 2. (A) N_2 adsorption-desorption isotherms at 77 K; (B) Cumulative pore size distribution and (C) Histogram of the size distribution of MIL-53-800, MIL-68-800, and MIL-100-800 based on nonlocal density functional theory (NLDFT) pore size analysis of nitrogen physisorption data; (D-F) Pore size distribution of MIL-53-800, MIL-68-800, and MIL-100-800, respectively.

to macropores with the help of the capillary effect. The successful confinement of Se and the exact weight ratio were studied by various characterization techniques. Figure 3A shows the XRD patterns of our MOF-derived samples after the confinement of Se. The pure Se exhibits its typical crystallized structure [PDF # 06-0362] with peaks at 23.5°, 29.7°, 41.3°, 43.6°, 45.4°, and 51.7°[55]. The MIL-53-800 gives two big broad peaks, indicating the loss of the crystalline structure of MIL-53 (Al) after the pyrolysis process. The peaks from Se are clearly identified for Se-MIL-53-800 (the mixture of Se and MIL-53-800 by ball milling). It is the same for the mixtures of Se-MIL-68-800 and Se-MIL-100-800, as shown in Supplementary Figure 4. However, the peaks of Se are not observed with Se@MIL-53-800 after the melt-diffusion process, indicating the amorphous state of Se in the MIL-53-800 porous structure[56,57]. The similar XRD patterns of Se@MIL-68-800 and Se@MIL-100-800 are observed, indicating that the Se remains in an amorphous state and effectively penetrated into the pores of MIL-68-800 and MIL-100-800, which will be confirmed by BET and EDX mapping measurements. However, there is a very weak peak of Se for Se@MIL-100-800, indicating the presence of a very small amount of crystalline Se in MIL-100-800. The probable reason would be the very limited pore volume of MIL-100-800 (0.84 $cm^3 g^{-1}$) and a high proportion of micropores, as indicated in Figure 2C and Supplementary Table 1.

Raman spectra [Figure 3B] also proved the successful Se confinement within the obtained porous carbon materials, as indicated by the total disappearance peak of 236.8 cm^{-1} for Se@MIL-53-800 and Se@MIL-68-800, which is the standard Raman peak of crystalline Se[58]. A very small peak is still observed at 236.8 cm^{-1} for Se@MIL-100-800, showing the presence of a very small amount of crystalline Se in this sample, which is perfectly consistent with XRD results. Furthermore, the peaks at approximately 1350 cm^{-1} and 1584 cm^{-1} are responsible for the carbon of MOF-derived porous carbon materials, which are also called D and G bands[59]. The intensity of D and G bands is responsible for the disordered and graphite carbon[60]. The similar intensity ratio (ID/IG) of around 1.02 for the three MOF-derived porous carbon materials indicates the similar ordered and disordered carbon state in these materials.

Supplementary Table 2 gives information on the surface area and pore volume before and after Se loading. The surface area sharply decreased from 1566 to 123 $m^2 g^{-1}$, 1053 to 139 $m^2 g^{-1}$, and 1412 to 21 $m^2 g^{-1}$ for MIL-53-800, MIL-68-800, and MIL-100-800, respectively, after Se infiltration. The sharp pore volume decreases from 2.33 to 0.33 $cm^3 g^{-1}$, 2.16 to 0.6 $cm^3 g^{-1}$, and 0.84 to 0.10 $cm^3 g^{-1}$ for MIL-53-800, MIL-68-800, and MIL-100-800, respectively, were also observed. The drastic reduction of surface area and pore volume

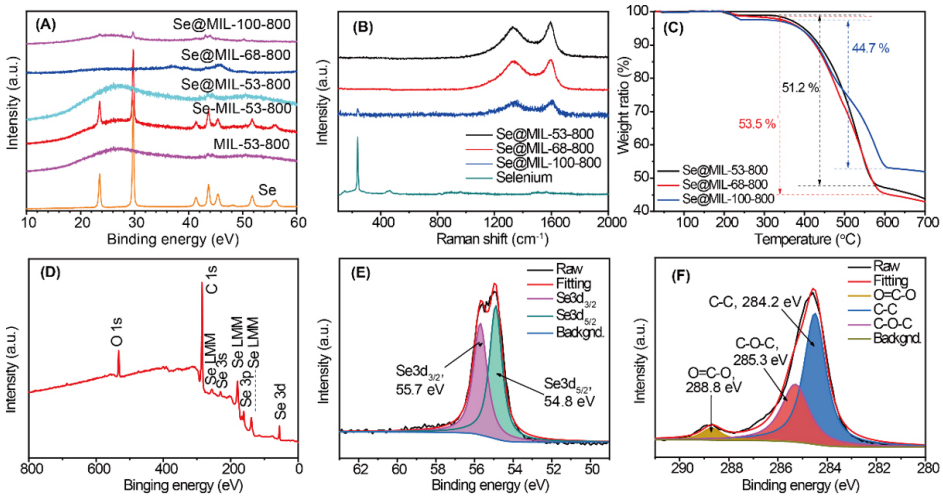

Figure 3. (A) XRD patterns of pure selenium, MIL-53-800, Se-MIL-53-800 mixture, Se@MIL-53-800, Se@MIL-68-800, and Se@MIL-100-800; (B) Raman spectrum of selenium, Se@MIL-53-800, Se@MIL-68-800, and Se@MIL-100-800; (C) TGA curves of Se@MIL-53-800, Se@MIL-68-800, and Se@MIL-100-800 under nitrogen with rate 5 °C min^{-1}. XPS spectrum of Se@MIL-53-800; (D) Survey scan curve (E) High-resolution Se3d and (F) C1s.

after Se infiltration directly evidences that the Se indeed diffuses into the pores of MOF-derived porous carbon materials. The SEM images after Se confinement and related energy dispersive X-ray spectroscopy EDX mapping are shown in Supplementary Figure 5. The uniform dispersion of Se and carbon can obviously be proved by the overlapped images.

The content of Se confined in MOF-derived porous carbon materials was measured by TGA. As shown in Figure 3C, the first weight loss is from 200 to 240 °C, responsible for the evaporation of bound water and moisture that adsorbed in micropores of MOF-derived porous carbon materials[61]. The main weight losses start from 340 to 600 °C. The weight loss in this temperature zone corresponds to the dispersed Se in the pores[62]. The Se@MIL-53-800 and Se@MIL-68-800 show the same shape with one important weight loss, while the MIL-100-800 at this range gives two weight losses with a turning point. That is due to the low pore volume and high micropores ratio of the MIL-100-800 composite; the diffusion of Se is limited by the lack of pathways, resulting in part of Se in the crystalline state. Compared with Se loaded in an amorphous state, the bulk Se confined with a crystalline state undergoes easier evaporation at lower temperature due to the weaker adsorption. While for MIL-53-800 and MIL-68-800, all the Se is in a well-dispersed amorphous state; thus, no turning point of the Se evaporation appears. This also indicates that micropores and mesopores are well interconnected, and tailoring the ratio between the micropores and mesopores of the hierarchically porous hosts has a significant influence on the system mass transfer. The total Se weight loss of Se@MIL-53-800, Se@MIL-68-800, and Se@MIL-100-800 are 53.5%, 51.2%, and 44.7%, respectively. As the pore volume of MIL-53-800 and MIL-68-800 is much higher than that of MIL-100-800, the higher loading of Se is observed in MIL-53-800 and MIL-68-800 than that in MIL-100-800.

The XPS is also applied to investigate the element composition, ratio, and electronic state of the specific elements. The survey scan of the Se@MIL-53-800 [Figure 3D] displays the peaks located at 533, 284, and 55.3 eV, corresponding to the O1s, C1s, and Se 3d, respectively. The high-resolution spectrum of Se 3d [Figure 3E] can be divided into two peaks (54.8 and 55.7 eV), corresponding to Se $3d_{5/2}$ and Se $3d_{3/2}$, respectively[63]. The peak of carbon [Figure 3F] can be deconvoluted into three peaks at 284.2, 285.3, and 288.8 eV, responsible for C-C, C-O, and C=O bonds, respectively[64]. The similar survey scan and high-

resolution spectrum of carbon and Se of Se@MIL-68-800 and Se@MIL-100-800 are shown in Supplementary Figure 6A and B and Supplementary Figure 6D-F, respectively. The weight ratio of Se from the survey scan of Se@MIL-53-800, Se@MIL-68-800, and Se@MIL-100-800 is 54.3%, 53.6%, and 45.4%, respectively, being in very excellent consistency with the results from TGA.

Electrochemical properties

The electrochemical properties of Se@MIL-53-800, Se@MIL-68-800, and Se@MIL-100-800 cathodes are presented in Figure 4 and Supplementary Figure 7, compared with pure Se electrode prepared as a reference. Cyclic voltammogram (CV) was collected at a scan rate of 0.1 mV s^{-1} with a potential range of 1.75–2.6 V *vs.* Li^+/Li in Figure 4A and Supplementary Figure 7A-C. All the Se cathodes with MOF-derived porous carbon host show two obvious reduction peaks at approximately 2.1 and 1.95 V in the first cycle, relevant to the stepwise electrochemical reaction from Se to (Li_2Se_n), finally to Li_2Se[65]. The oxidation peak, mainly at 2.25 V, and a shoulder peak at 2.35 V correspond to the Li_2Se back to Se with the intermediate Li_2Se_n, respectively. Compared with pure Se cathode, the reduction of Se@MIL-(53, 68, 100)-800 occurs on higher voltage in the first cycle, as the value labeled in Figure 4A and Supplementary Figure 7A-C, reflecting the accelerated electrochemical reaction kinetics on these three cathodes. The reduction peak at 2.1 V shifts to a higher potential of 2.21 V after six cycles of battery operation [Figure 4A]. The shift of the first cathodic peak is due to the activation of Se particles and the formation of a stable solid electrolyte interphase (SEI) layer[39,66,67]. The high potential shift of the first reduction peak means easier reduction reaction from Se to Li_2Se_n, indicating the Se cathodes were activated in the discharge/charge process. After activation through the first four cycles, the CV curves of these Se@MIL-X-800 (X = 53,68,100), overlapped well, demonstrating improved reversibility of these batteries[68]. The compared result of these three MOF-derived cathodes on the 5^{th} cycle is shown in Figure 4B. It can be seen that Se@MIL-68-800 possesses the smallest oxidation/reduction potential gap (ΔV) and the highest current density than Se@MIL-53-800 and Se@MIL-100-800, suggesting the accelerated reaction kinetics in Se@MIL-68-800 cathode[69]. It is worth noting that the pure Se cathode shows significantly different electrochemical behavior compared to the three MOF-derived porous carbon materials when used as carbon hosts for the Li-Se batteries. The pure Se cathode has the lowest reduction voltage at the first cycle due to the lack of pathways, while after five cycles, its reduction peak shifts to a higher voltage position than the other three cathodes. The phenomenon may be attributed to the easy diffusion and reaction of the polyselenides that have diffused out of the cathode, as they do not encounter significant interfacial barriers. Moreover, the detailed discharge/charge curves of the different electrodes at the 1^{st}, 50^{th}, 100^{th}, 150^{th}, and 200^{th} cycles are also shown in Figure 4C and Supplementary Figure 7D-F. The discharge curves show two typical platforms, in good consistence with the cyclic voltametric measurements containing two reduction peaks. The lowest gap between the discharge and charge platforms (overpotential) of Se@MIL-68-800 (0.1 V) among all the other three cathodes (Se@MIL-53 with 0.12 V, Se@MIL-100-800 with 0.17 V, and pure Se with 0.17 V) means its lowest polarization compared to the other three batteries, indicating the smallest reaction energy barrier[70].

The cycling performance and CE were evaluated at 0.2 C between 1.75–2.6 V. The initial discharge capacity of Se@MIL-53-800, Se@MIL-68-800, and Se@MIL-100-800 shows much higher values of 704.5, 648.3, and 473.7 mA h g^{-1}, respectively, compared to 342.3 mA h g^{-1} of pure Se cathode. The much higher initial capacity than pure Se cathode indicates the much higher utilization efficiency of Se for Se@MIL-53-800, Se@MIL-68-800, and Se@MIL-100-800. Because the highly porous carbon can lead to a large dispersion of Se in the carbon host system, facilitating the contact between carbon and Se for better electrochemical activity. The initial discharge capacity of Se@MIL-53-800 is higher than the theoretical value (675 mA h g^{-1}), and that of Se@MIL-68-800 is very similar to their theoretical value, while the Se@MIL-100-800 achieves a capacity value that is far from its theoretical value. This is due to the lack of interconnected micro-mesopores constructed electrolyte pathways for the Se@MIL-100-800 cathode, in spite of its high CE value

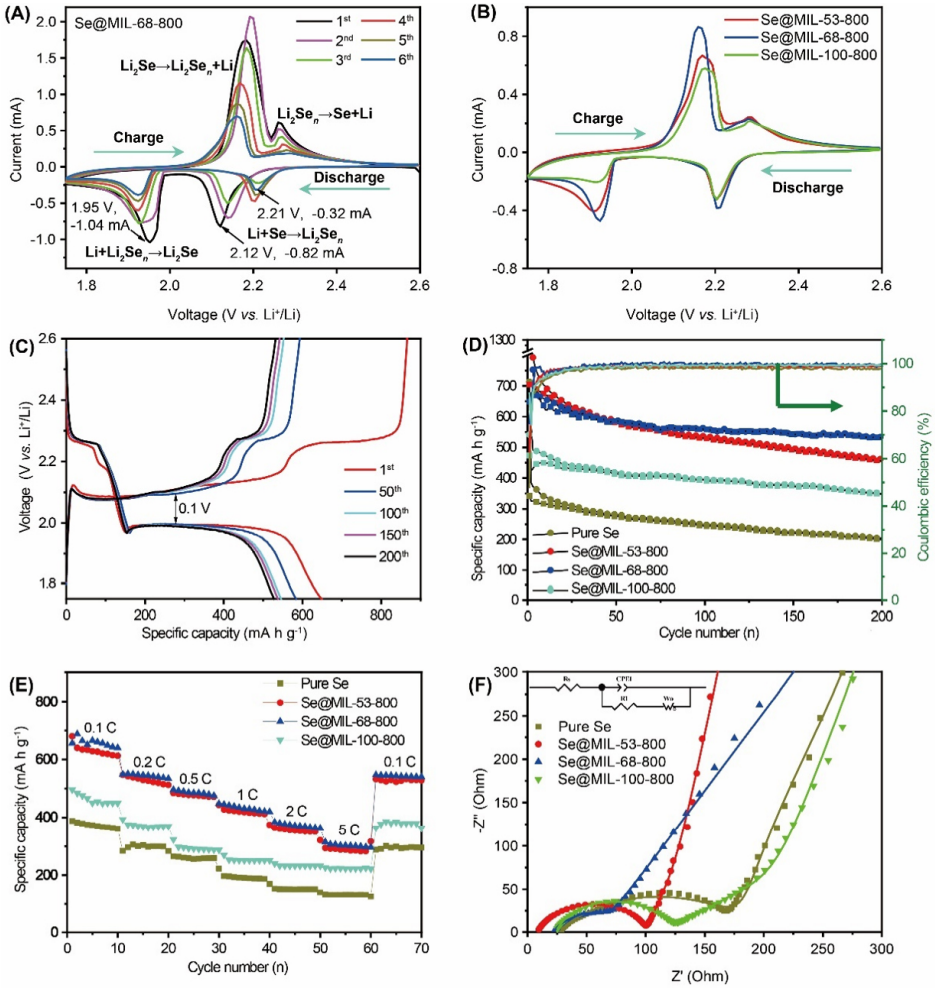

Figure 4. Cyclic voltammetry curves of (A) Se@MIL-53-800 and (B) Compared CV result of different cathodes in the 5th cycle at a voltage of 1.75–2.6 V *vs.* Li^+/Li with the scan rate of 0.1 mV s^{-1}; (C) The discharge/charge curves at different cycles at the voltage of 1.75-2.6 V *vs.* Li^+/Li with the current density of 0.2 C. The electrochemical properties of pure Se, Se@MIL-53-800, Se@MIL-68-800, and Se@MIL-100-800 cathodes in Li-Se cell; (D) Cycling performance and corresponding Coulombic efficiency at 0.2 C; (E) Rate capability and (F) Nyquist plots of these four different cathodes at fresh state.

of 87.5%. The initial CEs of Se@MIL-53-800 and Se@MIL-68-800 are 62.9% and 74.8%, respectively. The high initial capacity and low CE of these two cathodes can be attributed to the irreversible formation process of the SEI layer and electrolyte decomposition on the matrix materials in the first cycle[71]. The CE of Se@MIL-68-800 quickly increases to more than 95% in the first three cycles, which is attributed to the rapid formation of a stable SEI layer, leading to the decrease of irreversible side reaction between the Se cathode and electrolyte. This is much faster than that of Se@MIL-53-800, Se@MIL-100-800, and pure Se cathode to be stabilized because of its good Se dispersion and strong adsorption to polyselenides by optimized pores distribution[72]. As shown in Figure 4D, the discharge capacity of Se@MIL-53-800, Se@MIL-68-800, Se@MIL-100-800, and pure Se cathodes after 200 cycles is 457, 530.1, 347.9, and 199.3 mA h g^{-1}, respectively. The Se@MIL-53-800 shows comparable capacity in the first several cycles as Se@MIL-68-800. However, Se@MIL-68-800 keeps the capacity much better with high cycling stability after 200 cycles.

The rate capabilities of these three MOF-derived cathodes and the reference pure Se cathode is shown in Figure 4E. The capacity decreases with increased current density due to the polarization and the limited

utilization of Se[73]. The Se@MIL-68-800 and Se@MIL-53-800 exhibit very similar high discharge capacities, with the current density increasing from 0.1 C to 5 C due to the high proportion of mesopores and macropores in the corresponding two host materials. The capacity value of Se@MIL-68-800 (307 mA h g^{-1}) is higher than that of Se@MIL-53-800 (292 mA h g^{-1}) at the current density of 5 C, reflecting its better pore size cooperation to accelerate the transportation of electrons/ions. When the current density returns to 0.1 C, a high reversible capacity of 544 mA h g^{-1} is achieved for Se@MIL-68-800, indicating fast electrode reaction kinetics. The best rate capability of Se@MIL-68-800 is probably stemmed from its large proportion of large mesopores, which can ensure the rapid electrolyte transportation and shorten the distance between active Se in the cathode. The capacity of Se@MIL-100-800 and pure Se cathode can be only 220 and 130 mA h g^{-1} at 5 C and the reversible capacities of 380 and 295 mA h g^{-1} at 0.1 C, respectively, demonstrating deteriorated rate performance because of inappropriate porous structures. From the cycling performance, CE, and rate capability test, it is clearly seen that Se@MIL-68-800 performs better than Se@MIL-53-800, Se@MIL-100-800, and pure Se in Li-Se battery. Moreover, compared with the reported papers with similar Se host materials[74-76], the Se@MIL-68-800 cathode achieves a promising electrochemical performance, as shown in Supplementary Table 3.

To obtain further insight into the mechanism of improved cycle and rate performance, EIS analysis was carried out [Figure 4F]. The curves are composed of a semicircle at high frequency followed by a straight line at low frequency. The start point corresponds to the Ohmic resistance (R_Ω) of the whole battery[77-79], while the diameter of the semicircle corresponds to the interface resistance between electrode and electrolyte (also called charge transfer resistance, R_{ct})[80-82]. The fitted circuit diagram is shown in the inset. The interface resistance has a huge influence on the Li-ion and electron transportation. The R_{ct} values of Se@MIL-53-800, Se@MIL-68-800, Se@MIL-100-800, and pure Se cathode were 95, 48, 93, and 162 Ω, respectively. The smallest of Se@MIL-68-800 indicates its fastest reaction kinetics in the discharge/charge process.

Figure 5 schematically illustrates the mechanism of the MIL-53-800, MIL-68-800, and MIL-100-800 as hosts for Se. For the Se@MIL-53-800 composites (I), there are some interconnected large mesopores that traverse the whole particles, along with a large number of small mesopores and numerous micropores [Figure 2C] to carry selenium. This designed structure could ensure a high rate of electrolyte transfer and enough space for Se loading and reaction sites. For Se@MIL-68-800 (II), the difference in pores distribution compared to Se@MIL-53-800 is that the large mesopores occupy a larger proportion, while small mesopores are less abundant. At the same time, the number of micropores becomes a little bit less [Figure 2C], but it is still enough for Se loading. The enlarged pathways accelerate the mass transfer of ions and electrolytes. In the case of Se@MIL-100-800 (III), although there are plentiful micropores for loading Se, the lack of pathway of mesopores leads to slow mass transfer and inadequate reaction. The compromise between the efficient adsorption of polyselenides, fast electrolyte transfer, and fast Li-ion transportation should be well considered. Therefore, the balance of micropores (providing space for Se loading, reaction sites, and strong adsorption to polyselenides) and mesopores (pathways for Se loading and ions/electrons transportation) is critical for high reaction kinetics achievement. Se@MIL-68-800 cathode achieved the best electrochemical performances due to the optimized distribution and ratio of micropores and mesopores. The excellent electrochemical performances of Se@MIL-68-800 can be attributed to the following reasons: (1) High specific surface area and pore volume of high conductivity carbon materials are necessary to achieve good performance due to better Se dispersion, high utilization, and volume expansion suppression; (2) The rational range of micropores that provide Se loading space and interconnected with micropores-mesopores that shorten the pathways of the electrolyte can maximize the battery performance; (3) Most importantly, the favorable MOF-derived hierarchically porous carbon including the optimized ratio of micropores and

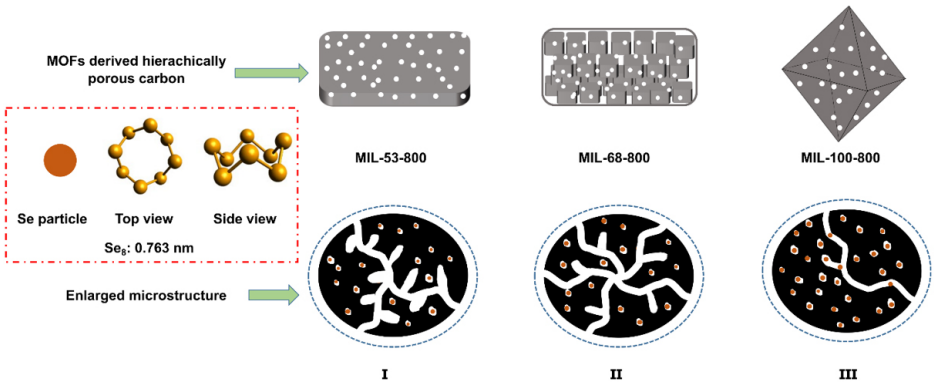

Figure 5. Schematic mechanism of the MOF-derived hierarchically porous carbon for selenium confinement and the synergistic effect of micropores and mesopores during the electrochemical reaction.

mesopores can achieve more efficient suppression of polyselenides dissolution and fast electrolyte transportation at the same time.

CONCLUSIONS

Hierarchically micro-mesoporous carbon materials have been synthesized to confine Se by facile carbonization of three kinds of aluminum-based MOFs. The hierarchically micro-mesoporous carbon structure can confine Se well and alleviate the volume expansion, especially enhancing the adsorption of soluble polyselenides, leading to improved battery performance. Especially, the micropores can efficiently decrease the polyselenides dissolution to inhibit the shuttle effect, and the mesopores interconnected with micropores can lead to good electrolyte transportation. These synergistic hierarchically micro-mesoporous characteristics with a well-balanced ratio of micropores and mesopores achieved a capacity of 456.6 mA h g^{-1} for Se@MIL-53-800 and 530.1 mA h g^{-1} for Se@MIL-68-800, compared to 348.4 mA h g^{-1} for their fewer mesopore counterparts Se@MIL-100-800 and 199.3 mA h g^{-1} for pure Se cathode after 200 cycles. The Se@MIL-68-800 also showed very good rate performance around 307 mA h g^{-1} at 5 C and a high reversible capacity of 544 mA h g^{-1} when back to 0.1 C. Furthermore, the electrochemical performance of the battery should be further improved through the modification of electrolytes to better match the prepared Se cathode[83-85]. Our strategy not only provides a facile way to obtain hierarchically porous carbon from MOFs but also gives insights on how to regulate the proportion of micropores and mesopores to achieve a better Li-Se or Li-S battery performance.

DECLARATIONS

Acknowledgments

Hongyan Li and Chao Li thank the financial support from the China Scholarship Council (CSC) and a scholarship from the Laboratory of Inorganic Materials Chemistry, Université de Namur. The authors thank the help of battery impedance analysis from Prof. Alexandru Vlad (Institute of Condensed Matter and Nanosciences, Université catholique de Louvain) and the support of bis(trifluoromethane)sulfonimide Li salt from Solvey company. The authors thank the help of TEM characterization from Mr. Weichun Huang (Shenzhen Engineering Laboratory of Phosphorene and Optoelectronics, Shenzhen University).

Authors' contributions

Provided financial support: Su BL, Li Y
Revised and finalized the manuscript: Su BL, Li Y

Designed the samples, performed experiments, and wrote the paper with support from: Su BL, Li Y, Li HY, Li C
Gave the experimental guidance and advice: Sun MH, Dong WD
Provided 3D image rendering: Wang YY
Help for data supplement: Zhang XK, Dong WD
All authors contributed to the general discussion.

Availability of data and materials
Not applicable.

Financial support and sponsorship
This work is supported by the National Key R&D Program of China (2016YFA0202602, 2021YFE0115800), National Key R&D Program, Intergovernmental Technological Innovation Special Cooperation Project: WBI International (Wallonia-Brussels)-Most (2021YFE0115800 and SUB/2021/IND493971/524448), National Natural Science Foundation of China (U20A20122, 52103285), Program of Introducing Talents of Discipline to Universities-Plan 111 from the Ministry of Science and Technology and the Ministry of Education of China (Grant No. B20002).

Conflicts of interest
All authors declared that there are no conflicts of interest.

Ethical approval and consent to participate
Not applicable.

Consent for publication
Not applicable.

REFERENCES
1. Yang CP, Yin YX, Guo YG. Elemental selenium for electrochemical energy storage. *J Phys Chem Lett* 2015;6:256-66. DOI PubMed
2. Abouimrane A, Dambournet D, Chapman KW, Chupas PJ, Weng W, Amine K. A new class of lithium and sodium rechargeable batteries based on selenium and selenium-sulfur as a positive electrode. *J Am Chem Soc* 2012;134:4505-8. DOI PubMed
3. Manthiram A, Fu Y, Su YS. Challenges and prospects of lithium-sulfur batteries. *Acc Chem Res* 2013;46:1125-34. DOI PubMed
4. Wang D, Zeng Q, Zhou G, et al. Carbon–sulfur composites for Li–S batteries: status and prospects. *J Mater Chem A* 2013;1:9382. DOI
5. Paraknowitsch JP, Thomas A. Doping carbons beyond nitrogen: an overview of advanced heteroatom doped carbons with boron, sulphur and phosphorus for energy applications. *Energy Environ Sci* 2013;6:2839. DOI
6. Li Z, Yuan L, Yi Z, Liu Y, Huang Y. Confined selenium within porous carbon nanospheres as cathode for advanced Li-Se batteries. *Nano Energy* 2014;9:229-36. DOI
7. Wang H, Li S, Chen Z, Liu HK, Guo Z. A novel type of one-dimensional organic selenium-containing fiber with superior performance for lithium–selenium and sodium-selenium batteries. *RSC Adv* 2014;4:61673-8. DOI
8. Youn HC, Jeong JH, Roh KC, Kim KB. Graphene-selenium hybrid microballs as cathode materials for high-performance lithium-selenium secondary battery applications. *Sci Rep* 2016;6:30865. DOI PubMed PMC
9. He J, Chen Y, Lv W, et al. Three-dimensional hierarchical graphene-CNT@Se: a highly efficient freestanding cathode for Li-Se batteries. *ACS Energy Lett* 2016;1:16-20. DOI
10. Fan S, Zhang Y, Li S, Lan T, Xu J. Hollow selenium encapsulated into 3D graphene hydrogels for lithium-selenium batteries with high rate performance and cycling stability. *RSC Adv* 2017;7:21281-6. DOI
11. Fan JM, Chen JJ, Zhang Q, et al. An amorphous carbon nitride composite derived from ZIF-8 as anode material for sodium-ion batteries. *Chem Sus Chem* 2015;8:1856-61. DOI
12. Wang H, Jiang Y, Manthiram A. Long cycle life, low self-discharge sodium-selenium batteries with high selenium loading and

suppressed polyselenide shuttling. *Adv Energy Mater* 2018;8:1701953. DOI
13. Xin S, Yu L, You Y, et al. The Electrochemistry with Lithium versus sodium of selenium confined to slit micropores in carbon. *Nano Lett* 2016;16:4560-8. DOI
14. Liu Y, Si L, Zhou X, et al. A selenium-confined microporous carbon cathode for ultrastable lithium-selenium batteries. *J Mater Chem A* 2014;2:17735-9. DOI
15. Hippauf F, Nickel W, Hao G, et al. The importance of pore size and surface polarity for polysulfide adsorption in lithium sulfur batteries. *Adv Mater Interfaces* 2016;3:1600508. DOI
16. Yang CP, Xin S, Yin YX, Ye H, Zhang J, Guo YG. An advanced selenium-carbon cathode for rechargeable lithium-selenium batteries. *Angew Chem Int Ed Engl* 2013;52:8363-7. DOI
17. Ji X, Lee KT, Nazar LF. A highly ordered nanostructured carbon-sulphur cathode for lithium-sulphur batteries. *Nat Mater* 2009;8:500-6. DOI PubMed
18. Liu L, Wei Y, Zhang C, et al. Enhanced electrochemical performances of mesoporous carbon microsphere/selenium composites by controlling the pore structure and nitrogen doping. *Electrochimica Acta* 2015;153:140-8. DOI
19. Park S, Park J, Kang YC. Selenium-infiltrated metal-organic framework-derived porous carbon nanofibers comprising interconnected bimodal pores for Li-Se batteries with high capacity and rate performance. *J Mater Chem A* 2018;6:1028-36. DOI
20. Liu T, Dai C, Jia M, et al. Selenium embedded in metal-organic framework derived hollow hierarchical porous carbon spheres for advanced lithium-selenium batteries. *ACS Appl Mater Interfaces* 2016;8:16063-70. DOI
21. Xia W, Qiu B, Xia D, Zou R. Facile preparation of hierarchically porous carbons from metal-organic gels and their application in energy storage. *Sci Rep* 2013;3:1935. DOI PubMed PMC
22. Li H, Dong W, Li C, et al. Boosting reaction kinetics and shuttle effect suppression by single crystal MOF-derived N-doped ordered hierarchically porous carbon for high performance Li-Se battery. *Sci China Mater* 2022;65:2975-88. DOI
23. Li C, Wang Y, Li H, et al. Weaving 3D highly conductive hierarchically interconnected nanoporous web by threading MOF crystals onto multi walled carbon nanotubes for high performance Li-Se battery. *J Energy Chem* 2021;59:396-404. DOI
24. Li H, Dong W, Li C, et al. Three-dimensional ordered hierarchically porous carbon materials for high performance Li-Se battery. *J Energy Chem* 2022;68:624-36. DOI
25. Song JP, Wu L, Dong WD, et al. MOF-derived nitrogen-doped core-shell hierarchical porous carbon confining selenium for advanced lithium-selenium batteries. *Nanoscale* 2019;11:6970-81. DOI
26. Dong WD, Yu WB, Xia FJ, et al. Melamine-based polymer networks enabled N, O, S Co-doped defect-rich hierarchically porous carbon nanobelts for stable and long-cycle Li-ion and Li-Se batteries. *J Colloid Interface Sci* 2021;582:60-9. DOI
27. Zhao Y, Song Z, Li X, et al. Metal organic frameworks for energy storage and conversion. *Energy Storage Mater* 2016;2:35-62. DOI
28. Wang L, Han Y, Feng X, Zhou J, Qi P, Wang B. Metal-organic frameworks for energy storage: Batteries and supercapacitors. *Coord Chem Rev* 2016;307:361-81. DOI
29. Liu X, Sun T, Hu J, Wang S. Composites of metal-organic frameworks and carbon-based materials: preparations, functionalities and applications. *J Mater Chem A* 2016;4:3584-616. DOI
30. Xu J, Lawson T, Fan H, Su D, Wang G. Updated metal compounds (MOFs, -S, -OH, -N, -C) used as cathode materials for lithium–sulfur batteries. *Adv Energy Mater* 2018;8:1702607. DOI
31. Tang J, Yamauchi Y. Carbon materials: MOF morphologies in control. *Nat Chem* 2016;8:638-9. DOI PubMed
32. Dang S, Zhu Q, Xu Q. Nanomaterials derived from metal–organic frameworks. *Nat Rev Mater* 2018:3. DOI
33. Lim S, Suh K, Kim Y, et al. Porous carbon materials with a controllable surface area synthesized from metal-organic frameworks. *Chem Commun* 2012;48:7447-9. DOI
34. Chaikittisilp W, Ariga K, Yamauchi Y. A new family of carbon materials: synthesis of MOF-derived nanoporous carbons and their promising applications. *J Mater Chem A* 2013;1:14-9. DOI
35. Wu HB, Lou XWD. Metal-organic frameworks and their derived materials for electrochemical energy storage and conversion: promises and challenges. *Sci Adv* 2017;3:eaap9252. DOI
36. Lai Y, Gan Y, Zhang Z, Chen W, Li J. Metal-organic frameworks-derived mesoporous carbon for high performance lithium–selenium battery. *Electrochimica Acta* 2014;146:134-41. DOI
37. Guo L, Sun J, Sun X, Zhang J, Hou L, Yuan C. Construction of 1D conductive Ni-MOF nanorods with fast Li^+ kinetic diffusion and stable high-rate capacities as an anode for lithium ion batteries. *Nanoscale Adv* 2019;1:4688-91. DOI PubMed PMC
38. Cai S, Meng Z, Cheng Y, et al. Three dimension Ni/Co-decorated N-doped hierarchically porous carbon derived from metal-organic frameworks as trifunctional catalysts for Zn-air battery and microbial fuel cells. *Electrochimica Acta* 2021;395:139074. DOI
39. Xu Q, Liu T, Li Y, et al. Selenium encapsulated into metal-organic frameworks derived N-doped porous carbon polyhedrons as cathode for Na-Se batteries. *ACS Appl Mater Interfaces* 2017;9:41339-46. DOI
40. He J, Lv W, Chen Y, et al. Three-dimensional hierarchical C-Co-N/Se derived from metal-organic framework as superior cathode for Li-Se batteries. *J Power Sources* 2017;363:103-9. DOI
41. Loiseau T, Serre C, Huguenard C, et al. A rationale for the large breathing of the porous aluminum terephthalate (MIL-53) upon hydration. *Chemistry* 2004;10:1373-82. DOI
42. Volkringer C, Meddouri M, Loiseau T, et al. The Kagomé topology of the gallium and indium metal-organic framework types with a MIL-68 structure: synthesis, XRD, solid-state NMR characterizations, and hydrogen adsorption. *Inorg Chem* 2008;47:11892-901. DOI

43. Yang Q, Vaesen S, Vishnuvarthan M, et al. Probing the adsorption performance of the hybrid porous MIL-68(Al): a synergic combination of experimental and modelling tools. *J Mater Chem* 2012;22:10210. DOI
44. Wang J, Yang J, Krishna R, Yang T, Deng S. A versatile synthesis of metal-organic framework-derived porous carbons for CO_2 capture and gas separation. *J Mater Chem A* 2016;4:19095-106. DOI
45. Yang J, Wang J, Deng S, Li J. Improved synthesis of trigone trimer cluster metal organic framework MIL-100Al by a later entry of methyl groups. *Chem Commun* 2016;52:725-8. DOI PubMed
46. Seoane B, Téllez C, Coronas J, Staudt C. NH_2-MIL-53(Al) and NH_2-MIL-101(Al) in sulfur-containing copolyimide mixed matrix membranes for gas separation. *Sep Purif Technol* 2013;111:72-81. DOI
47. Perea-cachero A, Romero E, Téllez C, Coronas J. Retracted article: insight into the reversible structural crystalline-state transformation from MIL-53(Al) to MIL-68(Al). *Cryst Eng Comm* 2018;20:402-6. DOI
48. García Márquez A, Demessence A, Platero-prats AE, et al. Green microwave synthesis of MIL-100(Al, Cr, Fe) nanoparticles for thin-film elaboration. *Eur J Inorg Chem* 2012;2012:5165-74. DOI
49. Zhou H, Zheng M, Tang H, Xu B, Tang Y, Pang H. Amorphous intermediate derivative from ZIF-67 and its outstanding electrocatalytic activity. *Small* 2020;16:e1904252. DOI PubMed
50. Zhang X, Li H, Lv X, et al. Facile Synthesis of highly efficient amorphous Mn-MIL-100 catalysts: formation mechanism and structure changes during application in CO oxidation. *Chemistry* 2018;24:8822-32. DOI
51. Zhou QY, Zhang Z, Cai JJ, et al. Template-guided synthesis of Co nanoparticles embedded in hollow nitrogen doped carbon tubes as a highly efficient catalyst for rechargeable Zn-air batteries. *Nano Energy* 2020;71:104592. DOI
52. Chen B, He X, Yin F, et al. MO-Co@N-Doped Carbon (M=Zn or Co): vital roles of inactive zn and highly efficient activity toward oxygen reduction/evolution reactions for rechargeable Zn-Air battery. *Adv Funct Mater* 2017;27:1700795. DOI
53. Jiang Y, Liu H, Tan X, et al. Monoclinic ZIF-8 nanosheet-derived 2D carbon nanosheets as sulfur immobilizer for high-performance lithium sulfur batteries. *ACS Appl Mater Interfaces* 2017;9:25239-49. DOI
54. Bardestani R, Patience GS, Kaliaguine S. Experimental methods in chemical engineering: specific surface area and pore size distribution measurements-BET, BJH, and DFT. *Can J Chem Eng* 2019;97:2781-91. DOI
55. Li Z, Yin L. MOF-derived, N-doped, hierarchically porous carbon sponges as immobilizers to confine selenium as cathodes for Li-Se batteries with superior storage capacity and perfect cycling stability. *Nanoscale* 2015;7:9597-606. DOI
56. Qu Y, Zhang Z, Jiang S, et al. Confining selenium in nitrogen-containing hierarchical porous carbon for high-rate rechargeable lithium –selenium batteries. *J Mater Chem A* 2014;2:12255. DOI
57. Xia Z, Zhang J, Fan M, Lv C, Chen Z, Li C. Se with Se-C bonds encapsulated in a honeycomb 3D porous carbon as an excellent performance cathode for Li-Se batteries. *New Carbon Materials* 2023;38:190-8. DOI
58. Zhou X, Gao P, Sun S, et al. Amorphous, crystalline and crystalline/amorphous selenium nanowires and their different (De)lithiation mechanisms. *Chem Mater* 2015;27:6730-6. DOI
59. Ribeiro-soares J, Oliveros M, Garin C, et al. Structural analysis of polycrystalline graphene systems by Raman spectroscopy. *Carbon* 2015;95:646-52. DOI
60. Liu Y, Lu YX, Xu YS, et al. Pitch-derived soft carbon as stable anode material for potassium ion batteries. *Adv Mater* 2020;32:e2000505. DOI
61. Zhou J, Yang J, Xu Z, Zhang T, Chen Z, Wang J. A high performance lithium-selenium battery using a microporous carbon confined selenium cathode and a compatible electrolyte. *J Mater Chem A* 2017;5:9350-7. DOI
62. Wang X, Zhang Z, Qu Y, Wang G, Lai Y, Li J. Solution-based synthesis of multi-walled carbon nanotube/selenium composites for high performance lithium-selenium battery. *J Power Sources* 2015;287:247-52. DOI
63. Wang P, Sun F, Xiong S, et al. WSe_2 Flakelets on N-doped graphene for accelerating polysulfide redox and regulating Li plating. *Angewandte Chemie* 2022:134. DOI
64. Hou H, Shao L, Zhang Y, Zou G, Chen J, Ji X. Large-area carbon nanosheets doped with phosphorus: a high-performance anode material for sodium-ion batteries. *Adv Sci* 2017;4:1600243. DOI PubMed PMC
65. Liu T, Zhang Y, Hou J, Lu S, Jiang J, Xu M. High performance mesoporous C@Se composite cathodes derived from Ni-based MOFs for Li-Se atteries. *RSC Adv* 2015;5:84038-43. DOI
66. Ma C, Wang H, Zhao X, et al. Porous bamboo-derived carbon as selenium host for advanced lithium/sodium–selenium batteries. *Energy Technol* 2020;8:1901445. DOI
67. Fang R, Xia Y, Liang C, et al. Supercritical CO_2-assisted synthesis of 3D porous SiOC/Se cathode for ultrahigh areal capacity and long cycle life Li-Se batteries. *J Mater Chem A* 2018;6:24773-82. DOI
68. Wang C, Dong W, Wang L, et al. Dual catalysis-adsorption function modified separator towards high-performance Li-Se battery. *Appl Surf Sci* 2022;599:153932. DOI
69. Mo Y, Guo L, Jin H, et al. Improved cycling stability of $LiNi_{0.6}Co_{0.2}Mn_{0.2}O_2$ through microstructure consolidation by TiO_2 coating for Li-ion batteries. *J. Power Sources* 2020;448:227439. DOI
70. Jiang Z, Zeng Z, Hu W, Han Z, Cheng S, Xie J. Diluted high concentration electrolyte with dual effects for practical lithium-sulfur batteries. *Energy Storage Materials* 2021;36:333-40. DOI
71. Wang X, Tan Y, Liu Z, et al. New insight into the confinement effect of microporous carbon in Li/Se battery chemistry: a cathode with enhanced conductivity. *Small* 2020;16:e2000266. DOI
72. Wang B, Zhang J, Xia Z, et al. Polyaniline-coated selenium/carbon composites encapsulated in graphene as efficient cathodes for Li-

Se batteries. *Nano Res* 2018;11:2460-9. DOI

73. Ryu HS, Guo Z, Ahn HJ, Cho GB, Liu H. Investigation of discharge reaction mechanism of lithium|liquid electrolyte|sulfur battery. *J Power Sources* 2009;189:1179-83. DOI
74. Yangdan L, Yichuan G, Yang T, Haichao T, Zhizhen Y, Jianguo L. Porous carbon derived from corncob as cathode host for Li-Se battery. *Ionics* 2022;28:2593-601. DOI
75. Ou J, Wang H, Wang J, Wu S. Porous carbon/Se composite derived from pistachio shell as high-performance Li-Se battery cathode. *Chem Lett* 2021;50:1797-800. DOI
76. Cao Y, Lei F, Li Y, et al. A MOF-derived carbon host associated with Fe and Co single atoms for Li-Se batteries. *J Mater Chem A* 2021;9:16196-207. DOI
77. Li HY, Li F, Wang YY, et al. Selenium confined in ZIF-8 derived porous carbon@MWCNTs 3D networks: tailoring reaction kinetics for high performance lithium-selenium batteries. *Chem Synth* 2022;2:8. DOI
78. Beer C, Barendse PS, Pillay P, Bullecks B, Rengaswamy R. Classification of high-temperature PEM fuel cell degradation mechanisms using equivalent circuits. *IEEE Trans Ind Electron* 2015;62:5265-74. DOI
79. Majasan JO, Cho JIS, Maier M, Dedigama I, Shearing PR, Brett DJ. Effect of anode flow channel depth on the performance of polymer electrolyte membrane water electrolyser. *ECS Trans* 2018;85:1593-603. DOI
80. Wu Q, Wang Y, Li P, Chen S, Wu F. MXene titanium carbide synthesized by hexagonal titanium aluminum carbide with high specific capacitance and low impedance. *Dalton Trans* 2022;51:3263-74. DOI
81. Yin J, Chen P, Lu M, et al. Cu-doped CoS_2 polyhedrons with high catalytic activity and long-term stability. *Sci China Mater* 2020;63:1337-44. DOI
82. Wang B, Li Z, Zhang J, et al. N-Doped 3D Interconnected carbon bubbles as anode materials for lithium-ion and sodium-ion storage with excellent performance. *J Nanosci Nanotechnol* 2019;19:7301-7. DOI
83. Hu Y, Fan L, Rao AM, et al. Cyclic-anion salt for high-voltage stable potassium-metal batteries. *Natl Sci Rev* 2022;9:nwac134. DOI PubMed PMC
84. Liu S, Li Y, Zhang Y, et al. In situ generation of AlF_3 in nanoporous carbon to enable cathode-lectrolyte interface construction for stable Li–Se batteries. *ACS Appl Nano Mater* 2023;6:5414-21. DOI
85. Zhou M, Dong W, Xu A, et al. Surface iodine modification inducing robust CEI enables ultra-stable Li-Se batteries. *Chem Eng J* 2023;455:140803. DOI

Su. *Chem Synth* 2023;3:46
DOI: 10.20517/cs.2023.62

Chemical Synthesis

Editorial

Open Access

Prof. Alain Krief, a brilliant scientist, a passionate chemist and a fantastic chemist trainer

Bao-Lian Su[1,2]

[1]Laboratory of Inorganic Materials Chemistry, University of Namur, Namur B-5000, Belgium.
[2]State Key Laboratory of Advanced technology for Materials Synthesis and Processing, Wuhan 430070, Hubei, China.

Correspondence to: Prof. Bao-Lian Su, Laboratory of Inorganic Materials Chemistry, University of Namur, Rue de Bruxelles 61, Namur B-5000, Belgium. E-mail: bao-lian.su@unamur.be

How to cite this article: Su BL. Prof. Alain Krief, a brilliant scientist, a passionate chemist and a fantastic chemist trainer. *Chem Synth* 2023;3:46. https://dx.doi.org/10.20517/cs.2023.62

Received: 5 Dec 2023 **Accepted:** 6 Dec 2023 **Published:** 6 Dec 2023

Academic Editor: Ying Wan **Copy Editor:** Pei-Yun Wang **Production Editor:** Pei-Yun Wang

It is my immense pleasure to lead this Special Issue in honor of Professor Alain Krief on the occasion of his 80th birthday. I would like to express my admiration for him and extend my heartfelt congratulations on the successful publication of Volume 3, Issue 4 of the Journal of *Chemical Synthesis* (*CS*).

Prof. Alain Krief was born in Tunis on 13th December 1942. He completed his Ph.D. in 1970 under the supervision of Prof. Jacqueline Ficini on cycloaddition of ynamines at the Université Pierre et Marie Curie in Paris, France. While working as a CNRS Research Associate (1968-1972), he made a ten-month postdoctoral stay at the laboratory of Prof. Elias J. Corey (Nobel Laureate, 1990) at Harvard University on sterol biosynthesis in 1970 (Prof. Krief contributed a research paper to this Special Issue on Sterol biosynthesis with a research highlight from double Nobel Laureate in Chemistry, Prof. K. B. Sharpless). In 1972, he was appointed as "Chargé de Cours" to head the newly established Laboratory of Organic Chemistry in Facultés Universitaires Notre-Dame de la Paix (now University of Namur), Belgium, a position he held until 1997. Subsequently, he became the Director of the Laboratoire de Chimie Organique de Synthèse (1997-2008). Notably, he was exceptionally promoted to a full professor in 1975 at the remarkable age of 33. Currently, Prof. Krief holds the status of an emeritus professor at the University of Namur (Belgium). Additionally, he serves as an adjunct professor at the University of Karachi (HEJ Research Institute, Pakistan) and a UNESCO research fellow at iThemba-Lab in Cape Town (South Africa).

Alain worked on a number of research subjects, demonstrating an abiding interest in bioorganic chemistry and the mechanism of sterol biosynthesis with an outstanding output of research that was summarized in more than 350 papers. Here, I would like to mention only two fields in which his impressive contributions have been highly recognized. The first one is on cyclopropane chemistry and pyrethroids. He developed novel syntheses of chrysanthemic acid and its analogs using elegant synthetic strategies. This essential methodology led to numerous synthetic methods of pyrethroids. The cornerstone of Alain's pyrethroid syntheses is the built-in flexibility of the approach, allowing for potential adaptability to expand the chemical space around their basic scaffold. The second one is about selenium chemistry. Alain stands as one of the pioneers of organoselenium chemistry and continues to be a leading authority in this field. For an extended period, selenium, as an element, held minimal significance in synthetic chemistry. However, owing to his groundbreaking studies, this has changed fundamentally.

Alain's pioneering work has been recognized by a number of scientific awards, such as the Prize of the French "Académie des Sciences" in 1985 and the International Wernaers Prize for Research and Broadcasting of Knowledge in 1999, and prestigious appointments, including Presidencies of the Janssen Prize for Creativity in Organic Synthesis (2002-2008) and the Société Royale de Chimie Belge (1993-1995). He has organized and been chairman of several congresses, including the famous Belgian Organic Synthesis Symposium (BOSS).

Not only a brilliant scientist and passionate chemist, but Alain was also a fantastic chemist trainer. Under his supervision, Alain mentored approximately 50 PhD and 100 Master students. His successful training for students who passed the FRIA (Fonds de Recherche pour l'Industrie et l'Agriculture, Belgium) scholarship remains a household story at the University of Namur. These students now hold significant positions in academic and industrial sectors. Alain's passion for chemistry remains unwavering. Even at 80 years old, he continues to visit the Laboratory daily, conducting various exploratory experiments and providing assistance to students.

Alain was heavily involved as a leader in the International Organization for Chemical Sciences in Development (IOCD), the first organization devoted to the role of the chemical sciences in global development. From 2009 to 2020, Alain Krief served as the Executive Director of the IOCD.

In this Special Issue honoring him, we have assembled 11 papers contributed by authors from around the world. Among them are two papers from a collaboration between my research groups in Belgium and China, focusing on Lithium-Selenium batteries[1-2]. Li-Selenium batteries have been recognized as very promising next-generation Lithium batteries with high energy density. Following these two research papers is a Research highlight from Editor[3]. Alain also contributed to this Special Issue on his passionate subject, "Schizophrenic behavior of 2,3-oxidosqualene sterol cyclase from pig liver towards 2,3-oxidosqualene analogs"[4]. The double Nobel Laureate in Chemistry, Prof. K. B. Sharpless, made a comment on Alain's last research[5]. "Biotransformation studies on bioactive compounds: 25 years of interesting research at the ICCBS" is from a Pakistan research group in honor of Prof. Krief[6]. Prof. Krief paid much attention to the research and higher education in Pakistan. He frequently visited Pakistan these last years in spite of COVID-19. Prof. Stefano A. Cerri from Italy contributed a paper entitled "Information, knowledge, and human learning for chemistry: the visionary contribution of Professor Alain Krief"[7]. We are deeply grateful to Prof. Vivian Wing-Wah Yam, the current and first female president of the IOCD, for her excellent contribution entitled "Luminescent alkynylplatinum(II) terpyridine-containing conjugated polymers: synthesis, characterization and photophysical studies"[8]. The excellent review paper from Prof. Wei Yan from Singapore and China on "Selenium nanomaterials enabled flexible and wearable electronics"[9] is

highly appreciated. This review illustrates the huge application of selenium nanomaterials. Prof. Hisashi Yamamoto contributed a feature article on "From Lewis acids to peptide chemistry"[10]. This Special Issue concludes with a perspective paper titled "Future prospects in boron chemistry: new boron compounds and Lewis acids for catalysis and materials science"[11], authored by Prof. Guillaume Berionni, a highly promising figure in organic chemistry from the University of Namur, with whom Prof. Krief shares a profound collaborative bond.

Through this Special Issue, we aim to bring you some novel developments in selenium and other chemistry, highlighting the significant contributions made by Prof. Krief.

DECLARATIONS

Author's contribution

The author contributed solely to this manuscript.

Availability of data and materials

Not applicable.

Financial support and sponsorship

None.

Conflicts of interest

The author declared that there are no conflicts of interest.

Ethical approval and consent to participate

Not applicable.

Consent for publication

Not applicable.

REFERENCES

1. Li HY, Li C, Wang YY, et al. Pore structure unveiling effect to boost lithium-selenium batteries: selenium confined in hierarchically porous carbon derived from aluminum based MOFs. *Chem Synth* 2023;3:30. DOI
2. Li HY, Li C, Wang YY, et al. Selenium confined in ZIF-8 derived porous carbon@MWCNTs 3D networks: tailoring reaction kinetics for high performance lithium-selenium batteries. *Chem Synth* 2022;2:8. DOI
3. Yamamoto H. Sterol biosynthesis: 2,3-oxidosqualene analogues. *Chem Synth* 2021;1:7. DOI
4. Krief A, Sable R, Ronvaux A, Dumont W, Sandra P, David F. Schizophrenic behavior of 2,3-oxidosqualene sterol cyclase from pig liver towards 2,3-oxidosqualene analogs. *Chem Synth* 2021;1:6. DOI
5. Sharpless KB. The "fittest sterol" - origin mysteries still fascinate. *Chem Synth* 2021;1:8. DOI
6. Siddiqui M, At, Choudhary MI, Au. Biotransformation studies on bioactive compounds: 25 years of interesting research at the ICCBS. *Chem Synth* 2023;3:25. DOI
7. Cerri SA. Information, knowledge, and human learning for chemistry: the visionary contribution of Professor Alain Krief. *Chem Synth* 2023;3:18. DOI
8. Cheng HK, Yam VWW. Luminescent alkynylplatinum(II) terpyridine-containing conjugated polymers: synthesis, characterization and photophysical studies. *Chem Synth* 2023;3:13. DOI
9. Dang C, Liu M, Lin Z, Yan W. Selenium nanomaterials enabled flexible and wearable electronics. *Chem Synth* 2023;3:14. DOI
10. Yamamoto H. From Lewis acids to peptide chemistry. *Chem Synth* 2022;2:14. DOI
11. Berionni G. Future prospects in boron chemistry: new boron compounds and Lewis acids for catalysis and materials science. *Chem Synth* 2021;1:10. DOI

AUTHOR INSTRUCTIONS

1. Submission Overview

Before you decide to publish with *Chemical Synthesis*, please read the following items carefully and make sure that you are well aware of Editorial Policies and the following requirements.

1.1 Topic Suitability

The topic of the manuscript must fit the scope of the journal. Please refer to Aims and Scope for more information.

1.2 Open Access and Copyright

The journal adopts Gold Open Access publishing model and distributes content under the Creative Commons Attribution 4.0 International License. Copyright is retained by authors. Please make sure that you are well aware of these policies.

1.3 Publication Fees

Chemical Synthesis is an open access journal. When a paper is accepted for publication, authors are required to pay Article Processing Charges (APCs) to cover its editorial and production costs. The APC for each submission is $1200. There are no additional charges based on color, length, figures, or other elements. For more details, please refer to OAE Publication Fees.

1.4 Language Editing

All submissions are required to be presented clearly and cohesively in good English. Authors whose first language is not English are advised to have their manuscripts checked or edited by a native English speaker before submission to ensure the high quality of expression. A well-organized manuscript in good English would make the peer review even the whole editorial handling more smoothly and efficiently.
If needed, authors are recommended to consider the language editing services provided by OAE to ensure that the manuscript is written in correct scientific English before submission. An extra charge is required to enjoy this service. Please visit https://www.oaepublish.com/index/author_services or contact English-Editing@oaepublish.com for more details.

1.5 Work Funded by the National Institutes of Health

If an accepted manuscript was funded by National Institutes of Health (NIH), the author may inform Editors of the NIH funding number. The Editors are able to deposit the paper to the NIH Manuscript Submission System on behalf of the author.

2. Submission Preparation

2.1 Cover Letter

A cover letter is required to be submitted accompanying each manuscript. It should be concise and explain why the study is significant, why it fits the scope of the journal, and why it would be attractive to readers, etc.
Here is a guideline of a cover letter for authors' consideration:
In the first paragraph: include the title and type (e.g., Original Article, Review, Case Report, etc.) of the manuscript, a brief on the background of the study, the question the author sought out to answer and why;
In the second paragraph: concisely explain what was done, the main findings and why they are significant;
In the third paragraph: indicate why the manuscript fits the Aims and Scope of the journal, and why it would be attractive to readers;
In the fourth paragraph: confirm that the manuscript has not been published elsewhere and not under consideration of any other journal. All authors have approved the manuscript and agreed on its submission to the journal. Journal's specific requirements have been met if any.
If the manuscript is contributed to a Special Issue, please also mention it in the cover letter.
If the manuscript was presented partly or entirely in a conference, the author should clearly state the background information of the event, including the conference name, time and place in the cover letter.

2.2 Types of Manuscripts

The journal publishes Research Article, Review Article, Short Communication, Feature Article, Commentary, Editorial, News, Research Highlight, Perspective, *etc*. For more details about paper type, please refer to the following table.

Manuscript Type	Definition	Word Limit	Abstract	Keywords	Main Text Structure

Research Article	A Research Article is a seminal and insightful research study and showcases that often involves modern techniques or methodologies. Authors should justify that their work are of novel findings.	8000max	The abstract should state briefly the purpose of the research, the principal results and major conclusions. No more than 250 words.	3-6 keywords.	The main content should include four sections: Introduction, Experimental, Results and discussion, and Conclusions.
Review	A Review Article should be an authoritative, well balanced and critical survey of recent progresses in an attractive or a fundamental chemical research field.	10000max	Unstructured abstract. No more than 250 words.	3-6 keywords.	The main text may consist of several sections with unfixed section titles. We suggest that the author include an "Introduction" section at the beginning, several sections with unfixed titles in the middle part, and a "Conclusion and outlook" section in the end. Corresponding authors are requested to provide a short biography (up to 200 words) and headshot for inclusion at the end of the published article.
Short Communication	Short Communications are for the urgent publication of a research which is of outstanding significance and interest to experts in the field and also to general chemistry readership. Authors should write in a clear and concise way to demonstrate the necessity of an urgent publication.	1500max	Unstructured abstract. No more than 150 words.	3-6 keywords.	The short Communication is a one body text with maximum 4 items (figures and tables) and 12 references.
Feature Article	A Feature Article is not a typical review. Feature article should highlight the author's contribution to a key field with a balanced discussion of related work from the field. A Feature Article should not, in principle, contain original research.	5000max	Unstructured abstract. No more than 250 words.	3-6 keywords.	The main text may consist of several sections with unfixed section titles. We suggest that the author include an "Introduction" section at the beginning, several sections with unfixed titles in the middle part, and a "Conclusion and outlook" section in the end.
Commentary	A Commentary is to provide comments on a newly published article or an alternative viewpoint on a certain topic.	2500max	Unstructured abstract. No more than 250 words.	3-6 keywords.	/
Editorial	An Editorial can be a comment about an important event in the world related or not to chemistry or a particular discovery in chemistry, needing a particular attention of chemistry community.	1000max	None required.	None required	/
News	A News comments an important event in the world related or not to chemistry, or a particular discovery in chemistry, needing a particular attention of chemistry community.	1500max	None required.	None required	/
Research Highlight	A Research Highlight article is peer-reviewed paper and highlights work recently published in the journal or in a recent issue of another journal.	1200max	None required.	3-6 keywords.	/

Perspective	A Perspective provides personal points of view on the state-of-the-art of a specific area of knowledge and its future prospects.	2000max	Unstructured abstract. No more than 150 words.	3-6 keywords.	/
Opinion	An Opinion usually presents personal thoughts, beliefs, or feelings on a topic.	2500max	Unstructured abstract (optional).No more than 250 words.	3-8 keywords.	/

2.3 Manuscript Structure

2.3.1 Front Matter

2.3.1.1 Title

The title of the manuscript should be concise, specific and relevant, with no more than 16 words if possible. When gene or protein names are included, the abbreviated name rather than full name should be used.

2.3.1.2 Authors and Affiliations

Authors' full names should be listed. The initials of middle names can be provided. Institutional addresses and email addresses for all authors should be listed. At least one author should be designated as corresponding author. In addition, corresponding authors are suggested to provide their Open Researcher and Contributor ID upon submission. Please note that any change to authorship is not allowed after manuscript acceptance.

2.3.1.3 Highlights

Highlights are mandatory because they can help increase the discoverability of your article through search engines. They consist of a short collection of bullet points that capture the novel results of your research as well as new methods that were used during the study (if any). They should be submitted in a separate editable file in the online submission system. Please use 'Highlights' in the file name and include 3 to 5 bullet points (maximum 85 characters per bullet point, including spaces).

2.3.1.4 Abstract

The abstract should be a single paragraph with word limitation and specific structure requirements (for more details please refer to Types of Manuscripts). It usually describes the main objective(s) of the study, explains how the study was done, including any model organisms used, without methodological detail, and summarizes the most important results and their significance. The abstract must be an objective representation of the study: it is not allowed to contain results which are not presented and substantiated in the manuscript, or exaggerate the main conclusions. Citations should not be included in the abstract.

2.3.1.5 Graphical Abstract

The graphical abstract is essential as this can catch first view of your publication by readers. We recommend you to submit an eye-catching figure. It should summarize the content of the article in a concise graphical form. It is recommended to use it because this can make online articles get more attention. The graphic abstract should be submitted as a separate document in the online submission system. Please provide an image with a minimum of 531 × 1,328 pixels (h × w) or proportionally more. The image should be readable at a size of 5 × 13 cm using a regular screen resolution of 96 dpi. Preferred file types: tiff, psd, AI, jpeg and eps files.

2.3.1.6 Keywords

Three to six keywords should be provided, which are specific to the article, yet reasonably common within the subject discipline.

2.3.2 Main Text

Manuscripts of different types are structured with different sections of content. Please refer to Types of Manuscripts to make sure which sections should be included in the manuscripts.

2.3.2.1 Introduction

The introduction should contain background that puts the manuscript into context, allow readers to understand why the study is important, include a brief review of key literature, and conclude with a brief statement of the overall aim of the work and a comment about whether that aim was achieved. Relevant controversies or disagreements in the field should be introduced as well.

2.3.2.2 Experimental

Experimental should contain sufficient details to allow others to fully replicate the study. New methods and protocols should be described in detail while well-established methods can be briefly described or appropriately cited. Experimental participants selected, the drugs and chemicals used, the statistical methods taken, and the computer software used should be identified precisely. Statistical terms, abbreviations, and all symbols used should be defined clearly. Protocol documents for clinical trials, observational studies, and other non-laboratory investigations may be uploaded as supplementary materials.

2.3.2.3 Results and Discussion

This section should contain the findings of the study and discuss the implications of the findings in context of existing research and highlight limitations of the study. Future research directions may also be mentioned. Results of statistical analysis should also be included either as text or as tables or figures if appropriate. Authors should emphasize and summarize only the most important observations. Data on all primary and secondary outcomes identified in the section Methods should also be provided. Extra or supplementary materials and technical details can be placed in supplementary documents.

2.3.2.4 Conclusions

It should state clearly the main conclusions and include the explanation of their relevance or importance to the field.

2.3.3 Back Matter

2.3.3.1 Acknowledgments

Anyone who contributed towards the article but does not meet the criteria for authorship, including those who provided professional writing services or materials, should be acknowledged. Authors should obtain permission to acknowledge from all those mentioned in the Acknowledgments section. This section is not added if the author does not have anyone to acknowledge.

2.3.3.2 Authors' Contributions

Each author is expected to have made substantial contributions to the conception or design of the work, or the acquisition, analysis, or interpretation of data, or the creation of new software used in the work, or have drafted the work or substantively revised it.

Please use Surname and Initial of Forename to refer to an author's contribution. For example: made substantial contributions to conception and design of the study and performed data analysis and interpretation: Salas H, Castaneda WV; performed data acquisition, as well as provided administrative, technical, and material support: Castillo N, Young V.

If an article is single-authored, please include "The author contributed solely to the article." in this section.

2.3.3.3 Availability of Data and Materials

In order to maintain the integrity, transparency and reproducibility of research records, authors should include this section in their manuscripts, detailing where the data supporting their findings can be found. Data can be deposited into data repositories or published as supplementary information in the journal. Authors who cannot share their data should state that the data will not be shared and explain it. If a manuscript does not involve such issue, please state "Not applicable." in this section.

2.3.3.4 Financial Support and Sponsorship

All sources of funding for the study reported should be declared. The role of the funding body in the experiment design, collection, analysis and interpretation of data, and writing of the manuscript should be declared. Any relevant grant numbers and the link of funder's website should be provided if any. If the study is not involved with this issue, state "None." in this section.

2.3.3.5 Conflicts of Interest

Authors must declare any potential conflicts of interest that may be perceived as inappropriately influencing the representation or interpretation of reported research results. If there are no conflicts of interest, please state "All authors declared that there are no conflicts of interest." in this section. Some authors may be bound by confidentiality agreements. In such cases, in place of itemized disclosures, we will require authors to state "All authors declare that they are bound by confidentiality agreements that prevent them from disclosing their conflicts of interest in this work.". If authors are unsure whether conflicts of interest exist, please refer to the "Conflicts of Interest" of *Chemical Synthesis* Editorial Policies for a full explanation.

2.3.3.6 Ethical Approval and Consent to Participate

Research involving human subjects, human material or human data must be performed in accordance with the Declaration of Helsinki and approved by an appropriate ethics committee. An informed consent to participate in the study should also be obtained from participants, or their parents or legal guardians for children under 16. A statement detailing the name of the ethics committee (including the reference number where appropriate) and the informed consent obtained must appear in the manuscripts reporting such research.

Studies involving animals and cell lines must include a statement on ethical approval. More information is available at Editorial Policies.

If the manuscript does not involve such issue, please state "Not applicable." in this section.

2.3.3.7 Consent for Publication

Manuscripts containing individual details, images or videos, must obtain consent for publication from that person, or in the case of children, their parents or legal guardians. If the person has died, consent for publication must be obtained from the next of kin of the participant. Manuscripts must include a statement that a written informed consent for publication was obtained. Authors do not have to submit such content accompanying the manuscript. However, these documents must be

available if requested. If the manuscript does not involve this issue, state "Not applicable." in this section.

2.3.3.8 Copyright

Authors retain copyright of their works through a Creative Commons Attribution 4.0 International License that clearly states how readers can copy, distribute, and use their attributed research, free of charge. A declaration "© The Author(s) 2022." will be added to each article. Authors are required to sign License to Publish before formal publication.

2.3.3.9 References

References should be numbered in order of appearance at the end of manuscripts. In the text, reference numbers should be placed in square brackets and the corresponding references are cited thereafter. If the number of authors is less than or equal to six, we require to list all authors' names. If the number of authors is more than six, only the first three authors' names are required to be listed in the references, other authors' names should be omitted and replaced with "et al.". Abbreviations of the journals should be provided on the basis of Index Medicus. Information from manuscripts accepted but not published should be cited in the text as "Unpublished material" with written permission from the source. In order to make submission as easy as possible for authors, the reference style in the initial submission is free, but DOI for each reference are required.

References should be described as follows, depending on the types of works:

Types	Examples
Journal articles by individual authors	Weaver DL, Ashikaga T, Krag DN, et al. Effect of occult metastases on survival in node-negative breast cancer. *N Engl J Med* 2011;364:412-21. [PMID: 21247310 DOI: 10.1056/NEJMoa1008108]
Organization as author	Diabetes Prevention Program Research Group. Hypertension, insulin, and proinsulin in participants with impaired glucose tolerance. *Hypertension* 2002;40:679-86. [PMID: 12411462]
Both personal authors and organization as author	Vallancien G, Emberton M, Harving N, van Moorselaar RJ; Alf-One Study Group. Sexual dysfunction in 1,274 European men suffering from lower urinary tract symptoms. *J Urol* 2003;169:2257-61. [PMID: 12771764 DOI: 10.1097/01.ju.0000067940.76090.73]
Journal articles not in English	Zhang X, Xiong H, Ji TY, Zhang YH, Wang Y. Case report of anti-N-methyl-D-aspartate receptor encephalitis in child. *J Appl Clin Pediatr* 2012;27:1903-7. (in Chinese)
Journal articles ahead of print	Odibo AO. Falling stillbirth and neonatal mortality rates in twin gestation: not a reason for complacency. BJOG 2018; Epub ahead of print [PMID: 30461178 DOI: 10.1111/1471-0528.15541]
Books	Sherlock S, Dooley J. Diseases of the liver and billiary system. 9th ed. Oxford: Blackwell Sci Pub; 1993. pp. 258-96.
Book chapters	Meltzer PS, Kallioniemi A, Trent JM. Chromosome alterations in human solid tumors. In: Vogelstein B, Kinzler KW, editors. The genetic basis of human cancer. New York: McGraw-Hill; 2002. pp. 93-113.
Online resource	FDA News Release. FDA approval brings first gene therapy to the United States. Available from: https://www.fda.gov/NewsEvents/Newsroom/PressAnnouncements/ucm574058.htm. [Last accessed on 30 Oct 2017]
Conference proceedings	Harnden P, Joffe JK, Jones WG, editors. Germ cell tumours V. Proceedings of the 5th Germ Cell Tumour Conference; 2001 Sep 13-15; Leeds, UK. New York: Springer; 2002.
Conference paper	Christensen S, Oppacher F. An analysis of Koza's computational effort statistic for genetic programming. In: Foster JA, Lutton E, Miller J, Ryan C, Tettamanzi AG, editors. Genetic programming. EuroGP 2002: Proceedings of the 5th European Conference on Genetic Programming; 2002 Apr 3-5; Kinsdale, Ireland. Berlin: Springer; 2002. pp. 182-91.
Unpublished material	Tian D, Araki H, Stahl E, Bergelson J, Kreitman M. Signature of balancing selection in Arabidopsis. *Proc Natl Acad Sci U S A*. Forthcoming 2002.

For other types of references, please refer to U.S. National Library of Medicine.
The journal also recommends that authors prepare references with a bibliography software package, such as EndNote to avoid typing mistakes and duplicated references.

2.3.3.10 Supplementary Materials

Additional data and information can be uploaded as Supplementary Materials to accompany the manuscripts. The supplementary materials will also be available to the referees as part of the peer-review process. Any file format is acceptable, such as data sheet (word, excel, csv, cdx, fasta, pdf or zip files), presentation (PowerPoint, pdf or zip files), image (cdx, eps, jpeg, pdf, png or tiff), table (word, excel, csv or pdf), audio (mp3, wav or wma) or video (avi, divx, flv, mov, mp4, mpeg, mpg or wmv). All information should be clearly presented. Supplementary materials should be cited in the main text in numeric order (e.g., Supplementary Figure 1, Supplementary Figure 2, Supplementary Table 1, Supplementary Table 2, etc.). The style of supplementary figures or tables complies with the same requirements on figures or tables in main text. Videos and audios should be prepared in English, and limited to a size of 500 MB or a duration of 3 minutes.

2.4 Manuscript Format

2.4.1 File Format

Manuscript files can be in DOC and DOCX formats and should not be locked or protected.

2.4.2 Length

There are no restrictions on paper length, number of figures, or amount of supporting documents. Authors are encouraged to present and discuss their findings concisely.

2.4.3 Language

Manuscripts must be written in English.

2.4.4 Multimedia Files

The journal supports manuscripts with multimedia files. The requirements are listed as follows:
Videos or audio files are only acceptable in English. The presentation and introduction should be easy to understand. The frames should be clear, and the speech speed should be moderate.
A brief overview of the video or audio files should be given in the manuscript text.
The video or audio files should be limited to a size of up to 500 MB.
Please use professional software to produce high-quality video files, to facilitate acceptance and publication along with the submitted article. Upload the videos in mp4, wmv, or rm format (preferably mp4) and audio files in mp3 or wav format.

2.4.5 Figures

Figures should be cited in numeric order (e.g., Figure 1, Figure 2) and placed after the paragraph where it is first cited;
Figures can be submitted in format of tiff, psd, AI or jpeg, with resolution of 300-600 dpi;
Figure caption is placed under the Figure;
Diagrams with describing words (including, flow chart, coordinate diagram, bar chart, line chart, and scatter diagram, *etc.*) should be editable in word, excel or powerpoint format. Non-English information should be avoided;
Labels, numbers, letters, arrows, and symbols in figure should be clear, of uniform size, and contrast with the background;
Symbols, arrows, numbers, or letters used to identify parts of the illustrations must be identified and explained in the legend;
Internal scale (magnification) should be explained and the staining method in photomicrographs should be identified;
All non-standard abbreviations should be explained in the legend;
Permission for use of copyrighted materials from other sources, including re-published, adapted, modified, or partial figures and images from the internet, must be obtained. It is authors' responsibility to acquire the licenses, to follow any citation instruction requested by third-party rights holders, and cover any supplementary charges.

2.4.6 Tables

Tables should be cited in numeric order and placed after the paragraph where it is first cited;
The table caption should be placed above the table and labeled sequentially (e.g., Table 1, Table 2);
Tables should be provided in editable form like DOC or DOCX format (picture is not allowed);
Abbreviations and symbols used in table should be explained in footnote;
Explanatory matter should also be placed in footnotes;
Permission for use of copyrighted materials from other sources, including re-published, adapted, modified, or partial tables from the internet, must be obtained. It is authors' responsibility to acquire the licenses, to follow any citation instruction requested by third-party rights holders, and cover any supplementary charges.

2.4.7 Abbreviations

Abbreviations should be defined upon first appearance in the abstract, main text, and in figure or table captions and used consistently thereafter. Non-standard abbreviations are not allowed unless they appear at least three times in the text. Commonly-used abbreviations, such as DNA, RNA, ATP, *etc.*, can be used directly without definition. Abbreviations in titles and keywords should be avoided, except for the ones which are widely used.

2.4.8 Italics

General italic words like *vs.*, *et al., etc.*, *in vivo*, *in vitro*; *t* test, *F* test, *U* test; related coefficient as *r*, sample number as *n*, and probability as *P*; names of genses; names of bacteria and biology species in Latin.

2.4.9 Units

SI Units should be used. Imperial, US customary and other units should be converted to SI units whenever possible. There is a space between the number and the unit (i.e., 23 mL). Hour, minute, second should be written as h, min, s.

2.4.10 Numbers

Numbers appearing at the beginning of sentences should be expressed in English. When there are two or more numbers in a paragraph, they should be expressed as Arabic numerals; when there is only one number in a paragraph, number < 10 should be expressed in English and number > 10 should be expressed as Arabic numerals. 12345678 should be written as 12,345,678.

2.4.11 Equations

Equations should be editable and not appear in a picture format. Authors are advised to use either the Microsoft Equation Editor or the MathType for display and inline equations.

2.5 Submission Link

Submit an article via https://oaemesas.com/login?JournalId=cs.

3. Research and Publication Ethics

3.1 Research Involving Human Subjects

All studies involving human subjects must be in accordance with the Helsinki Declaration and seek approval to conduct the study from an independent local, regional, or national review body (e.g., ethics committee, institutional review board, etc.). Such approval, including the names of the ethics committee, institutional review board, etc., must be listed in a declaration statement of Ethical Approval and Consent to Participate in the manuscript. If the study is judged exempt from ethics approval, related information (e.g., name of the ethics committee granting the exemption and the reason for the exemption) must be listed. Further documentation on ethics should also be prepared, as Editors may request more detailed information. Manuscripts with suspected ethical problems will be investigated according to COPE Guidelines.

3.3.1 Consent to Participate

For all studies involving human subjects, informed consent to participate in the studies must be obtained from participants, or their parents or legal guardians for children under 16. Statements regarding consent to participate should be included in a declaration statement of Ethical Approval and Consent to Participate in the manuscript. If informed consent is not required, the name of the ethics committee granting the exemption and the reason for the exemption must be listed. If any ethical violation is found at any stage of publication, the issue will be investigated seriously based on COPE Guidelines.

3.3.2 Consent for Publication

All articles published by *Chemical Synthesis* are freely available on the Internet. All manuscripts that include individual participants' data in any form (i.e., details, images, videos, *etc.*) will not be published without Consent for Publication obtained from that person(s), or for children, their parents or legal guardians. If the person has died, Consent for Publication must be obtained from the next of kin. Authors must add a declaration statement of Consent for Publication in the manuscript, specifying written informed consent for publication has been obtained.

3.2 Publication Ethics Statement

Chemical Synthesis fully adheres to the Code of Conduct and the Best Practice Guidelines of Committee on Publication Ethics (COPE).

The Editors of this journal enforce a rigorous peer-review process together with strict ethical policies and standards to guarantee to add high-quality scientific works to the field of scholarly publication. Unfortunately, cases of plagiarism, data falsification, image manipulation, inappropriate authorship credit, and the like, do arise. The Editors of *Chemical Synthesis* take such publishing ethics issues very seriously and are trained to proceed in such cases with zero tolerance policy.

Authors wishing to publish their papers in *Chemical Synthesis* must abide to the following:

The author(s) must disclose any possibility of a conflict of interest in the paper prior to submission.

The authors should declare that there is no academic misconduct in their manuscript in the cover letter.

Authors should accurately present their research findings and include an objective discussion of the significance of their findings.

Data and methods used in the research need to be presented in sufficient detail in the manuscript so that other researchers can replicate the work.

Authors should provide raw data if referees and the Editors of *Chemical Synthesis* request.

Simultaneous submission of manuscripts to more than one journal is not tolerated.

Republishing content that is not novel is not tolerated (for example, an English translation of a paper that is already published in another language will not be accepted).

The manuscript should not contain any information that has already been published. If you include already published figures or images, please get the necessary permission from the copyright holder to publish under the CC-BY license.

Plagiarism, data fabrication and image manipulation are not tolerated.

Plagiarism is not acceptable in *Chemical Synthesis.*

Plagiarism involves the inclusion of large sections of unaltered or minimally altered text from an existing source without appropriate and unambiguous attribution, and/or an attempt to misattribute original authorship regarding ideas or results, and copying text, images, or data from another source, even from your own publications, without giving credit to the source.

As to reusing the text that is copied from another source, it must be between quotation marks and the source must be cited. If a study's design or the manuscript's structure or language has been inspired by previous studies, these studies must be cited explicitly.

If plagiarism is detected during the peer-review process, the manuscript may be rejected. If plagiarism is detected after

publication, we may publish a Correction or retract the paper.

Falsification is manipulating research materials, equipment, or processes, or changing or omitting data or results so that the findings are not accurately represented in the research record.

Image files must not be manipulated or adjusted in any way that could lead to misinterpretation of the information provided by the original image.

Irregular manipulation includes: introduction, enhancement, moving, or removing features from the original image; grouping of images that should be presented separately, or modifying the contrast, brightness, or color balance to obscure, eliminate, or enhance some information.

If irregular image manipulation is identified and confirmed during the peer-review process, we may reject the manuscript. If irregular image manipulation is identified and confirmed after publication, we may publish a Correction or retract the paper.

Chemical Synthesis reserves the right to contact the authors' institution(s) to investigate possible publication misconduct if the Editors find conclusive evidence of misconduct before or after publication. OAE has a partnership with iThenticate, which is the most trusted similarity checker. It is used to analyze received manuscripts to avoid plagiarism to the greatest extent possible. When plagiarism becomes evident after publication, we will retract the original publication or require modifications, depending on the degree of plagiarism, context within the published article, and its impact on the overall integrity of the published study. Journal Editors will act under the relevant COPE Guidelines.

4. Authorship

Authorship credit of *Chemical Synthesis* should be solely based on substantial contributions to a published study, as specified in the following four criteria:

1. Substantial contributions to the conception or design of the work, or the acquisition, analysis, or interpretation of data for the work;

2. Drafting the work or revising it critically for important intellectual content;

3. Final approval of the version to be published;

4. Agreement to be accountable for all aspects of the work in ensuring that questions related to the accuracy or integrity of any part of the work are appropriately investigated and resolved.

All those who meet these criteria should be identified as authors. Authors must specify their contributions in the section Authors' Contributions of their manuscripts. Contributors who do not meet all the four criteria (like only involved in acquisition of funding, general supervision of a research group, general administrative support, writing assistance, technical editing, language editing, proofreading, *etc.*) should be acknowledged in the section of Acknowledgement in the manuscript rather than being listed as authors.

If a large multiple-author group has conducted the work, the group ideally should decide who will be authors before the work starts and confirm authors before submission. All authors of the group named as authors must meet all the four criteria for authorship.

AI and AI-assisted technologies should not be listed as an author or co-author.

5. Reviewers Exclusions

You are welcome to exclude a limited number of researchers as potential Editors or reviewers of your manuscript. To ensure a fair and rigorous peer review process, we ask that you keep your exclusions to a maximum of three people. If you wish to exclude additional referees, please explain or justify your concerns—this information will be helpful for Editors when deciding whether to honor your request.

6. Editors and Journal Staff as Authors

Editorial independence is extremely important and Editorial Office do not interfere with editorial decisions.

Editorial staff or Editors shall not be involved in the processing their own academic work. Submissions authored by editorial staff/Editors will be assigned to at least three independently outside reviewers. Decisions will be made by other Section Editors who do not have conflict of interests with the author. Journal staffs are not involved in the processing of their own work submitted to any OAE journals.

7. Policy of the Use of AI and AI-assisted Technologies in Scientific Writing

Generative AI and AI-assisted technologies (e.g., large language models) are expected to be increasingly used to create content. In the writing process of manuscripts, using AI and AI-assisted technologies to complete key researcher work, such as producing scientific insights, analyzing and interpreting data or drawing scientific conclusions, is not allowed, and they should only be used to improve the readability and language of manuscripts.

AI and AI-assisted technologies should be used under human control and supervision as they may generate incorrect or prejudiced output, and they should not be listed as an author or co-author, nor cited as an author.

The use of AI and AI-assisted technologies should be disclosed by authors in their manuscripts, and a statement will be required in the final publication.

OAE will keep monitoring the development and adjust the policy when necessary.

8. Conflict of Interests

Chemical Synthesis require authors to declare any possible financial and/or non-financial conflicts of interest at the end of their manuscript and in the cover letter, as well as confirm this point when submitting their manuscript in the submission system. If no conflicts of interest exist, authors need to state "The authors declare no conflicts of interest". We also recognize that some authors may be bound by confidentiality agreements, in which cases authors need to sate "The authors declare that they are bound by confidentiality agreements that prevent them from disclosing their competing interests in this work".

9. Editorial Process

9.1 Initial check

9.1.1 Initial manuscript check

New submissions are initially checked by the Managing Editor from the perspectives of originality, suitability, structure and formatting, conflicts of interest, background of authors, *etc*. Poorly prepared manuscripts may be rejected at this stage. If your manuscript does not meet one or more of these requirements, we will return it for further revisions.

9.1.2 Publishing ethics

All manuscripts submitted to *Chemical Synthesis* are screened using CrossCheck powered by iThenticate to identify any plagiarized content. Your study must also meet all ethical requirements as outlined in our Editorial Policies. If the manuscript does not pass any of these checks, we may return it to you for further revisions or decline to consider your study for publication.

9.2 Editorial assessment

Once your manuscript has passed the initial check, it will be assigned to an Assistant Editor, and then the Editor-in-Chief, or a Section Editor in the case of a conflict of interest, will be notified of the submission and invited to review. Regarding Special Issue paper, after passing the initial check, the manuscript will be successively assigned to an Assistant Editor, Guest Editor, and then to the Editor-in-Chief, or a Section Editor in the case of conflict of interest for the Editor-in-Chief to review. The Editor-in-Chief, or the Section Editor may reject manuscripts that they deem highly unlikely to pass peer review without further consultation. Once your manuscript has passed the editorial assessment, the Assistant Editor will start to organize peer-review.

9.3 Process

Chemical Synthesis operates a single-blind review process. The technical quality of the research described in the manuscript is assessed by a minimum of three independent expert reviewers. The Editor-in-Chief is responsible for the final decision regarding acceptance or rejection of the manuscript. For controversial manuscripts, the Editor-in-Chief is responsible for making the final decision.

9.4 Decisions

Your research will be judged on technical soundness only, not on its perceived impact as judged by Editors or referees. There are three possible decisions: Accept (your study satisfies all publication criteria), Invitation to Revise (more work is required to satisfy all criteria), and Reject (your study fails to satisfy key criteria and it is highly unlikely that further work can address its shortcomings).

10. Contact Us

Journal Contact
Chemical Synthesis Editorial Office
Suite 1504, Plaza A, Xi'an National Digital Publishing Base, No. 996 Tiangu 7th Road, Gaoxin District, Xi'an 710077, Shaanxi, China.
Tel: +86 (0)29 8954 0089

Siqing Hu
Managing Editor
editorialoffice@chesynjournal.com

www.oaepublish.com

Chemical Synthesis
(*CS*)
Los Angeles Office
245 E Main Street ste107, Alhambra,
CA 91801, USA
Tel: +1 323 9987086
E-mail: editorialoffice@chesynjournal.com
Website:www.oaepublish.com/cs